

# Remodeling of E-cadherin-mediated contacts via cortical flows

by

**Feyza Nur Arslan**

September, 2022

*A thesis submitted to the  
Graduate School  
of the  
Institute of Science and Technology Austria  
in partial fulfillment of the requirements  
for the degree of  
Doctor of Philosophy*

Committee in charge:  
Carl-Philipp Heisenberg  
Martin Loose  
Pierre-François Lenne  
Edouard Hannezo, Chair





The thesis of Feyza Nur Arslan, titled “Remodeling of E-cadherin-mediated contacts via cortical flows”, is approved by:

**Supervisor:** Carl-Philipp Heisenberg, ISTA, Klosterneuburg, Austria

Signature: \_\_\_\_\_

**Committee Member:** Martin Loose, ISTA, Klosterneuburg, Austria

Signature: \_\_\_\_\_

**Committee Member:** Pierre-François Lenne, IBDM, Marseille, France

Signature: \_\_\_\_\_

**Defense Chair:** Edouard Hannezo, ISTA, Klosterneuburg, Austria

Signature: \_\_\_\_\_

Signed page is on file



© by Feyza Nur Arslan, September, 2022

CC BY 4.0 The copyright of this thesis rests with the author. Unless otherwise indicated, its contents are licensed under a Creative Commons Attribution 4.0 International License. Under this license, you may copy and redistribute the material in any medium or format. You may also create and distribute modified versions of the work. This is on the condition that you credit the author.

ISTA Thesis, ISSN: 2663-337X

ISBN: 978-3-99078-025-1

I hereby declare that this thesis is my own work and that it does not contain other people's work without this being so stated; this thesis does not contain my previous work without this being stated, and the bibliography contains all the literature that I used in writing the dissertation.

I declare that this is a true copy of my thesis, including any final revisions, as approved by my thesis committee, and that this thesis has not been submitted for a higher degree to any other university or institution.

I certify that any republication of materials presented in this thesis has been approved by the relevant publishers and co-authors.

Signature: \_\_\_\_\_

Feyza Nur Arslan

September, 2022

Signed page is on file



# Abstract

Metazoan development relies on the formation and remodeling of cell-cell contacts. The binding of adhesion receptors and remodeling of the actomyosin cell cortex at cell-cell interaction sites have been implicated in cell-cell contact formation. Yet, how these two processes functionally interact to drive cell-cell contact expansion and strengthening remains unclear. Here, we study how primary germ layer progenitor cells from zebrafish bind to supported lipid bilayers (SLB) functionalized with E-cadherin ectodomains as an assay system for monitoring cell-cell contact formation at high spatiotemporal resolution. We show that cell-cell contact formation represents a two-tiered process: E-cadherin-mediated downregulation of the small GTPase RhoA at the forming contact leads to both depletion of Myosin-2 and decrease of F-actin. This is followed by centrifugal actin network flows at the contact triggered by a sharp gradient of Myosin-2 at the rim of the contact zone, with Myosin-2 displaying higher cortical localization outside than inside of the contact. These centrifugal cortical actin flows, in turn, not only further dilute the actin network at the contact disc, but also lead to an accumulation of both F-actin and E-cadherin at the contact rim. Eventually, this combination of actomyosin downregulation and flows at the contact contribute to the characteristic molecular organization implicated in contact formation and maintenance: depletion of cortical actomyosin at the contact disc, driving contact expansion by lowering interfacial tension at the contact, and accumulation of both E-cadherin and F-actin at the contact rim, mechanically linking the contractile cortices of the adhering cells. Thus, using a biomimetic assay, we exemplify how adhesion signaling and cell mechanics function together to modulate the spatial organization of cell-cell contacts.

# Acknowledgments

A developmental biologist, a biochemist and a naive rotation student enter a meeting room. The rotation student leaves with a project, between the two labs, with no idea that it would take 6 years to finish. It was not easy establishing an assay from scratch, but I managed with the support and help of many people.

CP accepted me into his lab with only a bachelor's degree, yet trusted me with my idea. I cannot imagine such freedom in any other lab. I learned a lot by exploring, and when I went in the wrong direction, he was there to steer me back, for which I am grateful. Martin has been a great foster boss; I could always jump into his office with my frustrations and leave hopeful. Towards the end of my project, I got to collaborate with Edouard, who helped put everything together so simply; I am thankful to him. Lastly, Pierre-François was a great external committee member who gave feedback at every opportunity, so I would also like to thank him.

I am grateful to the fish facility (especially Verena), the imaging & optics facility (especially Gabby, Nasser and Mo), and Jack Merrin from the nanofabrication facility, for keeping our fish alive, helping with imaging and making devices to confine cells, respectively. ISTA gave me a PhD excellence scholarship (Poettinger Agricultural Technology) for 3 years and rest of my work was supported by CP's ERC Advanced Grant (Interaction and feedback between cell mechanics and fate specification in vertebrate gastrulation, MECSPEC 742573), making this doctorate possible.

Being in the lab so long had its perks; I got to meet many great scientists and learn from them. Peng, Jana, Matt and Deborah mainly taught me the zebrafish basics. At the Loose Lab side, Urban and Natalia helped me take off the project as we started with the biochemistry part. I will be forever grateful to all these people. Natalia, later on, became a great friend and mentor. I know we will never lose connection and one day meet in SnSn too. I am happy I witnessed the evolution of so many exciting projects and spent a lot of time with Daniel, Conny, Roland, Nicoletta, Shayan, Silvia, David, Koni, Irene, Benoit, Karla, Diana, Ste, Alex and Suyash. Lab meetings and discussions with these people shaped my scientific brain significantly. Big parts of this lab culture are also the more recent citizens: Xin, Laura, Nikhil, Gayathri, Tushna and Naoya. Thanks to all, the lab continues to be a friendly, fun and helpful place. Shayan and Peng were my first buddies in the lab, though sometimes they tried to kick me out of their "elevated" discussions. With Alex we shared the pain of setting up new assays, so I am grateful for our support system - of complaining a lot. With Karla we had many over-coffee discussions about life, which I believe did not make either of us grow but it has and continues to be quite fun! I feel that we could elevate these discussions to philosophical levels with Nikhil, this is until he cracks a bad joke. And I did not think I would make new friends at the end of my PhD but I am very happy that I got to know Amrita, Gayathri and Inderburg more.

I was lucky enough to have great friends out of the lab as well. The 2015 cohort have made the PhD experience a lot of fun, to mention some of them, thanks to Paulinho, Saren, Rok, Sergey and Priscila. Amelie, I hope I got a little bit of your creativity through exposure. And thanks for opening your home to me when I was left to freeze in winters, best neighbor ever! Shamsi, thanks for feeding me on many occasions, teaching me so much about my language and bringing an awesome plus one to our friendship, Shirin. Lastly, Lena, I am so lucky that I found a BFF as an adult! One clearly depends on one a lot during 7 years of Austria. I sometimes feel like our minds came from some shared source and it is great to utilize this power when we make plans and travel the world, so let's go on!

Finally, I would like to thank my family. 14 yaşımдан beri sizden ayrı olmama rağmen, bunu hiç hissetmedim. Benimle bu kadar gurur duymasaydınız ve yaptığım her şeyin arkasında durmasaydınız bu doktora bitmezdi. Seviyorum sizi.

## About the Author

Feyza Nur Arslan graduated from the Molecular Biology and Genetics Department of Bilkent University, Turkey. During her undergraduate studies, she did internships at EMBL Heidelberg, Whitehead Institute for Biomedical Research and Max Planck Institute of Biochemistry, working with embryos of different model organisms. In 2015, she joined the ISTA PhD program as a recipient of the Pöttinger Scholarship and joined the group of Carl-Philipp Heisenberg in 2016. In her PhD project, Feyza worked on the reconstitution of cell-cell adhesion on supported lipid bilayers, in collaboration with Martin Loose, and presented her results at various conferences such as PhysCell, and Biophysical Society Thematic and Annual Meetings. In 2021 she published a review paper on cell-cell adhesion entitled “Holding It Together”. During her PhD studies, Feyza also participated in advocacy work and researched work-life balance in academia as a member of the elife Community Ambassadors.

## List of Publications

Arslan, F. N., Eckert, J., Schmidt, T. & Heisenberg, C.-P. Holding it together: when cadherin meets cadherin. *Biophys. J.* (2021) doi:10.1016/j.bpj.2021.03.025.

*“What I cannot create, I do not understand.”*  
*Richard Feynman*

*“I might not understand what I can create.”*  
*François Nédélec*

# Table of Contents

<b>Abstract</b>	<b>vii</b>
<b>Acknowledgments</b>	<b>viii</b>
<b>About the Author</b>	<b>ix</b>
<b>List of Collaborators and Publications</b>	<b>x</b>
<b>Table of Contents</b>	<b>xii</b>
<b>List of Figures</b>	<b>xiv</b>
<b>List of Tables</b>	<b>xv</b>
<b>List of Abbreviations</b>	<b>xvi</b>
<b>Introduction</b>	<b>1</b>
1.1 Cell-cell adhesion	1
1.1.1 Multicellularity	1
1.1.2 Intercellular adhesion proteins	3
1.1.3 Cell-cell adhesion through cadherins	5
1.2 Actin cytoskeleton in relation to the adhesion complex	177
1.2.1 Structural, functional and dynamical variability at adhesion sites	177
1.2.2 Cortical flows at adhesion sites	20
1.2.3 What kind of contacts are we looking at in the early zebrafish embryo?	23
1.3 Engineering cadherin adhesion	25
1.3.1 Reconstitution of biological processes	25
1.3.2 Reconstituting cadherin-based adhesion	266
1.3.2.1 Immobile ligands	266
1.3.2.2 Fluid Bilayers	29
<b>Materials and Methods</b>	<b>311</b>
2. 1 EcadECD protein expression, purification and characterization	311
2.1.1 Protein labeling	311
2.1.2 Bead Aggregation assay	311
2.1.3 Western blot	322
2. 2 Bilayer preparation	322
2. 3 Zebrafish lines and handling	333
2. 4 Cloning of expression constructs	333
2. 5 Embryo microinjections	344
2. 6 Embryo cell cultures	344
2. 7 Inhibitor treatments	34

2.8 Phalloidin staining	355
2. 9 Imaging tools	355
2.9.1 PDMS confinement	355
2.9.2 Hydrogel microwells	35
2. 10 Microscopy and Data Analysis	366
2.10.1 FRAP	36
2.10.2 Adherence assay	366
2.10.3 Average intensity and coverage at the contact	366
2.10.4 Colocalization and line profiles	377
2.10.5 Radial intensity profiles	377
2.10.6 F-actin and Ecad flows	37
2.10.7 Actin network density	38
2.10.8 Actin single particle tracking	38
2. 11 Statistics and Reproducibility	38
<b>Results</b>	<b>40</b>
3. 1 Reconstitution of adhesion on bilayers	40
3. 2 Contact formation dynamics	445
3.2.1 E-cadherin-mediated contact formation regulates cortical actomyosin	445
3.2.2 Small GTPases for contact regulation	467
3. 3 Centrifugal flows redistribute F-actin and E-cadherin	51
3. 4 Effects of turnover on contact dynamics	61
3.4.1 Reduced actin turnover increases rim accumulation	61
3.4.2 Molecular turnover measurements	63
3. 5 Actin architecture at the contact	655
3. 6 Contribution of blebs to F-actin and Ecad rim accumulation	688
<b>Discussion and Conclusions</b>	<b>71</b>
<b>References</b>	<b>778</b>

## List of Figures

- Figure 1. Cell sorting in ectoderm-mesoderm aggregates.
- Figure 2. Cell adhesion molecules.
- Figure 3. Characteristic architectures of various actin-adhesion complex structures.
- Figure 4. Examples of biochemical and cellular reconstitution.
- Figure 5. Tissues and substrates with a variety of stiffnesses.
- Figure 6. Effects of substrate on cadherin-adhesion organization.
- Figure 7. Schematic of the biomimetic cell-cell adhesion assay.
- Figure 8. Hybrid EcadFL-Ecad $\Delta$ cyto contacts compare to homotypic EcadFL-EcadFL contacts.
- Figure 9. Zebrafish EcadECD purification and activity.
- Figure 10. Mouse and zebrafish EcadECD on gel-phase bilayers.
- Figure 11. Optimization of fluid bilayers.
- Figure 12. Dynamics of contact formation.
- Figure 13. Rac1 inhibition does not affect cell-cell contacts.
- Figure 14. RhoA overactivity affects cell-cell doublets.
- Figure 15. RhoA-mediated changes at the contact.
- Figure 16. Contact architecture at the contact rim vs center.
- Figure 17. Radial intensity profiles at the contact.
- Figure 18. F-actin network density at the contact.
- Figure 19. Myosin-2-activity-dependent flows of F-actin and Ecad.
- Figure 20. Contractility-enhanced contact dynamics.
- Figure 21. Contact manipulations.
- Figure 22. Jasp-treated contacts.
- Figure 23. Actin single molecule imaging.
- Figure 24. Ecad recovery after bleaching.
- Figure 25. Actin at the contacts of cell doublets.
- Figure 26. Formin and Arp2/3 inhibitor treatments.
- Figure 27. Inhibitors of actin depolymerization.
- Figure 28. F-actin markers.
- Figure 29. Enrichment of proteins with bleb retractions.
- Figure 30. Ecad homophilic binding induced cortical acto-cadherin flows lead to rim accumulation.

## List of Tables

- Table 1. A summary of flow and turnover parameters at the contact.

# List of Abbreviations

AJ - adherens junction  
BSA - bovine serum albumin  
CHO - chinese hamster ovary  
CSK - cytoskeletal buffer  
cSMAC - central supramolecular activation cluster  
DMSO - Dimethyl sulfoxide  
DOPC - 1,2-dioleoyl-sn-glycero-3-phosphocholine  
DPPC - Dipalmitoylphosphatidylcholine  
dSMAC - distal supramolecular activation cluster  
Ecad - E(pithelial)-cadherin  
EcadECD - Ecad ectodomain  
ECM-extracellular matrix  
FBS - fetal bovine serum  
FRAP - fluorescence recovery after photobleaching  
GFP - green fluorescent protein  
GPI - glycosylphosphatidylinositol  
ICAM - intercellular cell adhesion molecule  
IgCAM - IgSF cell adhesion molecule  
IgSF - immunoglobulin superfamily  
LFA1 - Lymphocyte function-associated antigen 1  
LPA - 1-Oleoyl lysophosphatidic acid sodium salt  
MDCK - Madin-Darby canine kidney  
MHC - major histocompatibility complex  
mNG - mneongreen  
Ncad - N(eural)-cadherin  
NCAM - neural cell adhesion molecule  
NTA - Nitrilotriacetic acid  
PA - polyacrylamide  
PBS - phosphate buffered saline  
PDMS - polydimethylsiloxane  
PFA - paraformaldehyde  
pnBb - para-nitroblebbistatin  
pSMAC - peripheral supramolecular activation cluster  
RFP - red fluorescent protein  
RICM - reflection interference contrast microscopy  
SLB - supported lipid bilayer  
TCR - T-cell receptor  
TIRF - total internal reflection fluorescence  
ZA - zonula adherens

# 1. Introduction

## 1.1 Cell-cell adhesion

### 1.1.1 Multicellularity

A necessity for multicellular life is keeping cells together. Multicellularity has evolved several times across the tree of life through different mechanisms<sup>1</sup>. In cell-walled organisms such as plants, multicellularity is achieved by modifying the last step of cytokinesis so that the two daughter cells do not separate their interface after division. For metazoa, the supporting cell wall does not exist; therefore cell-cell adhesion is dependent on developing a glue for a single cell to stick to others.

Through multicellularity animals develop specific tissues with intercellular communication, which coordinate behavior to divide tasks, and run a developmental bauplan. Yet, examples of differentiation and tissue morphologies predate metazoa. Some hypothesize that in colonies of unicellular cells, which show self-aggregation dynamics, based on environmental cues patterns of two cell types can form; such as dividing inner layer and motile outer layer cell groups<sup>2</sup>, similar to structures formed in a blastula. The closest living relatives of animals, choanoflagellates go through single cell and multicellular colony forms through their life cycle. In the colony that forms by divisions of a single cell, cells differentiate to perform different mechanistic functions such as feeding or swimming<sup>3</sup>. Choanoflagellates show multicellular reactions such as activating actomyosin-mediated apical cell contractility in the polarized colony in response to light<sup>4</sup>. Another protozoan at the border of unicellular to multicellular switch, slime mould *Dictyostelium discoideum*, when it is starved, forms aggregates with differential cellular functions which can collectively migrate<sup>5</sup>. These observations show that tissue-like mechanics, which mimic processes shaping the developing embryo, emerge with increased cell-cell adhesion.

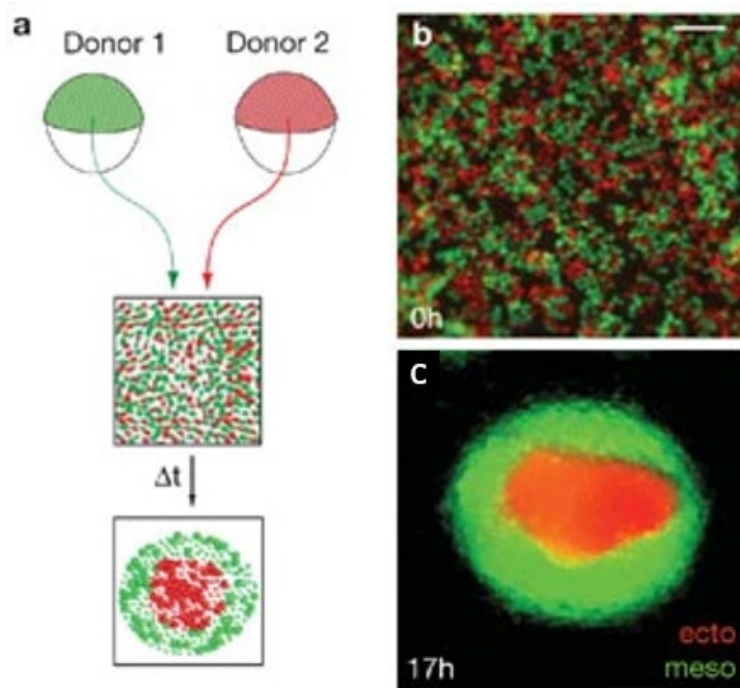


*Figure 1. Cell sorting in ectoderm-mesoderm aggregates. Mixed aggregates are made from progenitor cells dissociated from ectoderm- and mesoderm-induced zebrafish embryos are left to develop in hanging drops (a). Microscopy images at 0 hours (b) and after 17 hours (c) in cultures. Figure adapted from<sup>6</sup>.*

In principle, even weak electrostatic interactions due to the charge of the cell membrane lipids could account for some aggregation between cells<sup>7</sup>. Another contributing factor that is not well-studied is glycans; though glycocalyx is usually seen as a bulk repulsive layer between cells due to its overall negative charge, some carbohydrates on cell surface can make adhesion bonds as strong as some adhesion proteins via Van der Waals bonds thanks to their multivalent character<sup>8</sup>. Even early mouse embryo compaction was shown to depend on carbohydrate interactions<sup>9</sup>. Yet, cells often require stronger, and more importantly specific attachments letting them recognize similar cells from foreign cells. In a complex tissue, differential adhesion brings distinct aggregates of cells together, driving pattern formation (Fig. 1), a phenomenon often seen in developing embryos. Immune cells recognize other immune cells through their surface receptors to show a selective immune response against foreign antigens. Hundreds of proteins coat the cell surface and many of them participate in cell-cell adhesion to mediate this recognition and downstream communication. Specification and diversity of adhesion molecules allow animal cells to control cell-cell adhesion in space and time, leading to changes in cell fate and mechanics, as extracellular domains of adhesion receptors are often only the tip of the iceberg.

### 1.1.2 Intercellular adhesion proteins

Adhesion receptors are estimated to comprise at least 5% of the human genome<sup>10</sup>. Cadherins (**calcium-dependent adherent proteins**) are the primary molecules that mediate homophilic cell-cell adhesion during morphogenesis and hold many epithelial and endothelial sheets of cells together in adult tissues<sup>11</sup>. Cadherins have conserved cytoplasmic domains that bind to adapter proteins catenins which link them to the actin cytoskeleton, therefore mechanically linking neighboring cell cortices (1.1.3). Cadherins predate metazoa; there are several cadherins in choanoflagellates, however their function does not seem to be cell-cell adhesion and the nature of their connection to cytoskeleton is not clear<sup>12,13</sup>. Yet, it is unsurprising that these proteins have been repurposed in metazoa to mediate cell-cell adhesion.

The immunoglobulin superfamily (IgSF) is encoded by 765 human genes and contains immunoglobulin domains<sup>14</sup>. These surface receptors or soluble versions, such as antibodies, are mainly active in recognizing target cell antigens. Yet, members also include IgSF cell adhesion molecules (IgCAMs). For example, neural IgCAMs have been studied widely in neurodevelopment, functioning in axon guidance and synaptic junction formation. Another example is Nectins which were shown to be active at adherens junctions (cadherin-based adhesion domains mechanically linked to a circumferential actin belt in epithelial cells). Through Afadin adapter proteins, Nectins bind the actin cytoskeleton and the cadherin complex via interactions with alpha-catenin<sup>15,16</sup>. Recently more IgCAMs were found to be required for cell sorting, and their interactions with actomyosin were established and recent results strongly suggest they might be involved in mechanosensitivity of junctions<sup>17</sup>.

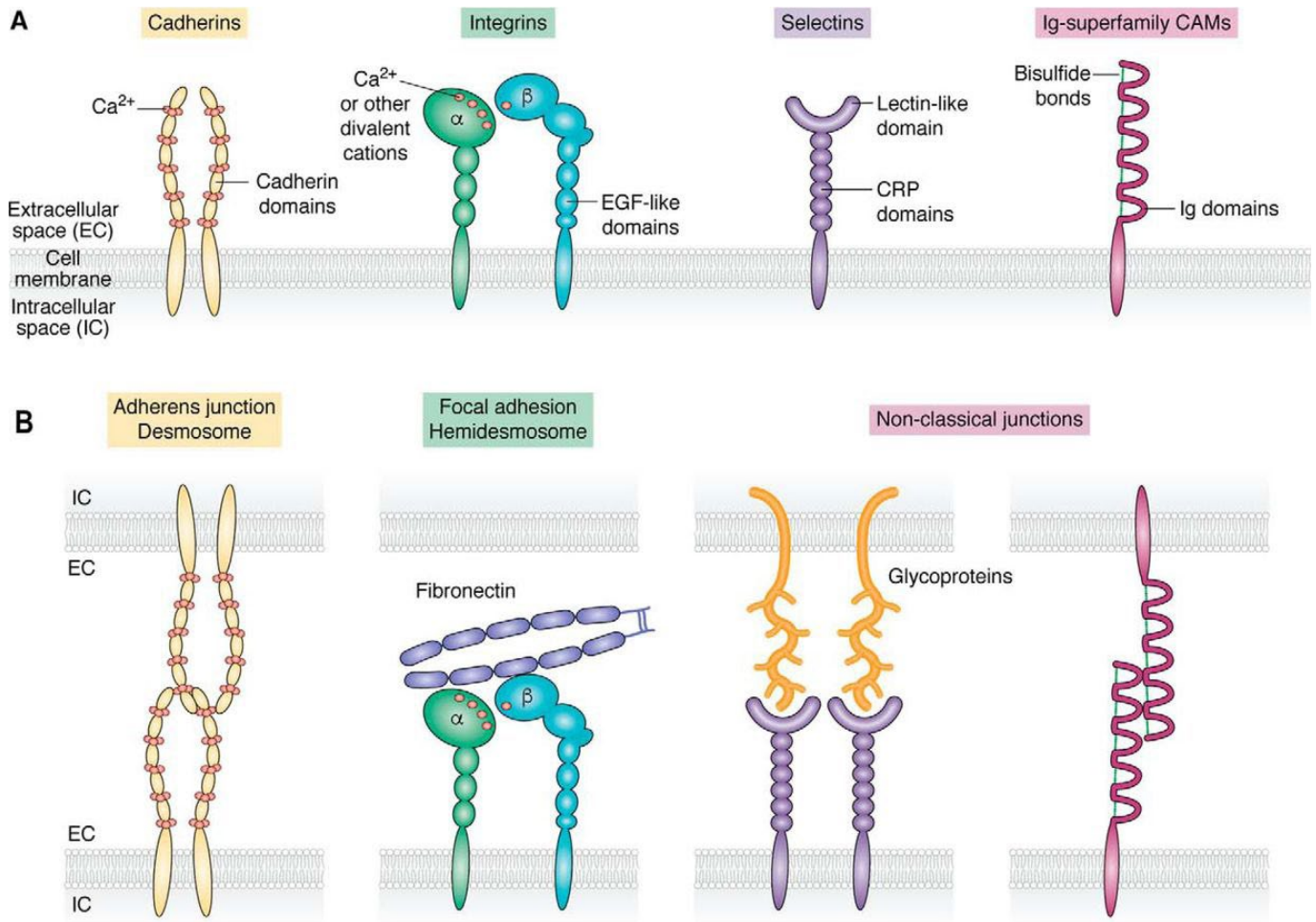


*Figure 2. Cell adhesion molecules. Schematic representations of four major classes of cell adhesion molecules (a). Different types of cellular junctions in which these adhesion molecules are involved (b). Figure adapted from<sup>18</sup>.*

IgSF and integrins mediate the adhesion of T cells to antigen-presenting cells. T-cell receptors (TCRs) of the IgSF bind to antigenic peptides only when they are presented in a complex with another IgSF, major histocompatibility complex (MHC) proteins on the cell surface, which activate T-cells. LFA-1, a member of the integrin family, mediates the antigen-independent adhesion of T-cells to IgSF members ICAM-1 or ICAM-2 on the target cell<sup>19</sup>. This exemplifies that integrins that are known to mediate cell-matrix adhesions commonly can also bind other cell surface receptors. Integrins link to the actin cytoskeleton through their cytoplasmic tails, participate in outside-in signaling to organize actin cytoskeleton and mediate further signaling events<sup>20</sup>, similar to cadherins.

One protein family that recognizes surface carbohydrates, including ones on glycoproteins, to mediate adhesion are cell surface lectins: selectins. Selectin-carbohydrate interactions are stronger than carbohydrate-carbohydrate interactions thanks to hydrogen bonds present. Selectins are heavily studied in the immune system context as leukocyte invasion into tissues occurs through an initial selectin-based adhesion which is followed by integrin activation downstream to selectins<sup>21</sup>. In a similar invasion mechanism, selectins also mediate the attachment of early mammalian embryos to the uterine wall<sup>22</sup>.

### 1.1.3 Cell-cell adhesion through cadherins

In the following section, we discuss the stereotypical features of classical cadherin-mediated cell-cell adhesion in animals, and remind the reader of related aspects of cell mechanics and topical terms, with a focus on how cadherins mediate processes affecting cell and tissue mechanics in a review paper.

# Holding it together: when cadherin meets cadherin

Feyza Nur Arslan,<sup>1</sup> Julia Eckert,<sup>2</sup> Thomas Schmidt,<sup>2</sup> and Carl-Philipp Heisenberg<sup>1,\*</sup>

<sup>1</sup>Institute of Science and Technology Austria, Klosterneuburg, Austria and <sup>2</sup>Physics of Life Processes, Leiden Institute of Physics, Leiden University, Leiden, the Netherlands

**ABSTRACT** Intercellular adhesion is the key to multicellularity, and its malfunction plays an important role in various developmental and disease-related processes. Although it has been intensively studied by both biologists and physicists, a commonly accepted definition of cell-cell adhesion is still being debated. Cell-cell adhesion has been described at the molecular scale as a function of adhesion receptors controlling binding affinity, at the cellular scale as resistance to detachment forces or modulation of surface tension, and at the tissue scale as a regulator of cellular rearrangements and morphogenesis. In this review, we aim to summarize and discuss recent advances in the molecular, cellular, and theoretical description of cell-cell adhesion, ranging from biomimetic models to the complexity of cells and tissues in an organismal context. In particular, we will focus on cadherin-mediated cell-cell adhesion and the role of adhesion signaling and mechanosensation therein, two processes central for understanding the biological and physical basis of cell-cell adhesion.

## INTRODUCTION

The basic unit of living systems is the cell, which gives rise to unicellular colonies and multicellular organisms. In multicellular organisms, cells are assembled into tissues (1), the formation of which depends on cell-cell adhesion complexes that couple cells to each other. Cell-cell adhesion plays essential roles in organismal development and homeostasis, such as tissue compaction (2), cell sorting (3), and cell migration (4), and misregulation of cell-cell adhesion is a hallmark of many developmental disorders and diseases (5–7).

Specific cell-cell adhesion receptors help two cells to interact and recognize each other (8). Among them, the cadherin family of cell-cell adhesion receptors was most intensively studied in the past and was shown to be essential for the formation and maintenance of tissues in countless organisms (9). Cadherins function by mechanically coupling cells to each other and modulating a wide array of effector processes that range from the regulation of the cytoskeleton to gene expression. Cadherin adhesion complexes typically consist of hundreds of proteins, some of which change their conformation and stoichiometry under mechanical stress, thereby linking the interacting surfaces of cells to their cyto-

skeleton and giving cells the ability to sense and respond to extracellular and intracellular signals (10).

Cell-cell adhesion is a complex and dynamic process. For years, physicists have been trying to measure and model cell-cell contacts, and biologists have identified new components, functions, and regulators of the cell-cell adhesion machinery. This led to various descriptions and interpretations of cell-cell adhesion as, for instance, the adhesion energy of molecular interactions at adhesive interfaces (11,12) or the resistance to cell-cell detachment forces (13,14). Moreover, adhesion-mediated cell-cell contact formation was proposed to be driven by the balance of interfacial/surface tensions, which again depend on tension exerted by the actomyosin cortex and its modulation via adhesion receptor signaling and the binding of adhesion molecules over the contact (15–18). In this review, we will summarize and discuss recent progress in defining cell-cell adhesion at multiple scales by both experiment and theory, predominantly focusing on the role of classical cadherins (generally referred to as cadherins) therein.

## THE TOOLBOX OF ADHESION

### Biological components of cell-cell adhesion

#### *Cadherin adhesion complex*

Cadherin adhesion complexes are protein assemblies consisting of cadherin adhesion receptors and their cytoplasmic interactors, such as catenins (19). Classical cadherins, such

Submitted December 16, 2020, and accepted for publication March 17, 2021.

\*Correspondence: [heisenberg@ist.ac.at](mailto:heisenberg@ist.ac.at)

Feyza Nur Arslan and Julia Eckert contributed equally to this work.

Editor: Stanislav Y. Shvartsman.

<https://doi.org/10.1016/j.bpj.2021.03.025>

© 2021



as E-cadherin (cdh1) and N-cadherin (cdh2), consist of an ectodomain of five repetitive extracellular cadherin (EC) subdomains with rigidity-providing  $\text{Ca}^{2+}$ -binding pockets in between those domains, a single-pass transmembrane domain, and a cytoplasmic tail. The ectodomains of cadherins of opposing cells interact by binding *in trans* over the contact, first by engaging in EC1-EC2 interactions, leading to the formation of intermediate fast binding X-dimers, followed by strand swapping to form the so-called S-dimers. Cadherins also interact *in cis* with other cadherins on the same cell surface, a process important for cadherin clustering (20,21). Intracellularly, the cadherin cytoplasmic tail interacts with adaptor proteins, such as p120- and  $\beta$ -catenins. They directly bind to subdomains in the cadherin tail and recruit other molecules, such as  $\alpha$ -catenins, which, by binding to filamentous actin (F-actin), connect cadherins to the actomyosin cytoskeleton (10). As new contacts form, cadherins, catenins, and hundreds of other components and interaction partners of the cadherin adhesion complex get recruited to the contact (19), where they control the establishment, strength, and stability of the contact by regulating cadherin clustering, turnover, and cytoskeletal anchoring. The cadherin adhesion complex also regulates downstream signaling mediators, which again modulate cytoskeletal organization and other cellular functions.

#### *Actin cortex*

The actin cortex is a thin, contractile F-actin network tethered to the plasma membrane shaping animal cells. The actin cortex can readily adapt to the microenvironment by rapidly turning over. Besides actin, the cortex contains various actin-binding proteins, such as actin nucleators (e.g., Arp2/3 and formins), which assemble and disassemble the F-actin network, actin cross-linkers, and motor proteins (most prominently myosin II), which can both pull and cross-link actin filaments. The coaction of these different proteins regulates the actin network architecture and function, thereby defining the mechanical properties of the cortex (22).

#### *Cell membrane*

The cell membrane (plasma membrane) is a phospholipid bilayer surrounding the cell, and forms the border between the interior and exterior of the cell. The cell membrane has a dynamically changing heterogeneous composition and structure. In particular, transient nanodomains of distinct lipid compositions were proposed to function as organizational hubs for recruiting proteins and thereby spatially restricting and modulating their activity (23,24).

#### *Glycocalyx*

The glycocalyx (pericellular matrix) is a carbohydrate-rich meshwork covering the cell membrane and consisting

primarily of glycopolymer chains decorated with bulky glycoproteins. Depending on the cell type, the glycocalyx can extend up to several micrometers from the cell membrane (25) and is thought to modulate cell-cell adhesion by physically keeping the cell membranes (and adhesion molecules therein) of adjacent cells at a distance.

#### *Extracellular matrix*

The extracellular matrix (ECM) is a three-dimensional network composed of proteoglycans (proteins with polysaccharide chains), fibrous proteins, and water, which is locally secreted by cells, connecting and surrounding them. The ECM supports cells structurally and regulates their activities. Cell-ECM adhesion is mediated through ECM receptors, mainly integrins (26).

#### *Junctions*

Junctions are cellular structures/multiprotein complexes that connect neighboring cells or cells with the ECM and are connected through adaptor proteins to the cytoskeleton (8). Most common cell-cell junctions are adherens junctions (containing cadherins), tight junctions, and gap junctions. Junctions experience mechanical forces and can convert those into biochemical signals in a process called mechanotransduction, which leads to changes in cell signaling and adhesion (Fig. 1; (14)).

## **Mechanical characterization of cell-cell adhesion**

#### *Mechanical stress*

Mechanical stress (Pascal, Pa) is equivalent to the force per surface area (Newton per square meter,  $\text{N/m}^2$ ) on an object applied by a neighboring object. At intercellular contacts, tensile stress and compressive stress act normally to the contact area. Tensile stress occurs when cells are pulled away from each other (Fig. 2 A), whereas compressive stress exists when cells are squeezed toward each other. In comparison, shear stress arises when forces act parallel to the contact area, as in the case of cells that move alongside each other. Furthermore, mechanical stress is equal to the mechanical energy per volume (Joule per cubic meter,  $\text{J/m}^3$ ).

#### *Cortical tension*

Cortical tension (Joule per square meter,  $\text{J/m}^2$ ) is the tension generated mainly by myosin motors contracting the thin actin cortex coupled to the cell membrane (27). Cortical tension is modulated by the composition and architecture of the actin cortex (22). Cortical tension must be in balance with the internal cellular pressure, thereby together controlling the cell shape. Cortical tension tends to decrease the surface and the contact area of a cell (Fig. 2 B).

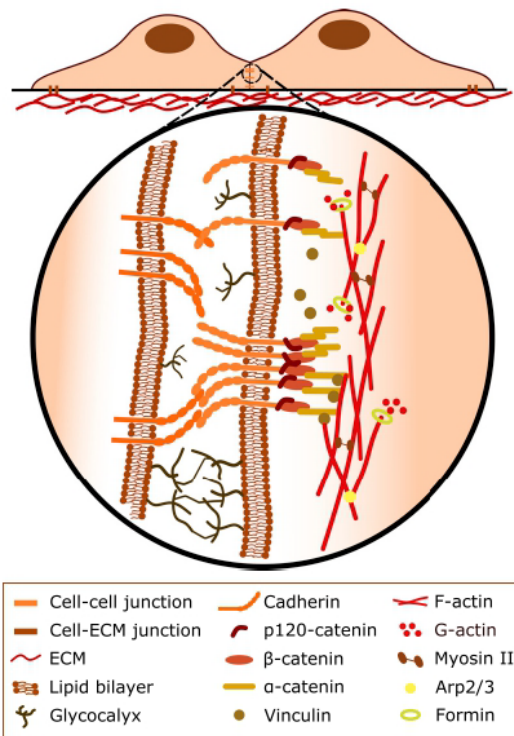


**FIGURE 1** Cells can undergo adhesions with other cells and the extracellular matrix (ECM) via junctions. Cadherins mediate specific cell-cell adhesions via *trans* interactions in the extracellular space, where glycocalices act as a repulsive barrier. Cadherins indirectly bind to the underlying actomyosin cortex via  $\beta$ - and  $\alpha$ -catenins. Mechanosensitive cadherin adhesion complexes can change their binding strength to the actin cortex by *cis* clustering and by recruiting adaptor proteins such as vinculin. These complexes can also lead to local changes in actomyosin contractility by regulating the architecture of the cortex.

### Surface tension

Analogous to water droplets, the surface tension (Joule per square meter,  $J/m^2$ ), as energy per surface area, acts to minimize the surface area of cells (28). Cortical tension together with the typically lower tension of the plasma membrane are the main regulators of cell surface tension. The concept of surface tension can also be applied to describe the mechanical properties of tissues. An aggregate of cells develops tissue surface tension, resulting from the difference in adhesion between cells of the aggregate and their surroundings (Fig. 3; (3)).

### Cell-cell interfacial tension

Cell-cell interfacial tension (Joule per square meter,  $J/m^2$ ) is the tension that is developed between two cells, described by the energy per contact area. The cell-cell interfacial tension is increased by the cortical tension, which shrinks the contact area, and decreased by adhesion tension because of the binding of adhesion molecules, which increases the contact area (Fig. 2 B; (18,29)).

### Adhesion tension

Adhesion tension (Joule per square meter,  $J/m^2$ ) is the total energy per unit area released when two cells come into contact (Fig. 2 B). The total adhesion energy (Joule, J) is given by the integral of the adhesion tension on the interaction area. Sometimes, the adhesion energy is translated as the detachment force (Newton, N), which determines the total work (Newton meter, Nm) needed to separate two objects.

### Cellular traction forces

Cellular traction forces (Newton, N) are in-plane pulling forces applied by adherent cells on substrates. They are generated by actomyosin contraction transmitted through the cell-matrix adhesion complexes to the ECM.

## CELL-CELL CONTACT FORMATION: FROM MOLECULES TO CELLS AND TISSUES

In the following section, we summarize and discuss how cell-cell adhesion is described by integrating biological components with quantitative terms inspired by polymer physics. We start with descriptions of cell-cell adhesion based on molecular interactions at the contacting membranes and then move on to descriptions on the cellular and tissue/organismal scale.

### The role of molecular interactions over the contact

For describing cell-cell adhesion on the molecular scale, biomimetic systems such as phospholipid membranes and vesicles were initially used. Here, adhesion is described based on the formation of specific molecular bonds and the role that the plasma membrane and the glycocalyx play therein. The theoretical basis for such description of cell-cell adhesion was first established by Bell (30), arguing that, aside from weak electrical forces between two cell membranes, attractive forces, generated by the specific binding of integral membrane proteins, must be considered to explain cell-cell detachment forces. This was soon followed by the identification of cadherin adhesion receptors capable of mediating attractive forces between cells (31). On the experimental side, various biomimetic systems were established that allowed controlling the identity, density, and mobility of adhesion molecules on surfaces. Specifically, giant vesicles and planar membranes decorated with adhesion molecules (attractive forces) and polymer cushions (repellent forces—inspired by glycocalyx) were employed to mimic interactions between two cells (32). On the theoretical side, various frameworks were developed to explain different aspects of adhesion in those biomimetic settings. They showed that the distance of an adhering vesicle to the contacting membrane is determined by the minimum of the free adhesion energy (11,12). At high

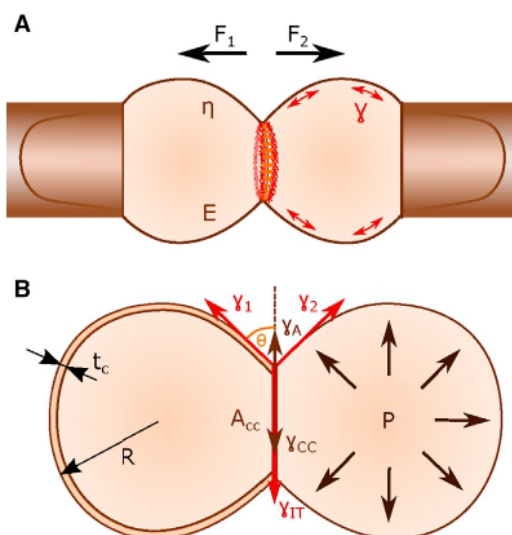


**FIGURE 2** (A) A schematic representation of dual pipette aspiration (DPA) is shown. Applied detachment forces,  $F_1 + F_2$ , on suspended cells with a given viscoelasticity (viscosity,  $\eta$ , and Young's modulus,  $E$ ) forming a contact, where E-cadherin and actin accumulate at the contact rim. (B) Radius,  $R$ , and the cortex thickness,  $t_c$ , define the cortical tensions,  $\gamma_1$  and  $\gamma_2$ , of the connected cells. For  $\gamma_1 = \gamma_2 = \gamma$ , cortical tensions at the contact-free area are counteracted by the interfacial tension,  $\gamma_{IT} = 2 \times \gamma \times \cos(\theta)$ , at the cell-cell adhesion area,  $A_{CC}$ . The interfacial tension,  $\gamma_{IT}$ , is determined by the difference in magnitude between the cortical tension of both cells at the cell-cell interface,  $2^* \gamma_{CC}$ , and the adhesion tension,  $\gamma_A$ , acting in antiparallel directions. The cortical tension is in balance with the internal cellular pressure,  $P$ .

receptor concentrations, contacts formed a homogenous tight adhesion zone, whereas at low receptor concentrations, contacts were composed of tight adhesion domains conferring strong adhesion separated by weak adhesion domains containing glycocalyx, corresponding to two minima of the free energy (33). Using a thermodynamic framework in which the adhesion energy depends on both the gain of enthalpy by the formation of bonds and the cost of entropy through the immobilization of receptors and suppression of membrane fluctuations, adhesion domains were predicted to preferentially localize to the rim of vesicle-bilayer contacts (34). This configuration is a result of bond dynamics, receptor crowding, and slowed-down diffusion upon adhesion molecule binding. These predictions were subsequently confirmed by experimental observations in a physiological context showing that cadherin adhesion molecules preferentially accumulate at the rim of cell-cell contacts (Fig. 2 A; (35,36)).

Biomimetic studies were also crucial for unraveling the role of cadherin clustering and mobility in cell-cell adhesion. Cadherins are known to form nanoclusters, which increase the cooperativity and stability of those molecules (37). Cadherin clustering depends on *cis* interactions of cadherins within the same cell and does not necessarily require cadherin *trans* binding given that cadherin ectodomains can form those clusters without engaging in *trans* interactions

over the contact (21). Changing the ability of cadherins to engage in *cis* clustering through membrane fluctuations was further found to influence their ability to form *trans* bonds, which are required for nucleation and growth of adhesion domains in model membranes (38). In a cellular context, intracellular interactions of cadherin nanoclusters with the cortical actomyosin network were shown to be critical for cadherin-mediated contact formation by decreasing the mobility of those clusters within the membrane (39). Yet, biomimetic studies predicted that some mobility of adhesion receptors is still required to form stronger contacts by allowing diffusion of those receptors into the contact zone and thus increasing their likelihood to participate in bond formation (33).

Finally, through biomimetic, single-molecule, and cell culture studies, the sensitivity of adhesion molecules to mechanical forces was shown to be a critical determinant of cell-cell adhesion strength. In contacts between bilayers and vesicles carrying mobile adhesion proteins, adhesion sites were found to enlarge and become more immobile in response to a pulling force at the contact as a result of the acquisition of new bonds at edges of already-dense sites or condensation of existing bonds (33). In addition to those general effects on adhesion site assembly, mechanical forces also affect the bonds between individual adhesion receptors. Typically, molecular interactions between adhesion receptors are studied by atomic force microscopy at the millisecond timescale, which is well below the timescale of molecular off-rates at which bond dissociation occurs even if no external force is applied (30). Atomic force microscopy measurements of cadherin bonds revealed that detachment forces between cadherins typically range from a few tens to hundreds of pN (40) and that the bond strength of cadherins depends on the type of cadherin and its specific off-rate. The analysis of detachment forces further showed that cadherin molecules preferably form homotypic bonds, with, for instance, homotypic E-cadherin bonds being stronger than homotypic N-cadherin bonds (41). Moreover, cadherin bonds also become more resistant to detachment with increased loading, a phenomenon explained by cadherin ectodomains forming X-dimers that function as catch bonds (42), increasing bond lifetime as a function of pulling force (43,44).

Collectively, biomimetic studies using model membranes and vesicles, together with single-molecule studies probing the characteristics of adhesion molecules, paved the way for understanding the molecular and physical processes by which cell-cell contacts are initiated and maintained. In particular, they provided insight into the role of several cell structures and processes, such as the glycocalyx and membrane fluctuations, for cell-cell contact formation, which is still difficult to rigorously address in a more physiological cell setting. By stepwise increasing the complexity of biomimetic assays—e.g., by encapsulating cytoskeletal components within vesicles to study the interaction between

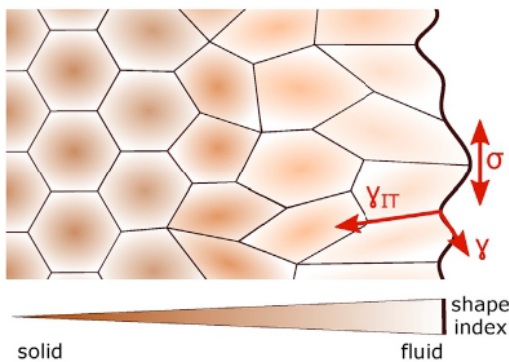


FIGURE 3 The tissue surface tension,  $\sigma$ , at the tissue edge results from the difference between the interfacial tension,  $\gamma_{IT}$ , at the cell-cell contact and the cortical tension,  $\gamma$ , at the contact-free surface. It minimizes the contact-free surface area by smoothing the tissue edge. Interfacial tension also contributes to determining the cell shape index, an indicator of tissue fluidity: cells within the cluster typically display more regular hexagonal shapes, are densely packed by surrounding neighbors, and thus behave more solid-like. Cells at the tissue edge, in contrast, are more elongated and mobile, and thus show a fluid-like behavior.

adhesion molecules and the cytoskeleton—those reconstituted systems might become even more powerful and provide a platform for systematically analyzing cell-cell adhesion independently from the specific features of entire cells, tissues, or organisms.

### The role of intercellular forces arising at the contact

In the following section, we discuss how experimental and theoretical studies of cell-cell adhesion forces on the cellular scale provided insight into the role of cell mechanics in cell-cell adhesion and contact formation. It is well established that most biological tissues are viscoelastic, behaving predominantly elastic at short timescales and viscous at long timescales (45). Consequently, cells have been modeled as solid elastic spheres or viscous liquid droplets depending on the specific cellular process studied. Assuming that the contacting cells behave as solid elastic spheres able to establish short-interaction-range adhesion, the Johnson-Kendall-Roberts (JKR) model used in polymer adhesion was applied to describe cell-cell contact detachment. The model permits the adhesion energy to be determined based on the pulling force needed to detach two spherical objects and their harmonic mean radii. For measuring detachment forces between contacting cells in the nN range, the dual pipette aspiration (DPA) technique is most commonly used (Fig. 2 A; (46)). Interestingly, the detachment force measured by DPA for nonspecific adhesion between culture cells displaying high elasticity could be well explained using the JKR model (47). However, for other cell types that display lower elasticity, only an extended version of the JKR model, in which cells are rep-

resented as thin shells with liquid cores that could be deformed as pulling forces were applied, was able to recapitulate experimental data (48,49).

The advantage of those coarse-grained theoretical models of cell detachment forces over the molecular-interaction-based theoretical models described in the previous chapter is the inclusion of the mechanical properties of cells. However, a caveat of taking detachment forces as a proxy for adhesion energy is the observation that cells can respond to mechanical forces by modulating their adhesion apparatus and thus adhesive properties. For instance, pulling on the contact zone increases E-cadherin and actin recruitment (Fig. 2 A; (50)), and applied forces can alter the mechanical properties of the cell cytoskeleton (51). Given that the detachment forces are thought to depend on mechanical properties of the actomyosin cortex of the adhering cells, such as its thickness, stiffness, and contractility (52); the equilibrium adhesion energy would be expected to change when detachment forces are applied.

The linkage of cadherins to the actomyosin cortex plays a central role for mechanosensation at cell-cell contacts (Fig. 1; (10)). Anchorage of cadherins to the actomyosin cortex is mediated by various molecules, including  $\beta$ -catenin,  $\alpha$ -catenin, and vinculin, and strengthens under force, a behavior characteristic of catch bonds (53). Specifically, whereas a single  $\beta$ -catenin/ $\alpha$ -catenin heterodimer forms a slip bond with F-actin, cooperativity of several heterodimers results in a catch-bond behavior (54). This is due to several  $\beta$ -catenin/ $\alpha$ -catenin heterodimers mediating longer-lasting contacts with F-actin, thereby allowing the tension-mediated unfolding of  $\alpha$ -catenin (55), which in turn reveals cryptic binding sites to vinculin, a molecule directly linking the cadherin/catenin complex to the actin cytoskeleton (56). This internal amplification mechanism, together with the observation that vinculin itself forms a catch bond with F-actin (57), provides an explanation for the mechanosensitivity of cadherin-mediated cell-cell contact sites.

Measured cell-cell detachment forces not only might change because of mechanosensitive feedback but also are dependent on the main direction of forces applied to the contact (normal or shear forces). Recent work suggests the direction of force to have different effects on cell-cell contacts: during *Drosophila* embryonic axis elongation, normal forces on cell-cell junctions, exerted by a medial actomyosin network within the apex of epithelial cells, increase E-cadherin levels and thus cell-cell adhesion, whereas shear forces through a junctional actomyosin network decrease E-cadherin levels (58). Such differential effects of normal versus shear forces might explain why detachment forces can vary depending on the specific measurement methods used, such as centrifugation, shear flow, or DPA.

In addition to cell-cell detachment force measurements, intercellular forces were determined by measuring traction forces of adhering cells through traction force microscopy

(59) and micropillar arrays (60), both of which allow the extraction of intercellular forces on the basis of the two-dimensional force balance (61,62). Those intercellular forces were found to positively correlate with cadherin levels at cell-cell contacts (63). Likewise, for endothelial cell doublets on a defined spreading area, intercellular forces linearly increased with cell-cell contact size (62). In contrast, epithelial cells grown on a free spreading area showed no apparent scaling between intercellular forces and cell-cell contact size (61), suggesting that the relation of contact size and intercellular forces is highly context dependent.

The analysis of traction forces might also give important insights into the interplay between cell-cell and cell-matrix adhesions. In migrating cell clusters, traction forces dominate at the edge (64,65) and intercellular stresses increase toward the center of the cluster as a result of traction forces of the outwardly moving cells being transmitted as intercellular forces to the trailing cells behind (66,67). Recently, the interplay between cell-cell-adhesion-mediated intercellular and cell-ECM-adhesion-mediated intracellular tension was found to be responsible for cell monolayers displaying either contractile or extensile behavior (68), suggesting that the nature of active forces in tissues depends on the cross talk between cell-cell and cell-ECM adhesion. In line with this, knockout of E-cadherin in epithelial cells caused a crossover from extensile to contractile tissue behavior along with relocalization of vinculin from cell-cell to cell-ECM contacts and an increase in cell-ECM adhesion (68). Thus, the strength of cell-cell adhesion—and, with that, the tissue behavior—strongly depends on the interactions with the extracellular environment and the adaptation of intracellular contractility.

Collectively, the analysis of cell-cell detachment forces was instrumental in identifying the adhesion energy and thus cell-intrinsic adhesion of adherent cells when separated. However, to understand the discrepancies in the adhesive behavior of different cell types, more parametric tests and models need to be developed to incorporate effects of cell viscoelasticity, contractility, and adhesion receptor mobility. In particular, changes in the distribution of adhesion molecules at heterogeneous cell-cell contact sites and the effect of cytoskeletal rearrangements that occur upon force application need to be quantified and incorporated in future computational models. Finally, the observation that intracellular bonds, linking the adhesion complex to the actomyosin cytoskeleton, break first when cell-cell contacts are being separated suggests that deadhesion and adhesion energies might be different (18,29). Current models of cell-cell detachment, however, do not distinguish between the two. In line with this, recent observations showed that experimentally measured detachment forces are higher than theoretically predicted on the basis of the adhesion energy, pointing at the possibility that cell-cell detachment forces might depend more on dissipative processes associ-

ated with the detachment process rather than the adhesion energy (69). Emerging tools for determining cell-cell adhesion forces, such as Förster resonance energy transfer sensors to measure endogenous molecular forces (70,71), DNA-based fluorescent force probes (72), oil droplets decorated with cadherin receptor ligands (73), and pressure probes that deform with local stresses (74), might lead to a deeper understanding of intercellular adhesion.

### The role of interfacial tension in cell aggregates

In analogy to liquids minimizing their surface area through surface tension as a result of the cohesion of their constituent molecules, the surface tension of cells and tissues is used as a proxy for cell-cell adhesion strength. In the following section, we discuss how cell-cell adhesion can be interpreted by the extent of surface tension, how surface tension is determined by tensions at different cellular interfaces, and how those surface/interfacial tensions were used in various models explaining cell/tissue shape changes and cell sorting. Originally, tissue surface tension was assumed to be determined by the adhesion energy, for instance, emerging from cadherin binding over the contact, a view supported with experiments in cell aggregates, which showed cadherin expression levels to linearly correlate with tissue surface tension (15,75). Subsequent work showed that, in addition or as an alternative to adhesion energy, tissue surface tension critically depends on the function of cortical actomyosin tension (17,59) and its modulation at cell-cell contacts (Fig. 3; (36,76)). Cortical tension is modulated not only by the binding of cadherin adhesion molecules over the contact (18) but also by unbound cadherins not engaged in *trans* binding, suggesting that a dynamic interplay between cadherins and the cortical actomyosin network determines the balance of interfacial tensions and thus surface tension of tissues (69).

At the cell-cell contact interface, interfacial tension is determined by both adhesion tension (a negative tension as a result of adhesion molecules binding over the contact), which expands the contact area, and cortical tension, which reduces it (Fig. 2 B). At contact-free interfaces, in contrast, surface tension is predominantly determined by cortical tension. Notably, cortical tension can differ at contact-free and adhering interfaces. Studies on zebrafish germ layer progenitor cells suggest that tissue surface tension arises from the difference between the two (77). This difference in tensions between the cell-cell versus contact-free interfaces is due to adhesion receptor signaling changing the actomyosin cortex, and thus cortical tension, at the cell-cell interface rather than adhesion tension lowering cell-cell interfacial tension (36). In line with adhesion receptors lowering cortical tension at the cell-cell contact are observations showing that E-cadherin-mutant mouse embryos fail in reducing myosin II from cell-cell contacts (78). Likewise, downregulation of C-cadherin in *Xenopus* embryonic aggregates prevents

proper reduction of actin from contacts (79). This suggests that adhesion receptor signaling reduces cortical tension at contacts by both diminishing myosin II activity and/or localization and modifying cortical actin density and organization. The molecular composition of the signaling cascade downstream of cadherin adhesion receptors modulating the actomyosin cortex is not yet entirely clear. The actin-severing protein cofilin was found to colocalize with E-cadherin at punctate adherens junctions (80), whereas other studies reported that interaction of the cadherin adhesion complex through  $\alpha$ -E-catenin with actin inhibits cofilin binding in vitro (81). Similarly, the branched actin nucleator Arp2/3 was proposed to be not only suppressed at nascent contacts through  $\alpha$ -E-catenin (81) but also recruited to cortical actin underlying cell-cell contacts (80,82). Moreover, the linear actin nucleator formin was shown to be recruited to adherens junctions by  $\alpha$ -E-catenin (83). These data suggest that cadherin adhesion receptors affect the cortical actin cytoskeleton by dynamically recruiting different types of actin nucleators, which could potentially control cortical tension by regulating actin filament length (84), and network density (85). Changes in cortical actin at cell-cell contacts might feed back on cortical myosin II recruitment given that, for instance, in mouse oocytes, cortical Arp2/3 enrichment leads not only to cortex thickening but also to myosin II depletion and, consequently, reduction in cortical tension (86).

The Rho family GTPases Rac, Cdc42, and RhoA play an important role in remodeling the actomyosin cortex at cell-cell adhesion sites. Rac, for instance, is transiently activated by cadherins at the edges of an expanding contact, leading to local activation of the Arp2/3 complex and thus branched actin polymerization (87,88). Activation of both Rac and Cdc42 were observed during the formation of cell aggregates, which contributed to the strengthening of cell-cell contacts (13). Cdc42 was also found to be involved in the initiation of cell-cell adhesion (89), possibly by promoting the formation of E-cadherin-containing filopodia, facilitating contact formation (90). RhoA is recruited to adherens junctions, where it activates cortical actomyosin contractility and recruits formins, promoting linear actin polymerization (91). At nascent contacts, in contrast, RhoA activity is inhibited by Rac, decreasing cortical actomyosin contraction and thus tension (88,92). Yet the exact spatiotemporal regulation and function of Rho family GTPases as signaling effectors of cadherin adhesion receptors in contact formation and maintenance remain to be fully explored.

To explain the effects of interfacial tension regulation by different effector mechanisms, several microscopic mechanical models based on energy minimization and interfacial tension balance were employed describing cell-cell contact dynamics both in vitro and in vivo. For instance, the cellular Potts model, in which each cell is defined as connected pixels, was developed to test the contribution of different levels of adhesion receptor expression in cell-sorting exper-

iments and the role of cell motility therein (93). Later, cortical tension was added to this model to capture the role of differential cell cortical tension in cell sorting (94,95). To more realistically capture the dynamics of confluent tissues on a cellular scale, vertex models, in which cells are defined as polygons whose vertices can move with mechanical forces, were developed. Vertex models were successfully applied for describing various morphogenetic processes, such as boundary formation, epithelial buckling, and wound healing, because of their ability to capture specific cellular processes, such as cell shape changes, divisions, extrusions, and rearrangements, as well as viscoelastic cell properties (96). As a hybrid of vertex models and self-propelled particle models, Voronoi models were recently developed in which not vertices but cell centers are tracked (97). These models were able to incorporate single-cell motility, missing from the vertex models, and predict more diverse shape distributions (98) and cellular rearrangements (99). More recently, vertex and Voronoi models were also used to describe abrupt and drastic changes in tissue material properties that might resemble transitions in states of matter, commonly referred to as phase transitions (100–102). Interestingly, phase transitions in confluent tissues appear to correlate to a “cell shape index,” a quantity that describes the cell geometry (Fig. 3; (100)). The cell geometry is regulated by the competition between cell-cell adhesion energy and cortical tension. An increase in cell-cell adhesion and a decrease in cortical tension lead to a change in cell shape and in turn to a transition of the whole tissue from solid-like to fluid-like behavior in a process called “unjamming transition”. The unjamming transition is characterized by increased irregularity in cell shapes and reduced number of contacts with neighboring cells, allowing cellular rearrangements (100,102). Recent studies also suggest the unjamming transition to be dominated by cellular traction forces (103). At the level of cell-cell contacts, force-mediated  $\alpha$ -catenin clustering was found to trigger a fluid-to-solid phase transition, suggesting that changes in the composition of cadherin adhesion complexes can locally modulate rheological properties of the contact (54). Tissue-scale phase transitions were observed not only in cultures but also within the physiologically relevant context of the developing embryo (104–107) and in disease-related processes such as wound healing (108) and tumor metastasis (109). Extension of existing vertex models (110) and application of new theoretical frameworks, such as rigidity percolation theory (111), were recently shown to accurately describe tissue phase transitions in nonconfluent embryonic tissues to understand these phenomena mechanistically.

So far, research on interfacial tensions of cells and tissues primarily focused on the role of adhesion tension and cortical tension in regulating interfacial tension. However, other factors might also be involved. Membrane tension, for instance, also contributes to surface tension, although

its specific contribution is difficult to determine because the plasma membrane is mechanically coupled to the underlying actomyosin cortex through proteins mediating membrane-to-cortex attachment and thus is difficult to disentangle from cortical tension. Although membrane tension was shown to be typically much smaller than cortical tension, there is increasing evidence in different cell types, such as keratocytes, that suggests membrane tension still significantly contributes to the overall surface tension of those cells (112). In addition to membrane tension, high adhesion tension between dynamically cross-linking components of interacting glycocalices was recently proposed to contribute to tissue surface tension in systems such as chick embryos and various mammalian cell lines, in which surface tension clearly exceeds the theoretically expected values based on cadherin-mediated adhesion and cortical tension alone (113). Finally, external factors, such as the presence of ECM and the osmolarity of the interstitial fluid, were shown to affect interfacial tensions of cells and tissues. ECM interactions can contribute to cell sorting by regulating cell-ECM and cell-cell interfacial tensions in monolayers and surface tension in cell aggregates (68,114), whereas osmolarity was recently demonstrated as an important regulator of tissue surface tension by regulating membrane tension and cortical tension via changes in the internal cellular pressure and volume (115).

Beyond cadherins, comparably little is known about upstream regulators of cell/tissue interfacial tensions. Living tissues have a remarkably diverse cell surface proteome, suggesting that several other of those proteins might be involved in controlling interfacial tensions. For instance, the differential expression of proteins mediating cell repulsion, such as Eph-ephrin receptor-ligand pairs, or signaling receptors, such as leucine-rich repeat family receptors (including Toll-like receptors), were shown to mediate differences in cortical tension, which is important for boundary formation in developing vertebrate and invertebrate embryos (116,117). The potential role of those and many other cell surface proteins in regulating interfacial tensions in different model systems remains to be investigated.

## CONCLUSIONS AND PERSPECTIVES

Cell-cell adhesion has been studied for many decades by both biologists and physicists. In those studies, different views of adhesion emerged, which can be roughly categorized as 1) the affinity of molecular bonds, 2) a cohesive force supported by a force-sensing and force-transducing machinery, and 3) the modulation of interfacial tensions through adhesion receptor signaling. These different views are nonexclusive because they simply emphasize different functions of the adhesion apparatus that together define adhesion. In evolution, these different functions seem to have coevolved because, for instance, the core adhesion complex, consisting of cadherins and catenins that bind to

F-actin, emerged together with the appearance of metazoans (118). Moreover, cadherins predating this complex already carry intracellular domains that can possibly interact with actin-binding proteins (119), suggesting that cadherin extracellular binding and intracellular signaling could have been directly adapted with the appearance of multicellularity.

Initially, the degree of cell-cell adhesion was thought to correspond to the adhesion strength of cell-cell contacts at steady state. However, observations of cell-cell contacts in their physiological context show that cell-cell adhesion is a rather dynamic process, with the duration and size of cell-cell contacts constantly changing. Contact size and duration represent critical parameters modulating not only the extent by which cells rearrange in cohesive tissues (120) but also the activity of various signaling pathways involved in cell fate specification in embryos (121,122). Recently, cell-cell contact dynamics were shown to be important parameters determining tissue material properties and the transitions between different material phases (45). How those dynamic cell-cell contact properties are regulated on a molecular and cellular scale have only begun to be understood. For example, the size of cell-cell contacts was originally thought to increase with the ratio of cortical tension at the contact-free to the cell-cell interfaces (36). Surprisingly, most recently, this view was challenged by showing that the relationship between cell-cell contact size and cortical tension of the contact-free cortex is nonmonotonic, reversing at high levels of cortical tension because of tension-mediated E-cadherin stabilization, which limits contact expansion (123). Further work is needed to elucidate the relationship between various features of cell-cell contacts to determine their multifaceted functions in multicellular settings.

Cell-cell adhesion is regulated through both intracellular and extracellular cues, possibly involving various feedback loops between them. For instance, myosin II activity was shown not only to increase cytoskeletal anchoring of cadherins (70) but also to slow down actin turnover, which affects E-cadherin mobility at the cell-cell contacts and thus contact expansion (35,123). In turn, the stability of cadherin clusters was shown to regulate actin turnover, suggesting a bidirectional coupling between actin and cadherin dynamics (80). Many questions remain as to the regulation and function of cell-cell adhesion. What distinguishes the adhesion apparatus from the cell cytoskeleton? Does cell-cell adhesion simply function as a molecular linker connecting the cytoskeleton of neighboring cells? That said, could the adhesion complex be regarded as a specialized cytoskeletal component needed for the assembly, dynamic regulation, and coordination of supracellular cytoskeletal networks? Would such supracellular cytoskeletal networks just represent a permutation of intracellular cytoskeletal networks, or would the addition of cell-cell adhesion sites provide emergent features that cannot be found in unconnected cytoskeletal networks? To answer those questions, synthetic approaches

for engineering cell-cell contacts might be helpful because they would allow the systematic study of different properties of cell-cell contacts in the presence and absence of cytoskeletal anchoring. Likewise, theoretical models need to be developed to connect molecular-scale interactions and dynamics of adhesion and cytoskeletal molecules to tissue-scale functions of cell-cell adhesion, such as tissue morphogenesis and material properties (124).

Cell-cell adhesion is integral to the evolution of multicellularity. Studying cell-cell adhesion, therefore, provides the basis for understanding how multicellularity has emerged. Although in the past, cell-cell adhesion has been predominantly studied on the basis of the extracellular bindings of adhesion receptors and their affinity and strength, it becomes increasingly clear that the coupling of those receptors to the cytoskeleton is equally important. This highlights two essential and tightly intertwined functions of adhesion: providing selectivity in cellular interactions and regulating the mechanical and biochemical cross talk between neighboring cells. This naturally involves both biochemical and mechanical signals; thus, understanding their interaction through mechanosensation will be indispensable for elucidating the basis of cell-cell adhesion.

## ACKNOWLEDGMENTS

T.S. acknowledges funding by the research program “The Active Matter Physics of Collective Metastasis,” which is financed by the Dutch Research Council (NWO).

## REFERENCES

- Miller, J. G. 1973. Living systems. II. The organism. *Quad. Criminol. Clin.* 48:92–276.
- Turlier, H., and J.-L. Maître. 2015. Mechanics of tissue compaction. *Semin. Cell Dev. Biol.* 47–48:110–117.
- Lecuit, T., and P.-F. Lenne. 2007. Cell surface mechanics and the control of cell shape, tissue patterns and morphogenesis. *Nat. Rev. Mol. Cell Biol.* 8:633–644.
- Collins, C., and W. J. Nelson. 2015. Running with neighbors: coordinating cell migration and cell-cell adhesion. *Curr. Opin. Cell Biol.* 36:62–70.
- Berx, G., and F. van Roy. 2009. Involvement of members of the cadherin superfamily in cancer. *Cold Spring Harb. Perspect. Biol.* 1:a003129.
- El-Amraoui, A., and C. Petit. 2010. Cadherins as targets for genetic diseases. *Cold Spring Harb. Perspect. Biol.* 2:a003095.
- Janiszewska, M., M. C. Primi, and T. Izard. 2020. Cell adhesion in cancer: beyond the migration of single cells. *J. Biol. Chem.* 295:2495–2505.
- Yamada, S., and W. J. Nelson. 2007. Synapses: sites of cell recognition, adhesion, and functional specification. *Annu. Rev. Biochem.* 76:267–294.
- Halbleib, J. M., and W. J. Nelson. 2006. Cadherins in development: cell adhesion, sorting, and tissue morphogenesis. *Genes Dev.* 20:3199–3214.
- Huveneers, S., and J. de Rooij. 2013. Mechanosensitive systems at the cadherin-F-actin interface. *J. Cell Sci.* 126:403–413.
- Bell, G. I., M. Dembo, and P. Bongrand. 1984. Cell adhesion. Competition between nonspecific repulsion and specific bonding. *Biophys. J.* 45:1051–1064.
- Bruinsma, R., A. Behrisch, and E. Sackmann. 2000. Adhesive switching of membranes: experiment and theory. *Phys. Rev. E Stat. Phys. Plasmas Fluids Relat. Interdiscip. Topics.* 61:4253–4267.
- Chu, Y.-S., W. A. Thomas, ..., S. Dufour. 2004. Force measurements in E-cadherin-mediated cell doublets reveal rapid adhesion strengthened by actin cytoskeleton remodeling through Rac and Cdc42. *J. Cell Biol.* 167:1183–1194.
- Charras, G., and A. S. Yap. 2018. Tensile forces and mechanotransduction at cell-cell junctions. *Curr. Biol.* 28:R445–R457.
- Steinberg, M. S. 1963. Reconstruction of tissues by dissociated cells. Some morphogenetic tissue movements and the sorting out of embryonic cells may have a common explanation. *Science.* 141:401–408.
- Harris, A. K. 1976. Is cell sorting caused by differences in the work of intercellular adhesion? A critique of the Steinberg hypothesis. *J. Theor. Biol.* 61:267–285.
- Brodland, G. W. 2002. The differential interfacial tension hypothesis (DITH): a comprehensive theory for the self-rearrangement of embryonic cells and tissues. *J. Biomech. Eng.* 124:188–197.
- Winklbauer, R. 2015. Cell adhesion strength from cortical tension - an integration of concepts. *J. Cell Sci.* 128:3687–3693.
- Zaidel-Bar, R. 2013. Cadherin adhesome at a glance. *J. Cell Sci.* 126:373–378.
- Brasch, J., O. J. Harrison, ..., L. Shapiro. 2012. Thinking outside the cell: how cadherins drive adhesion. *Trends Cell Biol.* 22:299–310.
- Thompson, C. J., V. H. Vu, ..., D. K. Schwartz. 2019. Cadherin extracellular domain clustering in the absence of *trans*-interactions. *J. Phys. Chem. Lett.* 10:4528–4534.
- Chugh, P., and E. K. Paluch. 2018. The actin cortex at a glance. *J. Cell Sci.* 131:jcs186254.
- Simons, K., and E. Ikonen. 1997. Functional rafts in cell membranes. *Nature.* 387:569–572.
- Truong-Quang, B.-A., and P.-F. Lenne. 2014. Membrane microdomains: from seeing to understanding. *Front Plant Sci.* 5:18.
- Clariss, B. J., and J. R. Fraser. 1968. On the pericellular zone of some mammalian cells in vitro. *Exp. Cell Res.* 49:181–193.
- Frantz, C., K. M. Stewart, and V. M. Weaver. 2010. The extracellular matrix at a glance. *J. Cell Sci.* 123:4195–4200.
- Salbreux, G., G. Charras, and E. Paluch. 2012. Actin cortex mechanics and cellular morphogenesis. *Trends Cell Biol.* 22:536–545.
- Helfrich, W. 1973. Elastic properties of lipid bilayers: theory and possible experiments. *Z. Naturforsch. C.* 28:693–703.
- Maître, J.-L., and C.-P. Heisenberg. 2013. Three functions of cadherins in cell adhesion. *Curr. Biol.* 23:R626–R633.
- Bell, G. I. 1978. Models for the specific adhesion of cells to cells. *Science.* 200:618–627.
- Takeichi, M., T. Atsumi, ..., T. S. Okada. 1981. Selective adhesion of embryonal carcinoma cells and differentiated cells by Ca<sup>2+</sup>-dependent sites. *Dev. Biol.* 87:340–350.
- Sackmann, E. 1996. Supported membranes: scientific and practical applications. *Science.* 271:43–48.
- Smith, A.-S., and E. Sackmann. 2009. Progress in mimetic studies of cell adhesion and the mechanosensing. *ChemPhysChem.* 10:66–78.
- Schmidt, D., T. Bühr, ..., A.-S. Smith. 2015. Crowding of receptors induces ring-like adhesions in model membranes. *Biochim. Biophys. Acta.* 1853:2984–2991.
- Engl, W., B. Arasi, ..., V. Viasnoff. 2014. Actin dynamics modulate mechanosensitive immobilization of E-cadherin at adherens junctions. *Nat. Cell Biol.* 16:587–594.
- Maître, J.-L., H. Berthoumieux, ..., C.-P. Heisenberg. 2012. Adhesion functions in cell sorting by mechanically coupling the cortices of adhering cells. *Science.* 338:253–256.

37. Yap, A. S., G. A. Gomez, and R. G. Parton. 2015. Adherens junctions revisualized: organizing cadherins as nanoassemblies. *Dev. Cell.* 35:12–20.
38. Fenz, S. F., T. Bühr, ..., A.-S. Smith. 2017. Membrane fluctuations mediate lateral interaction between cadherin bonds. *Nat. Phys.* 13:906–913.
39. Chandran, R., G. Kale, ..., S. Mayor. 2021. Distinct actin-dependent nanoscale assemblies underlie the dynamic and hierarchical organization of E-cadherin. *Curr. Biol* Published online February 12, 2021. <https://doi.org/10.1016/j.cub.2021.01.059>.
40. Baumgartner, W., P. Hinterdorfer, ..., D. Drenckhahn. 2000. Cadherin interaction probed by atomic force microscopy. *Proc. Natl. Acad. Sci. USA.* 97:4005–4010.
41. Panorchan, P., M. S. Thompson, ..., D. Wirtz. 2006. Single-molecule analysis of cadherin-mediated cell-cell adhesion. *J. Cell Sci.* 119:66–74.
42. Dembo, M., D. C. Torney, ..., D. Hammer. 1988. The reaction-limited kinetics of membrane-to-surface adhesion and detachment. *Proc. R. Soc. Lond. B Biol. Sci.* 234:55–83.
43. Pittet, P., K. Lee, ..., B. Hinz. 2008. Fibrogenic fibroblasts increase intercellular adhesion strength by reinforcing individual OB-cadherin bonds. *J. Cell Sci.* 121:877–886.
44. Rakshit, S., Y. Zhang, ..., S. Sivasankar. 2012. Ideal, catch, and slip bonds in cadherin adhesion. *Proc. Natl. Acad. Sci. USA.* 109:18815–18820.
45. Petridou, N. I., and C.-P. Heisenberg. 2019. Tissue rheology in embryonic organization. *EMBO J.* 38:e102497.
46. Sung, K. L., L. A. Sung, ..., S. Chien. 1986. Determination of junction avidity of cytolytic T cell and target cell. *Science.* 234:1405–1408.
47. Chu, Y.-S., S. Dufour, ..., F. Pincet. 2005. Johnson-Kendall-Roberts theory applied to living cells. *Phys. Rev. Lett.* 94:028102.
48. Pierrat, S., F. Brochard-Wyart, and P. Nassoy. 2004. Enforced detachment of red blood cells adhering to surfaces: statics and dynamics. *Biophys. J.* 87:2855–2869.
49. Brochard-Wyart, F., and P.-G. de Gennes. 2003. Unbinding of adhesive vesicles. *C. R. Phys.* 4:281–287.
50. Gao, X., B. R. Acharya, ..., V. Viasnoff. 2018. Probing compression versus stretch activated recruitment of cortical actin and apical junction proteins using mechanical stimulations of suspended doublets. *APL Bioeng.* 2:026111.
51. Schwarz, U. S., and S. A. Safran. 2013. Physics of adherent cells. *Rev. Mod. Phys.* 85:1327–1381.
52. Smeets, B., M. Cuvelier, ..., H. Ramon. 2019. The effect of cortical elasticity and active tension on cell adhesion mechanics. *Biophys. J.* 116:930–937.
53. Buckley, C. D., J. Tan, ..., A. R. Dunn. 2014. Cell adhesion. The minimal cadherin-catenin complex binds to actin filaments under force. *Science.* 346:1254211.
54. Arbore, C., M. Sergides, ..., M. Capitanio. 2020.  $\alpha$ -catenin switches between a slip and a cooperative catch bond with F-actin to regulate cell junction fluidity. *bioRxiv* <https://doi.org/10.1101/2020.04.15.035527>.
55. Yonemura, S., Y. Wada, ..., M. Shibata. 2010.  $\alpha$ -Catenin as a tension transducer that induces adherens junction development. *Nat. Cell Biol.* 12:533–542.
56. Huveneers, S., J. Oldenburg, ..., J. de Rooij. 2012. Vinculin associates with endothelial VE-cadherin junctions to control force-dependent remodeling. *J. Cell Biol.* 196:641–652.
57. Huang, D. L., N. A. Bax, ..., A. R. Dunn. 2017. Vinculin forms a directionally asymmetric catch bond with F-actin. *Science.* 357:703–706.
58. Kale, G. R., X. Yang, ..., T. Lecuit. 2018. Distinct contributions of tensile and shear stress on E-cadherin levels during morphogenesis. *Nat. Commun.* 9:5021.
59. Harris, A. K., D. Stopak, and P. Wild. 1981. Fibroblast traction as a mechanism for collagen morphogenesis. *Nature.* 290:249–251.
60. Tan, J. L., J. Tien, ..., C. S. Chen. 2003. Cells lying on a bed of micro-needles: an approach to isolate mechanical force. *Proc. Natl. Acad. Sci. USA.* 100:1484–1489.
61. Maruthamuthu, V., B. Sabass, ..., M. L. Gardel. 2011. Cell-ECM traction force modulates endogenous tension at cell-cell contacts. *Proc. Natl. Acad. Sci. USA.* 108:4708–4713.
62. Liu, Z., J. L. Tan, ..., C. S. Chen. 2010. Mechanical tugging force regulates the size of cell-cell junctions. *Proc. Natl. Acad. Sci. USA.* 107:9944–9949.
63. Ng, M. R., A. Besser, ..., G. Danuser. 2014. Mapping the dynamics of force transduction at cell-cell junctions of epithelial clusters. *eLife.* 3:e03282.
64. du Roure, O., A. Saez, ..., B. Ladoux. 2005. Force mapping in epithelial cell migration. *Proc. Natl. Acad. Sci. USA.* 102:2390–2395.
65. Mertz, A. F., Y. Che, ..., V. Horsley. 2013. Cadherin-based intercellular adhesions organize epithelial cell-matrix traction forces. *Proc. Natl. Acad. Sci. USA.* 110:842–847.
66. Trepatt, X., M. R. Wasserman, ..., J. J. Fredberg. 2009. Physical forces during collective cell migration. *Nat. Phys.* 5:426–430.
67. Tambe, D. T., C. C. Hardin, ..., X. Trepatt. 2011. Collective cell guidance by cooperative intercellular forces. *Nat. Mater.* 10:469–475.
68. Balasubramaniam, L., A. Doostmohammadi, ..., B. Ladoux. 2021. Investigating the nature of active forces in tissues reveals how contractile cells can form extensile monolayers. *Nat. Mater* Published online February 18, 2021. <https://doi.org/10.1038/s41563-021-00919-2>.
69. Aladin, D. M. K., Y. S. Chu, ..., J. P. Thiery. 2020. Extracellular domains of E-cadherin determine key mechanical phenotypes of an epithelium through cell- and non-cell-autonomous outside-in signaling. *bioRxiv* <https://doi.org/10.1101/2020.03.17.996181>.
70. Borghi, N., M. Sorokina, ..., A. R. Dunn. 2012. E-cadherin is under constitutive actomyosin-generated tension that is increased at cell-cell contacts upon externally applied stretch. *Proc. Natl. Acad. Sci. USA.* 109:12568–12573.
71. Conway, D. E., M. T. Breckenridge, ..., M. A. Schwartz. 2013. Fluid shear stress on endothelial cells modulates mechanical tension across VE-cadherin and PECAM-1. *Curr. Biol.* 23:1024–1030.
72. Zhao, B., N. Li, ..., M. You. 2020. Quantifying tensile forces at cell-cell junctions with a DNA-based fluorescent probe. *Chem. Sci. (Camb.)* 11:8558–8566.
73. Campàs, O., T. Mammoto, ..., D. E. Ingber. 2014. Quantifying cell-generated mechanical forces within living embryonic tissues. *Nat. Methods.* 11:183–189.
74. Chan, C. J., and T. Hiiragi. 2020. Integration of luminal pressure and signalling in tissue self-organization. *Development.* 147:dev181297.
75. Foty, R. A., and M. S. Steinberg. 2005. The differential adhesion hypothesis: a direct evaluation. *Dev. Biol.* 278:255–263.
76. Youssef, J., A. K. Nurse, ..., J. R. Morgan. 2011. Quantification of the forces driving self-assembly of three-dimensional microtissues. *Proc. Natl. Acad. Sci. USA.* 108:6993–6998.
77. Manning, M. L., R. A. Foty, ..., E.-M. Schoetz. 2010. Coaction of intercellular adhesion and cortical tension specifies tissue surface tension. *Proc. Natl. Acad. Sci. USA.* 107:12517–12522.
78. Maître, J.-L., R. Niwayama, ..., T. Hiiragi. 2015. Pulsatile cell-autonomous contractility drives compaction in the mouse embryo. *Nat. Cell Biol.* 17:849–855.
79. David, R., O. Luu, ..., R. Winklbauer. 2014. Tissue cohesion and the mechanics of cell rearrangement. *Development.* 141:3672–3682.
80. Indra, I., R. B. Troyanovsky, ..., S. M. Troyanovsky. 2020. Sensing actin dynamics through adherens junctions. *Cell Rep.* 30:2820–2833.e3.
81. Hansen, S. D., A. V. Kwiatkowski, ..., W. J. Nelson. 2013.  $\alpha$ E-catenin actin-binding domain alters actin filament conformation and regulates

- binding of nucleation and disassembly factors. *Mol. Biol. Cell.* 24:3710–3720.
82. Kovacs, E. M., M. Goodwin, ..., A. S. Yap. 2002. Cadherin-directed actin assembly: E-cadherin physically associates with the Arp2/3 complex to direct actin assembly in nascent adhesive contacts. *Curr. Biol.* 12:379–382.
  83. Kobiela, A., H. A. Pasolli, and E. Fuchs. 2004. Mammalian formin-1 participates in adherens junctions and polymerization of linear actin cables. *Nat. Cell Biol.* 6:21–30.
  84. Chugh, P., A. G. Clark, ..., E. K. Paluch. 2017. Actin cortex architecture regulates cell surface tension. *Nat. Cell Biol.* 19:689–697.
  85. Xia, S., Y. B. Lim, ..., P. Kanchanawong. 2019. Nanoscale architecture of the cortical actin cytoskeleton in embryonic stem cells. *Cell Rep.* 28:1251–1267.e7.
  86. Chaigne, A., C. Campillo, ..., M. E. Terret. 2015. A narrow window of cortical tension guides asymmetric spindle positioning in the mouse oocyte. *Nat. Commun.* 6:6027.
  87. Kitt, K. N., and W. J. Nelson. 2011. Rapid suppression of activated Rac1 by cadherins and nectins during de novo cell-cell adhesion. *PLoS One.* 6:e17841.
  88. Yamada, S., and W. J. Nelson. 2007. Localized zones of Rho and Rac activities drive initiation and expansion of epithelial cell-cell adhesion. *J. Cell Biol.* 178:517–527.
  89. Collins, C., A. K. Denisin, ..., W. J. Nelson. 2017. Changes in E-cadherin rigidity sensing regulate cell adhesion. *Proc. Natl. Acad. Sci. USA.* 114:E5835–E5844.
  90. Biswas, K. H., K. L. Hartman, ..., J. T. Groves. 2015. E-cadherin junction formation involves an active kinetic nucleation process. *Proc. Natl. Acad. Sci. USA.* 112:10932–10937.
  91. Acharya, B. R., S. K. Wu, ..., A. S. Yap. 2017. Mammalian diaphanous 1 mediates a pathway for E-cadherin to stabilize epithelial barriers through junctional contractility. *Cell Rep.* 18:2854–2867.
  92. Wildenberg, G. A., M. R. Dohn, ..., A. B. Reynolds. 2006. p120-catenin and p190RhoGAP regulate cell-cell adhesion by coordinating antagonism between Rac and Rho. *Cell.* 127:1027–1039.
  93. Glazier, J. A., and F. Graner. 1993. Simulation of the differential adhesion driven rearrangement of biological cells. *Phys. Rev. E Stat. Phys. Plasmas Fluids Relat. Interdiscip. Topics.* 47:2128–2154.
  94. Krieg, M., Y. Arboleda-Estudillo, ..., C.-P. Heisenberg. 2008. Tensile forces govern germ-layer organization in zebrafish. *Nat. Cell Biol.* 10:429–436.
  95. Glazier, J. A., A. Balter, and N. J. Poplawski. 2007. Magnetization to morphogenesis: a brief history of the Glazier-Graner-Hogeweg model. In *Single-Cell-Based Models in Biology and Medicine*. A. R. A. Anderson, M. A. J. Chaplain, and K. A. Rejniak, eds. Birkhäuser, pp. 79–106.
  96. Alt, S., P. Ganguly, and G. Salbreux. 2017. Vertex models: from cell mechanics to tissue morphogenesis. *Philos. Trans. R. Soc. Lond. B Biol. Sci.* 372:20150520.
  97. Bi, D., X. Yang, ..., M. L. Manning. 2016. Motility-driven glass and jamming transitions in biological tissues. *Phys. Rev. X.* 6:021011.
  98. Sánchez-Gutiérrez, D., M. Tozluoglu, ..., L. M. Escudero. 2016. Fundamental physical cellular constraints drive self-organization of tissues. *EMBO J.* 35:77–88.
  99. Barton, D. L., S. Henkes, ..., R. Sknepnek. 2017. Active vertex model for cell-resolution description of epithelial tissue mechanics. *PLoS Comput. Biol.* 13:e1005569.
  100. Bi, D., J. H. Lopez, ..., M. L. Manning. 2015. A density-independent rigidity transition in biological tissues. *Nat. Phys.* 11:1074–1079.
  101. Farhadifar, R., J.-C. Röper, ..., F. Jülicher. 2007. The influence of cell mechanics, cell-cell interactions, and proliferation on epithelial packing. *Curr. Biol.* 17:2095–2104.
  102. Park, J.-A., J. H. Kim, ..., J. J. Fredberg. 2015. Unjamming and cell shape in the asthmatic airway epithelium. *Nat. Mater.* 14:1040–1048.
  103. Saraswathibhatla, A., and J. Notbohm. 2020. Traction and stress fibers control cell shape and rearrangements in collective cell migration. *Phys. Rev. X.* 10:011016.
  104. Petridou, N. I., S. Grigolon, ..., C.-P. Heisenberg. 2019. Fluidization-mediated tissue spreading by mitotic cell rounding and non-canonical Wnt signalling. *Nat. Cell Biol.* 21:169–178.
  105. Mongera, A., P. Rowghanian, ..., O. Campàs. 2018. A fluid-to-solid jamming transition underlies vertebrate body axis elongation. *Nature.* 561:401–405.
  106. Jain, A., V. Ulman, ..., A. Pavlopoulos. 2020. Regionalized tissue fluidization is required for epithelial gap closure during insect gastrulation. *Nat. Commun.* 11:5604.
  107. Saadaoui, M., D. Rocancourt, ..., J. Gros. 2020. A tensile ring drives tissue flows to shape the gastrulating amniote embryo. *Science.* 367:453–458.
  108. Tetley, R. J., M. F. Staddon, ..., Y. Mao. 2019. Tissue fluidity promotes epithelial wound healing. *Nat. Phys.* 15:1195–1203.
  109. Oswald, L., S. Grosser, ..., J. A. Käs. 2017. Jamming transitions in cancer. *J. Phys. D Appl. Phys.* 50:483001.
  110. Kim, S., M. Pochitaloff, ..., O. Campàs. 2020. Embryonic tissues as active foams. *bioRxiv* <https://doi.org/10.1101/2020.06.17.157909>.
  111. Petridou, N. I., B. Corominas-Murtra, ..., E. Hannezo. 2021. Rigidity percolation uncovers a structural basis for embryonic tissue phase transitions. *Cell.* 184:1914–1928.
  112. Sens, P., and J. Plastino. 2015. Membrane tension and cytoskeleton organization in cell motility. *J. Phys. Condens. Matter.* 27:273103.
  113. Winklbauer, R. 2019. Dynamic cell-cell adhesion mediated by pericellular matrix interaction - a hypothesis. *J. Cell Sci.* 132:jcs231597.
  114. Caicedo-Carvajal, C. E., T. Shinbrot, and R. A. Foty. 2010.  $\alpha 5 \beta 1$  integrin-fibronectin interactions specify liquid to solid phase transition of 3D cellular aggregates. *PLoS One.* 5:e11830.
  115. Gabriele Krens, S. F., J. H. Veldhuis, ..., C.-P. Heisenberg. 2017. Interstitial fluid osmolarity modulates the action of differential tissue surface tension in progenitor cell segregation during gastrulation. *Development.* 144:1798–1806.
  116. Fagotto, F. 2020. Tissue segregation in the early vertebrate embryo. *Semin. Cell Dev. Biol.* 107:130–146.
  117. Sharrock, T. E., and B. Sanson. 2020. Cell sorting and morphogenesis in early *Drosophila* embryos. *Semin. Cell Dev. Biol.* 107:147–160.
  118. Miller, P. W., D. N. Clarke, ..., W. J. Nelson. 2013. The evolutionary origin of epithelial cell-cell adhesion mechanisms. *Curr. Top. Membr.* 72:267–311.
  119. Abedin, M., and N. King. 2008. The premetazoan ancestry of cadherins. *Science.* 319:946–948.
  120. Guirao, B., and Y. Bellaïche. 2017. Biomechanics of cell rearrangements in *Drosophila*. *Curr. Opin. Cell Biol.* 48:113–124.
  121. Barone, V., M. Lang, ..., C.-P. Heisenberg. 2017. An effective feedback loop between cell-cell contact duration and morphogen signaling determines cell fate. *Dev. Cell.* 43:198–211.e12.
  122. Shaya, O., U. Binshtok, ..., D. Sprinzak. 2017. Cell-cell contact area affects notch signaling and notch-dependent patterning. *Dev. Cell.* 40:505–511.e6.
  123. Slováková, J., M. Sikora, ..., C.-P. Heisenberg. 2020. Tension-dependent stabilization of E-cadherin limits cell-cell contact expansion. *bioRxiv* <https://doi.org/10.1101/2020.11.20.391284>.
  124. Lenne, P.-F., J.-F. Rupprecht, and V. Viasnoff. 2021. Cell junction mechanics beyond the bounds of adhesion and tension. *Dev. Cell.* 56:202–212.

## 1.2 Actin cytoskeleton in relation to the adhesion complex

### 1.2.1 Structural, functional and dynamical variability at adhesion sites

As discussed above, the previous description of cell-cell adhesion receptors as sticky surface proteins is evolving towards being a module of mechanochemical signal transduction. Even though cytoskeletal elements, microtubules and intermediate filaments are also involved with adhesion complexes at certain structures, such as in orientation of the spindles<sup>23,24</sup> and desmosomes<sup>25</sup>, almost all adhesion modules are supported by actin. The actomyosin cytoskeleton provides the base that is required for adhesions with substrates or other cells to form, and it can cause conformational changes through force in adhesion molecules changing their force-bearing capability and architecture of adhesion sites. While it is itself modulated by regulatory proteins in adhesion complexes and mechanical signals sensed from outside of the cells, it can also affect the properties such as stability of adhesion sites inside-out.

At integrin-based contacts of migratory cells, nascent and mature adhesion sites differ in structure. At the more peripheral lamellipodia where Myosin-2 activity is low, nascent adhesion sites form and disassemble while mature focal adhesions are more commonly found in lamellum, the inner domain, where there is Myosin-2 and tropomyosin activity. Interestingly, only the crosslinking but not motor activity of Myosin-2 is required to transform a nascent adhesion site into a mature adhesion site<sup>26</sup>. In both these regions, super-resolution studies revealed individual clusters  $\sim 100 \pm 20$  nm in size as functional modules, independent of ligand density and substrate rigidity<sup>27</sup>. At nascent adhesions in lamellipodia, Arp2/3-enriched and less dense branched actin is found, whereas at mature adhesions actin network thickens and forms linear actin bundles stratified with alpha-actinin, centripetal arcs. This suggests that mature adhesion sites might be signaling hubs where its associated proteins are brought together in a dense environment through actin. Yet, as recent studies show that passive crosslinkers might provide contractile forces to the actin network<sup>28</sup>, further studies are needed to check whether Myosin-2 motor activity independence of mature adhesions corresponds to no difference in force profiles of these distinct adhesion sites or not. Similar to cadherins, integrin adhesion complexes respond to force. Actomyosin-based recruitment of vinculin to the linker protein talin induces active integrin clustering and increases its residency time, maturing focal adhesions<sup>29</sup>. Vinculin itself also binds actin, which contributes to the dense protein plaque formed at integrin adhesion sites and likely to stabilization of actin. The turnover of integrins in mature adhesions has a halftime of  $\sim 3$  minutes, which is faster than that of the full adhesion site, yet is faster than other components of the adhesion; vinculin having a halftime of  $\sim 20$  seconds and talin  $\sim 2$  minutes<sup>27</sup>. About one-third of integrin at a focal adhesion is immobilized while the rest goes into temporary cycles of diffusion and immobilization with exchanges between the adhesion site and the free membrane<sup>30</sup>.

At immune synapses, several regions of different actin organizations exist. Distal supramolecular activation cluster (dSMAC) consists of an Arp2/3 generated dendritic network at the outer one-third of the contact, and is analogous to lamellipodial actin

network of migratory cells. This network disassembles at the peripheral SMAC (pSMAC) boundary, where actomyosin that is formin generated forms concentric arcs, analogous to lamella, surrounding the central SMAC (cSMAC). pSMAC also disassembles at the cSMAC boundary. There also exists Arp2/3-dependent actin foci within pSMAC and dSMAC, some of which colocalize with TCRs however their exact function is not known. The cSMAC consists of a sparse actin network of both straight and branched filaments. Its nucleators have not been clearly described; both Arp2/3 and formins have been indicated through indirect experiments and simulations<sup>31</sup>. The function of this region in natural killer cells is mainly secretion of lytic granules to a target cell, and therefore the actin network mesh size is thought to regulate the size-dependent secretion of granules, as upon synaptic activation actin network gets less dense<sup>32,33</sup>, yet the mechanism driving this actin remodeling is not discovered so far. Interestingly, Myosin-2 inhibition does not change the overall structure of the immune synapse, yet it increases the network density at cSMAC and reduces exocytosis. Myosin-2 was also found to be not only at the contact site but also above, as the T cell's equatorial plane seemed to align with the peripheral to central F-actin boundaries at the contact site<sup>34</sup>. There is a partition of proteins in the immune synapse in correlation with changes in actin architecture. For instance, the main integrin at immune synapses LFA1 is found mainly at pSMAC, where actomyosin force is highest; providing an analogy to nascent adhesions at dSMAC and mature adhesions at pSMAC. As for why integrins do not get transported to the cSMAC, LFA1-ICAM1 pairs have been found to be excluded due to their bulky size in comparison to TCR-MHC interactions which brings two membranes closer at the cSMAC<sup>35</sup>.

In traditional electron microscopy studies two groups of adherens junctions were defined; linear adherens junctions that form at the apex of lateral membranes in epithelia that associate with an actomyosin ring along the cell circumference and reach microscyles and punctate adherens junctions that are smaller and more mobile adhesion points observed mainly in mesenchymal cell-cell contacts. Super-resolution studies revealed that adhesion sites form as assemblies of nanoclusters<sup>36,37</sup>. The size distribution of these nanoclusters is quite broad in *Drosophila* epithelial tissues, and it is actin-dependent. Actin network interactions decrease fission rates of small clusters<sup>36</sup>. Multimers of cadherins do not bind actin while nanoclusters do. Stable nanoclusters, forming in an actomyosin contractility-dependent manner, act as building blocks for mature adhesion sites<sup>38</sup>. The F-actin interaction makes the clusters more stable as seen by increased lifetimes when the cadherin cytoplasmic domain is mutated into an actin-binding domain<sup>39</sup>, and the actin network binding these nanoclusters is also more stable while the surrounding actin network is contractile and turns over rapidly<sup>40</sup>, these observations could be explained by both inside-out and outside-in interactions between cadherin complex and actomyosin, influencing each other's stability.

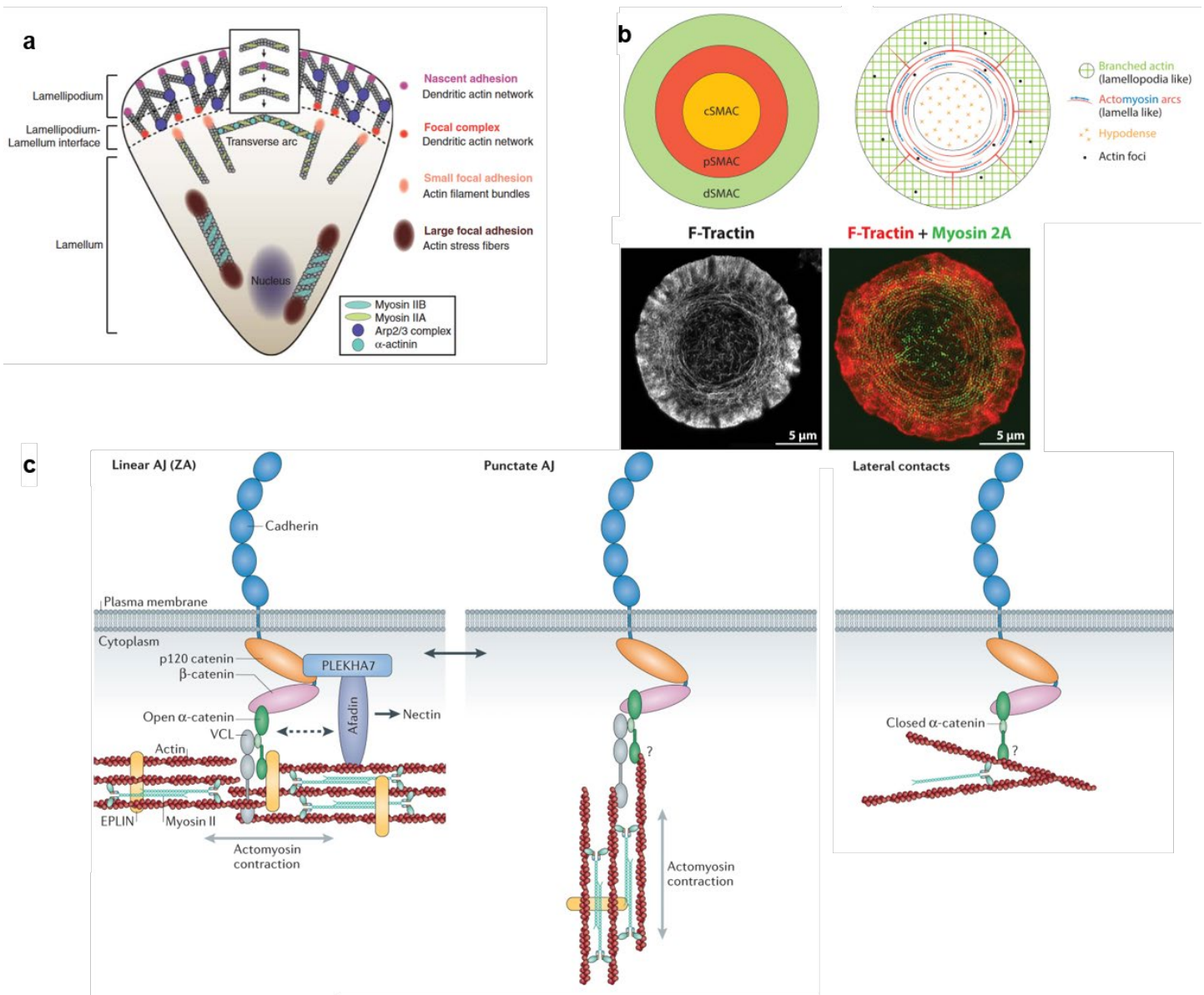


**Figure 3. Characteristic architectures of various actin-adhesion complex structures. At contacts of migratory cells with ECM, nascent adhesions emerge within the lamellipodia with dendritic actin network, which are precursors of larger focal adhesion sites that are associated with myosin decorated actin bundles (a). Schematic of four actin networks at the immune synapse is given above. An example of a synapse where networks are sharply seen and symmetric is given below; the loose network at the cSMAC that is mostly overlooked is evident with the actin marker Ftractin (b). Schematics of three possible cadherin-adhesion sites in epithelial cells. Actin filaments run parallel subapical at high-tension linear AJs, actin filaments perpendicularly terminate at punctate AJs, and lateral contacts below linear AJs provide less specialized contacts, which might be more similar to early embryonic contacts (c). ECM: extracellular matrix, SMAC: supramolecular activation cluster, cSMAC: central SMAC, dSMAC: distal SMAC, pSMAC: peripheral SMAC, AJ: adherens junctions, ZA: zonula adherens, VCL: vinculin. Figure adapted from<sup>35,41,42</sup>.**

Cadherin junction dynamics is less defined as results seem to differ with cell type as well as the measurement method. In pancreatic cells, within clusters of E-cadherin, around half were found to be mobile as free E-cadherin diffused into clusters while the rest was immobile. Recovery time for E-cadherin in this model's mobile fractions of adhesive clusters changed from 10 to 40 seconds. FRAP experiments of differing bleached areas showed that the recovery time within clusters was mainly limited by molecular turnover, whereas for freely diffusing cadherin on the surface, which lacked actin interactions, this rate was determined by lateral diffusion<sup>37</sup>, showing that actin interactions affect E-cadherin lifetime. This could be attributed to the force-responsive behavior of E-cadherin under increased actomyosin tension at cell-cell interfaces<sup>43,44</sup>. The cadherin turnover depends on the dynamics of junctional actin, as the turnover of actin was recently shown to affect E-cadherin stability independent of actomyosin tension<sup>45-47</sup>. Another set of FRAP and single molecule tracking data, by contrast, showed that nearly all of cadherin in junctions could be replaced in a maximum of 2 minutes, with average lifetimes in order of seconds, while the overall morphology of adherens junctions could appear unchanged<sup>46,48</sup>. This proves that further studies are required to understand the dynamics of cadherin clusters, and importantly, the dynamics should be studied within defined structures to link function and stability.

As for actin dynamics, in the free cell cortex, two subpopulations were observed. One subpopulation with a lifetime of less than 1 second forms most of the cortex as short filaments, while the second population has a lifetime of around 25 seconds<sup>49</sup>. Turnover of actin is essential to maintain the force balance of adhesion<sup>50</sup>, yet actin turnover is significantly slower under cadherin clusters. At murine cell doublets with E-cadherin expression, FRAP experiments show actin to recover in ~30 seconds, this recovery time decreases when E-cadherin levels at junctions decrease. When resolved spatially more, punctate adherens junctions were shown to consist of a bundled F-actin stalk and a tip interacting with cadherin clusters; actin turnovers were shown to differ at the stalk (~50 seconds) and the tip (~20 seconds)<sup>51,52</sup>. Out of cadherin-associated contacts, the turnover was faster (~10 seconds). Remarkably, when changing E-cadherin lifetime using mutants, authors in this study<sup>52</sup> also observed changes in actin lifetime, proving outside-in effects on the cytoskeleton, suggesting that at contacts the dynamics of one cell can be translated to the neighboring cells. The molecular architecture of the actin network at most cadherin-mediated contacts is not understood well enough to have such comparative analysis as in this study. F-actin is thought to form an Arp2/3-mediated network in adherens junctions<sup>53</sup>, but in some studies, junctions are depleted of Arp2/3<sup>54,55</sup>. In MDCK cells, FRAP experiments showed that actin recovers in seconds, similar to lamellipodial branched actin<sup>56</sup>, while other studies report a half-life of minimum one minute<sup>40,57</sup>. Formins were found to localize to contacts, promoting actin cable assemblies as well<sup>58</sup> and VASP-promoted actin bundle formation<sup>59</sup>. In short, actin organization differs significantly, possibly at different contacts as and stages of adhesion formation.

### 1.2.2 Cortical flows at adhesion sites

In a seminal paper, Bray and White predicted that the cortical flows of actin might act as the driving mechanism of cytokinesis, animal cell movements, antigen aggregation at the

immune synapse and more<sup>60</sup>. The treadmill dynamics in the commonly polarized actin network, and more prominently, the active stresses, for instance, through motors, generates flows of actin<sup>61</sup>, which can translocate molecules and cells.

During cell division, an actomyosin contractile ring performs the membrane constriction in animal cells<sup>62</sup>. Due to contraction at the cell equator or relaxation at the mitotic poles, a gradient of contractility results in fast actomyosin flows towards the contractile ring<sup>63</sup>. When labeled fluorescently, concanavalin A, a label for surface glycoproteins, was shown to translocate towards the cytokinetic ring, not necessarily colocalizing with F-actin there<sup>64</sup>. *Caenorhabditis elegans* embryos partition membrane-bound and freely-diffusing PAR proteins into anterior and posterior poles via passive advective transport (via a net global fluid flow) by the cortical flows<sup>65,66</sup>. Outer-leaflet GPI-anchored proteins were shown to nanocluster locally in CHO cells, where actomyosin asters formed at the inner-leaflet of the cell membrane<sup>67</sup>. A recent study showed that the cell membrane moves in the direction of cortical flows at immune synapses, suggesting not only proteins directly linked to the cytoskeleton but associated proteins might be carried through passive interactions as well<sup>68</sup>. The flows of actin and membrane seem coupled, and long-range membrane flows alone seem unlikely as the cell membranes do not transmit flows for longer than a few micrometers<sup>69</sup>. The cortex and membrane are physically close to each other and highly crosslinked in many settings, which explains the coupled flows, including of transmembrane proteins<sup>70,71</sup>, especially where there is cell-substrate interaction; disturbance of it, such as when a cell is de-adhered from another cell or a substrate, results in the formation of blebs due to membrane ripping from the actin cortex.

Integrin adhesion sites are often stationary, while the actin network above them shows retrograde flows due to polymerization at the front end of the cell and contractions at the rear end, the exact mechanism driving the substrate-dependent migration. This non-correlation indicates slippages at the actin cortex-adhesion site linkage. Still, with no links in between, migration cannot occur (unless cells are in a confined environment where pressure gradients within the cell due to deformations drive the movement of the cell<sup>72</sup>). A clutch, where mechanical coupling between actin and extracellular matrix is provided under force, is thought to support the movement. As stretch-relaxation cycles of 4-16 seconds were measured for talin<sup>73</sup>, this supports the idea that the clutch might be transient at a molecular level yet intact at a macro scale. The clutch results in actin flow velocities getting affected by the formation of adhesion sites as this interaction affects the effective friction. Nascent adhesions form in the presence of lamellipodial fast flows, yet within seconds these adhesion sites start maturing and reach the lamellum, where retrograde flow is slower<sup>74</sup>. This supports the idea that interactions with the adhesion sites slow the retrograde flow of actin.

Similarly, at immune synapses, retrograde actin flows, which gradually decay towards the center, carry numerous receptors such as the TCR to form the cSMAC; actin flows slow down where the membrane receptors are artificially trapped, supporting a frictional model of TCR coupling to actin flow with slippages<sup>75</sup>. When clusters are enhanced, for instance via phase separation in case of LAT proteins, they can be carried for longer distances by actin flows as their frictional coupling gets enhanced<sup>76</sup>. TCR receptors' flow velocity

matches with actin flow velocities in corresponding regions of the immune synapse<sup>35</sup>. At pSMAC, TCRs do not directly bind actin arcs but instead get swept by them<sup>77</sup>, as they lose the effector protein Nck which links them to actin at dSMAC/pSMAC boundary. At dSMAC, actin moves quite fast, with  $\sim 6 \mu\text{m}/\text{min}$  velocity with a retrograde flow perpendicular to the cell edge. At pSMAC, actin flows are more telescopic and circular and flow with  $\sim 2 \mu\text{m}/\text{min}$  velocity. Within cSMAC that is less studied as it can only be observed with super-resolution techniques, unlike the dSMAC and pSMAC networks, no actin flows have been detected so far.

At epithelia, changes in E-cadherin amounts were shown to be a driver of actomyosin flows, independent of the initial distribution of Myosin-2. This is exemplified in *Drosophila* epithelial cytokinesis, as dividing cell pulls on the neighboring cells during cytokinesis, their junctions elongate, resulting in a dilution of E-cadherin locally. This results in less effective friction at these ingressing junctions. Since whether an actomyosin gel will break symmetry depends on its contractility and the gel's properties, including its friction coefficient, actomyosin flows can theoretically appear without a contractility increase but with a physical cue, such as local elongation of a junction. Experiments indeed show actomyosin flows towards the neighboring cells from the ingression and a local actomyosin accumulation as a result<sup>78</sup>. The actomyosin pool at the junctions seems to be more stable than the medial pool at the apical surfaces of epithelia. Large-scale flows at medial pools are observed, for instance, towards vertical shrinking junctions. The directions of flows in this setting were based on anchorage points at cell-cell junctions; the flows were directed towards higher E-cadherin-containing junctions as the amounts of E-cadherin at junctions pulsated<sup>79</sup>. Additional work is necessary to see if the first model applies to flows at medial junctions, as medial flows seem to precede junctional changes in E-cadherin amounts<sup>80</sup>.

Cadherin and actomyosin flows can also be seen in a coupled fashion; so far, such observations have been made with retrograde flows. In migratory multicellular tissues and epithelia, only when a new contact was forming, VE-cadherin flows from basal to subapical sides of the cells, where one cell crawled under another one, were observed<sup>81</sup>. These flows were inhibited by Cytochalasin D, supporting actin involvement in the flows, and cadherins seemed to localize on actin fibers, also moved with similar velocities ( $\sim 0.3 \mu\text{m}/\text{min}$ ), even though transient dissociations occurred. Myosin-2 did not show such localization but flows halted with Myosin-2 inhibition via Blebbistatin. Y-27632 did not have such a response, and as it is known to stop flows at actin arcs but not lamellipodia, this raises the question of whether an Arp2/3-dependent and not ROCK-dependent actomyosin network might be mediating the flows at lateral junctions. The cadherin flows in this study were suggested to facilitate the movement of cells under or over other cells. Similarly, a recent study showed that cortical retrograde flows in opposing directions at neighboring cells' junction unfold alpha-catenin<sup>82</sup> and enhance cis-clustering, even though cadherin flows were  $\sim 8$  times slower than actin flows in this study. Authors observed adherens junctions to form only when actin-dependent flows mechanically activated the cadherin complex, yet the flows stopped when junctions matured. When cadherin interactions driving apical movement of clusters were dissected, *trans*-dimerization was shown to increase cluster stability and stop cluster movements, while a

cytoplasmic tail mutant could make fast random movements while it turned over more rapidly than wild types<sup>39</sup>. An actin-binding site gave direction to cluster movements, given they could still turnover, and Latrunculin A treatment destabilized clusters, showing actin linkage is required and can control the direction of dynamic cadherin clusters apically. The reason actin and cadherin clusters move apically could be due to tension differences at the lateral interface. At the subapical zone where zonula adherens is, there is an actomyosin belt, yet below zonula adherens also an actomyosin cortex is visible<sup>57</sup>. Laser ablations show the whole lateral junction to have contractile forces; however they are higher at zonula adherens, which could explain the direction of the flow there. Interestingly, E-cadherin seemed to contribute to establishing these contractile force instabilities, as interfering with E-cadherin reduced oscillations of other membrane proteins. Cadherin clusters were also shown to move in a retrograde fashion at the lateral interfaces of collectively migrating cells, following the retrograde actin flows that appear during cell migration, and their stability impacted the polarity and speed of leader cells<sup>83</sup>. These studies with actin-mediated cadherin cluster migration indicate cadherin clusters to be essential for mediating coordination between migrating cells. Yet, it remains to be elucidated more clearly whether such movements might be necessary for adherens junction assembly and localization at a subcellular level.

### 1.2.3 What kind of contacts are we looking at in the early zebrafish embryo?

In a complex adult system, there are thousands of different tissues with specific function and shape. Nevertheless, cell-cell adhesion's molecular basis and regulation are not fully understood even in a more straightforward system of three cell layers, such as the gastrulating zebrafish embryo we study. To study cadherin-based adhesions, we use the zebrafish model in our lab, taking advantage of optically transparent embryos. The deep cells that form the embryo proper depend on cadherin-based adhesions, and the enveloping layer also carries tight junctions<sup>6,84</sup>. As a result, *cdh1* knockdown or knockouts, for instance, results in a loss of cell adhesion in deep cells and halts tissue movements during gastrulation<sup>85</sup>. In the early stages of gastrulation, zebrafish embryos go through cell sorting as the ectoderm and mesendoderm cells differentiate and segregate from each other<sup>6</sup>. Zebrafish reach gastrulation only 6 hours post fertilization, and the different germ layer progenitors show differential contractility, as well as molecular differences starting with cadherins they express. Heterotypic adhesions are weaker than homophilic adhesions, as ectoderm progenitors only express E-cadherin, while mesendoderm progenitors also express N-cadherin.

Previous studies from our lab used a primary cell culture of germ layer progenitors to study the adhesion of cell doublets in a minimalistic system<sup>6,47,86</sup>. These studies revealed cortical tension as the primary determinant of adhesion strength, while cadherins act as the transmembrane linkers connecting the adhering cell cortices. Another vital function of cadherins in this context is their signaling, as the cortical tension gets reduced at cell-cell contacts downstream to cadherin binding, helping the contact-free cortical tension to drive contact expansion. This expansion appears bigger and leads to stronger contacts in ectoderm cells as they downregulate Myosin-2 more efficiently at their contacts<sup>86</sup>. This phenomenon seems common to many early embryos, such as *Drosophila* and mouse<sup>87,88</sup>, even though most cadherin-mediated mature contacts at adult tissues or

embryonic epithelial tissues recruit Myosin-2<sup>89</sup>, indicating differences in overall structures of adhesion complexes and their coupling to contractile apparatus between early embryos and more specialized structures.

Early embryos are pretty soft and fluid tissues. For instance, the tissue surface tension of *Xenopus* and zebrafish germ layer progenitor aggregates are less than 1 mJ/m<sup>2</sup>, while for many human cancer and tumor lines this value is around 10-25 mJ/m<sup>2</sup><sup>90</sup>. Again, for cortical tensions, in zebrafish single cells, the values for endoderm, mesoderm and ectoderm have been measured as 0.03, 0.05 and 0.08 mJ/m<sup>2</sup> respectively<sup>6</sup>; while for mouse embryo pre-compaction and post-compaction cortical tensions are 0.2 and 0.4 mJ/m<sup>2</sup><sup>88</sup>. Meanwhile, in many cell lines these values reach 0.5 to 2.5 mJ/m<sup>2</sup><sup>90</sup>. These values can be expected to correlate with adhesion strengths in many models; zebrafish progenitors do not seem to make strong adhesions, as is also evident by the lack of vinculin at wild-type contacts which only gets recruited to contacts when cortical tension is artificially enhanced<sup>47</sup>.

It is conceivable that the adhesions in early embryos may not be very strong as at these stages embryos constantly remodel. The zebrafish embryo reaches ~ 1000 cells in 3 hours at its 10th division cycle, so cell cycles are without intervening gaps<sup>91</sup>. With each division, especially after interstitial fluid accumulation<sup>92</sup>, cell contacts get dissolved by mitotic rounding<sup>93</sup>. Large cellular rearrangements start with gastrulation, such as involution, intercalation and directed single cell migrations, which are conserved in most vertebrates and during which adhesion-regulated remodeling plays a critical role<sup>94</sup>.

Even though the adhesions in early embryos seem transient, adhesion takes place quite fast and matures within a few minutes, indicative of a very efficient system to make adhesions. Remarkably, progenitors in zebrafish show differences in their contact architecture: while ectoderm progenitors accumulate E-cadherin and F-actin at the contact rim in a ring-like fashion (similar to what has been observed in other cell doublets of MDCK cells, embryonic stem cells and sarcoma line cells<sup>45</sup>), mesoderm and endoderm progenitors show a more homogenous distribution of the two. Understanding the differences between different germ layer progenitor contacts would be valuable for the developmental biology community, as differential adhesion complex and actin cytoskeleton remodeling is intercalated with differentiation and material properties of embryonic tissues<sup>93</sup>. Furthermore, understanding how the contact architectures form in zebrafish progenitors would help us elucidate contact formation, maintenance and remodeling in early embryos, a question that would apply to many other model systems; maybe to even different adhesion molecule-cortex-mediated processes discussed as analogous mechanisms in previous chapters. One efficient method to look at contacts is reconstituting these contacts. In the next chapter, I will discuss different methods to do so, building toward my methodology of choice for this thesis work, reconstitution of cadherin-based adhesion with functionalized lipid bilayers.

## 1.3 Engineering cadherin adhesion

### 1.3.1 Reconstitution of biological processes

Reconstitution is building a system from its components. This is a valuable method which proofreads one's understanding of the system at hand and figures the critical parameters of a biological event. Reconstituted systems are composed of a reduced set of components, yet as our understanding increases, they become more complex, like the natural environment within a cell, with steps towards even reconstituting a functional synthetic cell. At cellular scales, the discoveries range from the first synthesis of DNA<sup>95</sup> to a synthetic chromosome<sup>96</sup>; from the first meeting of actin, myosin and ATP *ex cellulo*<sup>97</sup> to actomyosin-based constriction of giant vesicles resembling furrow formation in dividing cells<sup>98</sup>.

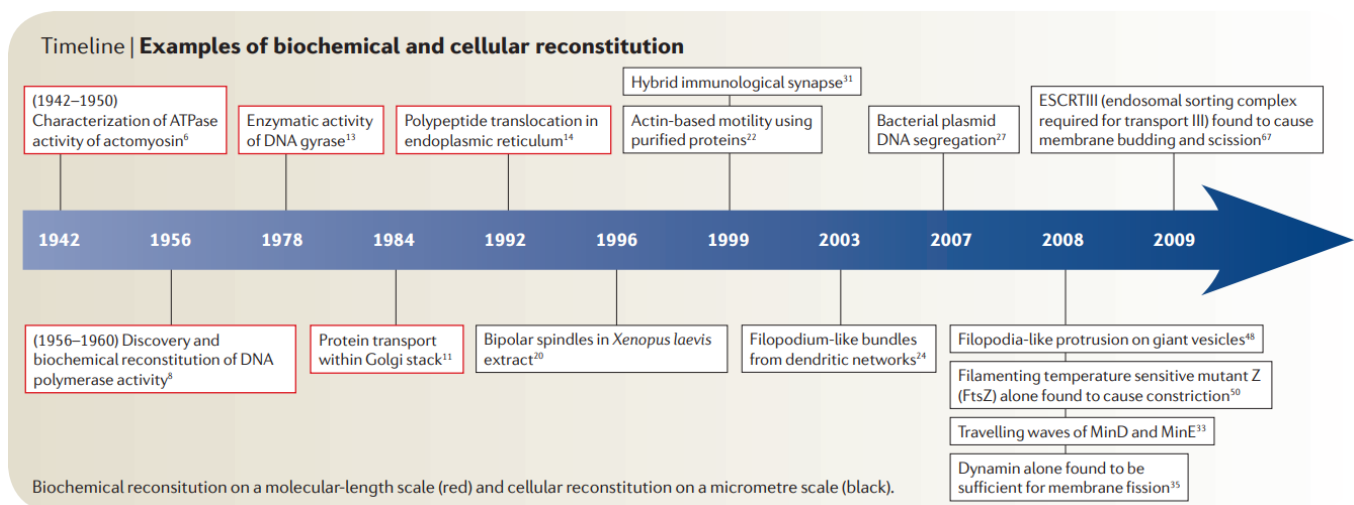


**Figure 4. Examples of biochemical and cellular reconstitution. Biochemical reconstitution at molecular length scale (red) and cellular reconstitution at micrometer length scale (black). The figure is taken from<sup>99</sup>.**

Cell adhesion sites are quite interesting as they provide a defined signaling interface with biochemical and mechanical signaling. As many adhesion receptors and ligands retain functionality in isolation, essays with reconstituted substrates can be used to induce cell-matrix or cell-cell adhesion. The most common methods involve a defined geometry via patterning ligands on solid substrates of varied rigidity, changing from crosslinked soft polymers to hydrogels to glass.

For the reconstitution of membrane-bound processes, such as cell junction formation, supported lipid bilayers (SLBs) are useful approximations of cell membranes that can be controlled to a great extent<sup>100</sup>. SLBs can be formed of smaller phospholipid vesicles on a solid substrate such as silica or glass. The lipid bilayer retains fluid character as it forms over a ~5 nm water layer above the glass surface. This system provides a cell-surface model where receptors are correctly oriented, and non-specific interactions are limited. Moreover, it provides control over receptor density and mobility. Around 20 years ago,

SLBs started to be used to recapitulate interactions at cellular interfaces, as such a reductionist approach allowed the contact interactions to occur within ~100 nm of the glass coverslip, allowing high-spatiotemporal imaging methods such as total internal reflection microscopy (TIRF) and reflection interference contrast microscopy (RICM) to be used on contacts that were not resolved before.

### 1.3.2 Reconstituting cadherin-based adhesion

Cell membranes are very complex structures with hundreds of different lipids in possibly different phases and different types of proteins; some embedded within the membrane, some soluble and some decorating the cell surface. This environment gets even more complex with modifications to proteins and lipids, which can be part of an even more diverse glycocalyx. It is only understandable that in such a complex environment receptors that also have self- or nonself-interactions behave in very different ways. It is well known, for example, that in antigen-presenting cells, some ligands move freely while some exhibit constrained movement<sup>101</sup>. One needs to consider that during recapitulation, neither immobile nor fluid substrates capture the bona fide complexity of the membrane alone. Both these approaches completely lack the cytoskeletal interactions which are important to mechanosensitive proteins such as cadherins and their interaction partners<sup>102</sup>. Cell type might be another concern in deciding what substrate is better. For example, at cadherin contact sites involving integrins, such as in endothelial cells, mechanotransduction via VE-cadherins activate the integrin response, which requires high traction forces<sup>103</sup>. Based on the process studied, both immobile and mobile ligand approaches might be helpful tools. In the following, I discuss some previous studies of cadherin-based adhesion reconstitution.

#### 1.3.2.1 Immobile ligands

Cadherin adhesions are very specific. For example, only homophilic but not heterotypic classical cadherin adhesions mediated mechanotransduction<sup>104</sup>. Nevertheless, they have remarkably low affinity; for instance, while the dissociation constant of integrin and ICAM interactions are at the nanomolar range<sup>105,106</sup>, Ecad interactions are in the micromolar range<sup>107</sup>. This supports the idea that most of the adhesion strength in cell-cell contacts comes from reorganizing the actin cytoskeleton underlying the contact rather than receptor affinities. Still, a critical function of cadherin receptors is to link the underlying cytoskeletons of cells to each other<sup>86</sup>. For neighboring cells to expand cell-cell contacts, the ligands - cadherins - need to resist the piconewton forces generated by cells during contact spreading. Cadherin cytoplasmic domain mutants or contact missing the linker alpha-catenin, which do not bind the cytoskeleton, cannot expand cell-cell contacts<sup>45,47</sup>. This suggests that a reconstitution system should provide enough support to cadherins so that they can resist forces. Immobile substrates have been useful to provide this.

The immobile substrate needs to be carefully recruited. For instance, immobile RGD ligands activate integrin response only if they are in less than 60 nm apart clusters<sup>108</sup>, and for the immune synapse, T cells can only be activated on immobile substrates if the TCR ligands are at the center of the immune contact, surrounded by ICAM-1 molecules as in a mature contact<sup>109</sup>. Such configurations must be allowing the maximum mimicry one

could achieve with a solid substrate, of TCR-MHC engagement, which consists of assembly into microclusters and transport of clusters to cSMAC<sup>110</sup>.

Cadherin-coated solid substrates allow the spreading of cells as cells can spread on any adhesive surface, given that it creates enough adhesion energy, as well as can induce migration of mesenchymal cells as a clutch could be activated with drag force applied on a solid substrate. However, it is not clear whether a solid cadherin surface would recapitulate the natural response and remodeling at cell-cell contacts, such as the accumulation of cadherin under adhering surfaces (see 1.1.3) or long-range redistribution of cadherins seen as flows (see 1.2.2). In addition, a concern is whether the solid ligands would mimic the effects of having ECM interactions, as actomyosin organization correlates with substrate stiffness (*Fig. 5*). Previous studies measuring forces on even soft PDMS (1 kPa) adhesive substrates showed the stresses measured to be an order of magnitude higher than at cell-cell junctions<sup>111</sup>. Compared to fibronectin-coated substrates, these forces were very similar; actin showed similar distribution at the cell edge<sup>112</sup>.

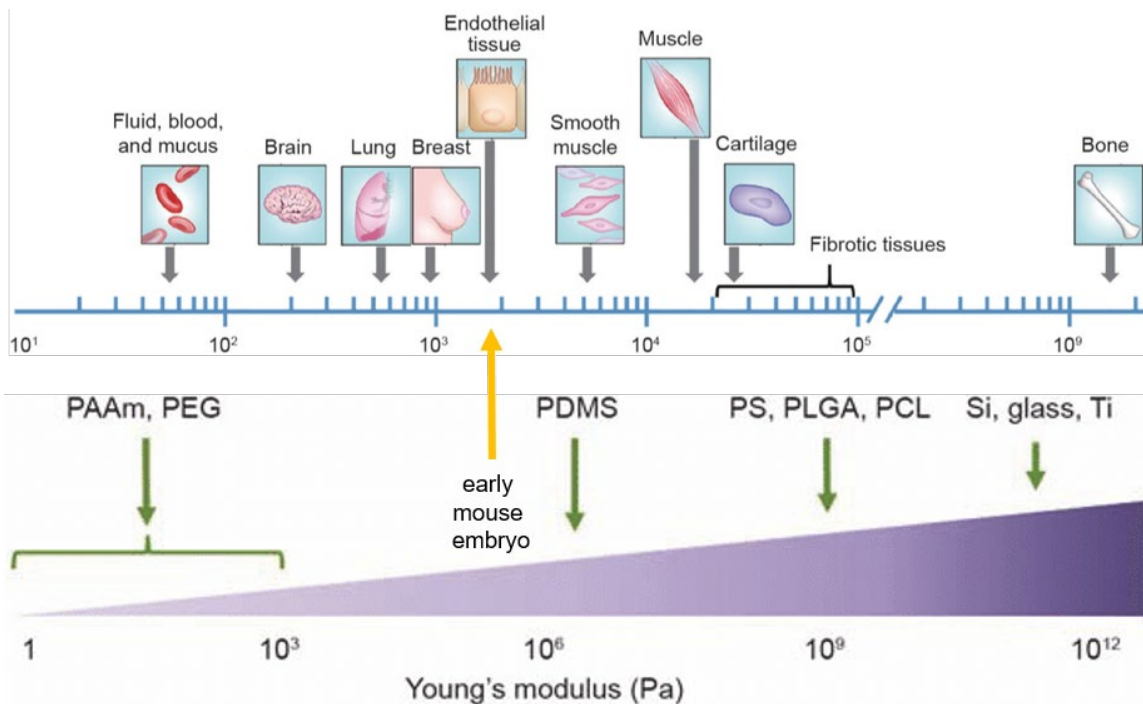


*Figure 5. Tissues and substrates with a variety of stiffnesses. Early embryos are relatively soft tissues, exemplary mouse embryo data taken from<sup>113</sup>. PAA: polyacrylamide, PEG: polyethyleneglycol, PDMS: polydimethylsiloxane, PS: polystyrene, PLGA: polylactic-co-glycolic acid, PCL: polycaprolactone. Figure adapted from<sup>114</sup>.*

The signaling response of cadherin adhesions was highlighted to differ on different substrate stiffnesses in one study, where E-cadherin-coated polyacrylamide (PA) hydrogels were used to study the adhesions of MDCK cells<sup>115</sup>. For instance, Cdc42 activity and formins were required for adhesion to 30 kPa PA gel yet not for 60 kPa PA gel, which induced Arp2/3-mediated adhesions, showing cadherin-actin complex

architecture depends on the reconstitution assay; both mechanisms may be used for contact formation and maturation at the same time in natural contacts. Previous studies of cadherin reconstitution very often used glass as a solid substrate ( $\sim 100\text{GPa}$ )<sup>53,116</sup>, which induced large adhesion plaques and a highly organized actin network, also seen on more rigid PA gels of 95 kPa<sup>117</sup>; these structures look different from small clusters often observed on softer substrates as well as real contacts. (Fig. 6)

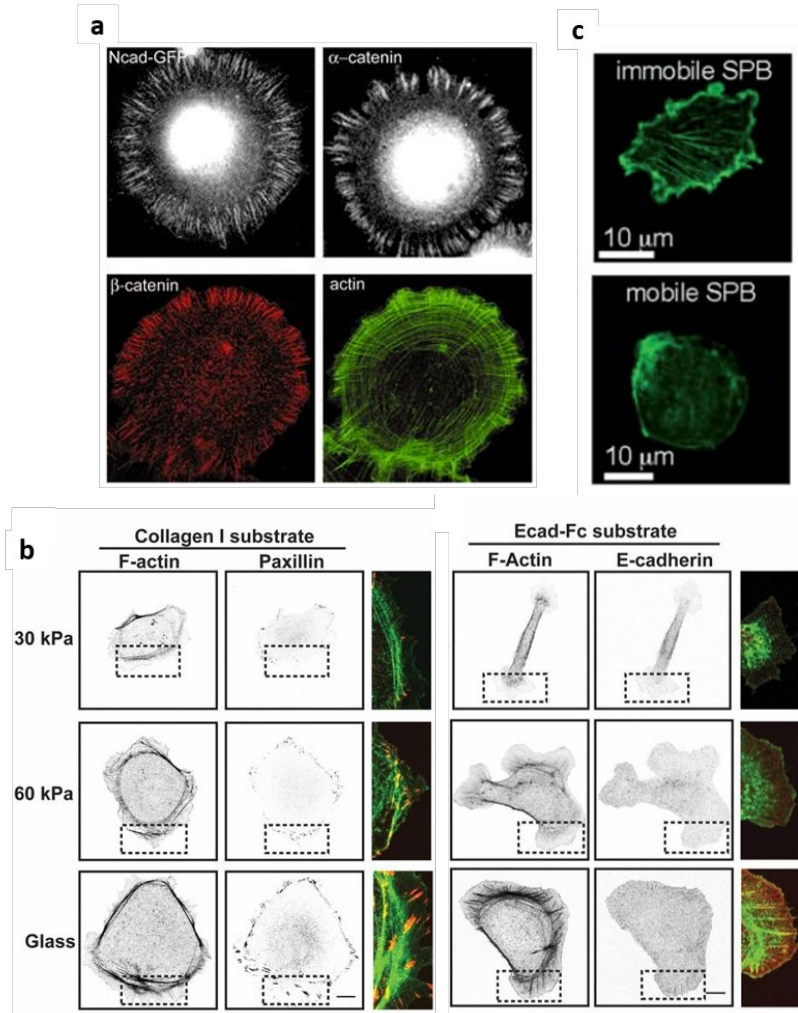


**Figure 6. Effects of substrate on the cadherin-adhesion organization.** Immobile N-cadherin-Fc substrates on glass lead to cell spreading. Immunolabeling of cadherin-actin complex proteins is shown. Cadherin/catenin proteins show a radial distribution at lamellipodia, and strong vesicle-like immunostaining is found in the central area; actin arcs and radial arcs are visualized in the actin channel (a). Effects of integrin- and E-cadherin-based rigidity sensing on collagen-coated substrates (left) and E-cadherin-Fc functionalized substrates (right) of different moduli are shown (b). Effects of supported lipid bilayer mobility on cadherin-based adhesions. F-actin forms organized structures on immobile substrates reminiscent of stress fibers; on mobile substrates, it accumulates at the edge and has a less organized central distribution (c). Figure adapted from<sup>115,116,118</sup>.

### 1.3.2.2 Fluid Bilayers

SLBs can provide a dynamic reconstitution system where cadherin receptors can get recruited, cluster and spatially reorganize, capturing many details of these receptors within the cell membrane. As used for immune synapse reconstitution for more than 20 years (The first hybrid immune synapse was formed between a T cell and an SLB decorated with MHC peptide and ICAM1, mimicking the surface of an antigen-presenting cell<sup>119</sup>), these systems provide a large toolset and modifications to play with. Fluid bilayers activate immune synapse activity with considerably fewer ligands than immobile substrates<sup>101</sup>. Neuronal synapses were recapitulated using SLBs functionalized with neuroligin-1 proteins<sup>120</sup>. Recently, SLBs were also used to reconstitute Eph-Ephrin signaling on bilayers decorated with ephrinA1 ligands intermixed with immobile RGD peptides<sup>121</sup>.

Previous studies showed cadherins to diffuse slower when they are in density-induced clusters on fluid membranes<sup>122</sup>, which seem to stabilize their binding to the cytoskeleton<sup>123</sup>, suggesting a mobile substrate might induce different adhesions than an immobile substrate. In line with this, E-cadherin-dependent Rac1 responses of epithelial cells were shown to be enhanced on laterally mobile substrates of E-cadherin compared to immobilized counterparts<sup>124</sup>. However, due to the weak cadherin interactions, mobile ligand systems have not been easy to activate, especially considering the lack of actin cytoskeleton that could have increased the adhesion energy of cadherin receptors<sup>125</sup>.

First trials used fluid bilayers to induce cadherin adhesion between bilayers and cells. In one such study decorating bilayers via GPI-anchored E-cadherin ectodomain, epithelial cells did not spread on the bilayer 6 hours after seeding, even though about 30% of the cells increased ligand concentrations underneath, suggesting some diffusion trap to be active<sup>126</sup>, probably suggesting nascent adhesions could be induced. However, maturation could not take place due to low shear viscosity. This study went on to induce cell spreading using fibronectin micropatterns within the bilayers. However, this might complicate the cellular adhesion response, as some proteins involved with cadherin adhesions, such as alpha-catenin<sup>127</sup> and vinculin, also take part in integrin-mediated adhesions. Therefore such modification possibly affects the amount of available pools of these proteins to cell-cell vs. cell-matrix adhesions. Indeed, in another study where epithelial cells showed polarization on E-cadherin/Fc functionalized bilayers, in the presence of integrin adhesion, E-cadherin clustering was reduced<sup>128</sup>. The fluidity of bilayers in this study was unclear as they were composed of mainly fluid DOPC but formed on PDMS, which can affect the fluidity differently. When looking at the actin cytoskeleton, a switch from gel-phase to fluid bilayers was shown to induce a switch from stress-fiber-like actin bundles to more diffuse actin<sup>118</sup>, supporting the idea that immobile cadherin adhesions might have features of cell-matrix interactions. Notably, the same substrate was used by changing the temperature of the bilayers and taking advantage of phase transitions, attributing this change in actin structure very likely to E-cadherin mobility. In this study, again performed on PDMS wells, the DOPC lipid diffusion was recorded to be significantly lower than on glass substrates, suggesting the better cell-bilayer adhesion in the Charnley et al. and Andreasson-Ochsner et al. papers compared to Perez et al. might also be a consequence of decreased bilayer fluidity. When this

hypothesis was systematically addressed, indeed, partially-fluidized bilayers were shown to induce adhesion more efficiently than fluid bilayers<sup>129</sup>. Importantly, in this study, the authors also tried trapping the ligands with nanogrids, but it did not prove successful, showing that the drag forces or the long-range mobility of ligands might be necessary in contact maturation. In model membranes, the 2D diffusion coefficient of a membrane-bound protein is typically between 1-10  $\mu\text{m}^2/\text{s}$ . For E-cadherin, the diffusion coefficient was estimated to be 0.1-0.3  $\mu\text{m}^2/\text{s}$  on free membranes<sup>130,131</sup>, whereas, at epithelial adhesion sites, this value drops to 0.005-0.06  $\mu\text{m}^2/\text{s}$ <sup>40</sup>, reflecting changes in dynamics via trans and cis interactions, cytoskeletal links and possibly specific lipid environments.

Another way to decrease the mobility of ligands and capture the natural state of transmembrane proteins is to deploy the bilayers on polymers so that the bilayer is at a 5-100 nm distance from the solid support, allowing transmembrane proteins to be incorporated within the bilayer without affecting their diffusivity due to physical constraints. Although chemically challenging, polymer tethered bilayers can be deployed as multi-bilayer stacks, linked to each other with spacers, which also allows the adjustment of frictional coupling as lipid diffusion on such bilayers can be adjusted<sup>132</sup>. Based on the number of layers, substrate stiffness can be varied; this system was used with N-cadherin functionalization and provided a substrate on which myoblasts could spread and migrate, as N-cadherin was shown to accumulate and assemble in clusters under the adhered cells, independent of ligand density within the range tried, as linker distances of 48 nm and 68 nm did not make a difference<sup>133</sup>.

For our study, we decided to recruit E-cadherin-based adhesion of zebrafish ectoderm progenitors on SLBs to study contact formation and maturation, given the importance of ligand mobility in cadherin-based adhesions. In order to make homogenous partially-fluid bilayers, we opted for introducing cholesterol into fluid bilayer preparation, so that we could adjust diffusion precisely without introducing bulky lipid moieties or heterogenous layers<sup>100</sup>.

## 2. Materials and Methods

### 2.1 EcadECD protein expression, purification and characterization

cDNA encoding the zebrafish E-cadherin ectodomain (Q90Z37\_DANRE, EC1 to EC5, residues G141 to D672), with an N-terminal human CD33 signaling peptide and C-terminal 12xHistidine purification tag was codon optimized and ordered as a gBlocks Gene Fragment with overhangs for Gibson assembly (NEB). The sequence was engineered to have a single Cys in the EC5 domain for site-specific labeling<sup>129</sup>. The product was inserted between EcoRI and XbaI sites of pcDNA3.1(-) mammalian expression vector (Invitrogen).

EcadECD was expressed in suspension FreeStyle 293-F cells (Thermo Fisher Scientific) in Freestyle 293 Expression medium at 37°C and 8% CO<sub>2</sub>. HEK293 F cells were transiently transfected using polyethylenimine (Polysciences, #23966) diluted in Opti-MEM Reduced Serum Medium (Thermo Fisher Scientific). Cultures were supplemented with 5 mM CaCl<sub>2</sub> 2 days after transfection<sup>134</sup> and culture media containing secreted EcadECD was collected 5 days later. Secreted protein from filtered and conditioned media was loaded to HisTrap Fast Flow Crude column (Cytiva) for affinity chromatography on an AEKTA pure fast protein liquid chromatography system (Cytiva) and eluted with an imidazole gradient. Clean fractions, checked by SDS-PAGE, were pooled together, and dialyzed overnight in storage solution (100 mM NaCl, 20 mM Tris-HCl pH 8, 3 mM CaCl<sub>2</sub>) or buffer was exchanged using PD10 desalting columns (Cytiva). The identity of the protein was verified with N-terminal sequencing. Clean protein was aliquoted at a final 50 µg/ml concentration and snap frozen for long-term storage at -80°C with 5% glycerol.

#### 2.1.1 Protein labeling

In order to perform FRAP experiments to determine the protein diffusion constant, EcadECD was labeled at the Cys residue using Sulfo-C5-maleimide (Lumiprobe). First, the sample was incubated for 20 min with TCEP (100 molar fold excess of protein) at RT. Then maleimide dye (10 molar fold excess of protein) was added to the sample and incubated at RT for 1 hour. Excess dye was removed using a 7K MWCO Zeba™ Spin Desalting Column (Thermo Fisher Scientific).

#### 2.1.2 Bead Aggregation assay

10 µl of Cobalt-based Dynabeads (Invitrogen) were mixed with 2 µg of EcadECD and slowly shaken at 4°C. Beads were rinsed and resuspended in a storage buffer (500 mM NaCl, 3mM CaCl<sub>2</sub> and 20 mM Tris-HCl). Using a magnetic rack, beads were washed 3 times with a washing buffer (100 mM NaCl, 20 mM Tris, pH 7.3) and resuspended in 600 µl washing buffer. Preparation was sonicated briefly to disperse the beads, split into half and put into two wells of a 12-well plate. To one well 2 mM CaCl<sub>2</sub> was added while the other was kept calcium-free.

### 2.1.3 Western blot

Eluted protein fraction was incubated at 70°C in NuPAGE LDS Sample Buffer and NuPAGE Sample Reducing Agent (Invitrogen) for 10 min before getting loaded to a 4-12% NuPAGE Bis-Tris protein gel. After SDS-PAGE, proteins in the gel were transferred to a membrane using the iBlot Western Blotting System (Invitrogen) according to the manufacturer's protocol. For the immunodetection of EcadECD, the membrane was blocked with blocking buffer (3%BSA, 0.2% Tween 20 in PBS) for 1 hour at RT and incubated overnight with rabbit anti-zebrafish E-cadherin antibody<sup>86</sup> (1:5000) in blocking solution. After 3x10 min washes with PBT (PBS with 0.2% Tween), the membrane was incubated with Peroxidase AffiniPure Goat Anti-Rabbit IgG (H+L) (1:20000) (Jackson ImmunoResearch Laboratories, Inc.) for 45 min at RT and washed 4 x 5min with PBT, then 2x5 min with PBS. The membrane was developed with Clarity Western ECL Substrate (Bio-Rad) before imaging.

## 2. 2 Bilayer preparation

To make small unilamellar vesicles, 1,2-dioleoyl-sn-glycero-3-phosphocholine (DOPC), 1,2-dioleoyl-sn-glycero-3-[(N-(5-amino-1-carboxypentyl)iminodiacetic acid)succinyl] (nickel salt), 1,2-distearoyl-sn-glycero-3-phosphoethanolamine-N-[amino(polyethylene glycol)-2000] (ammonium salt) (DSPE-PEG2000) (Avanti Polar Lipids), and freshly dissolved cholesterol (Sigma Aldrich) lipid mixtures in chloroform with a molar ratio of 55.9:4:0.1:40 (unless otherwise stated) were prepared in glass vials and evaporated under N<sub>2</sub> stream to get a homogenous thin film. To make gel-phase bilayers, DOPC was replaced by 1,2-dipalmitoyl-sn-glycero-3-phosphocholine (DPPC) (Avanti Polar Lipids). Lipids were further vacuumed for 1 hour to remove the remaining solvent and frozen at -20°C unless freshly used. For FRAP experiments, 0.1% (1,2-dioleoyl-sn-glycero-3-phosphoethanolamine-N-(lissamine rhodamine B sulfonyl) (Rhodamine-DOPE) was added to the lipid mixture. Lipid film was resuspended in a vesicle buffer (75 mM NaCl, 3mM CaCl<sub>2</sub>, 20 mM Hepes) at 37°C by vortexing, with a final concentration of 1.5mM and freeze-thawed in liquid nitrogen 5 times before aliquoting. Aliquots were kept at -20°C and used within 2 weeks, after diluting the solution to 0.2 mM with vesicle buffer and bath sonication for 15 minutes.

To form the lipid bilayers on, 24-x50-mm high precision coverslips (no. 1.5H; Marienfeld) were cleaned in Piranha solution (3:1, 98% H<sub>2</sub>SO<sub>4</sub> (Merck):30% H<sub>2</sub>O<sub>2</sub> (Sigma-Aldrich)) for 1 hour. The coverslips were further washed with deionized water and kept in water to be used within 2 weeks. Before use, coverslips were dried, PCR tubes were attached to the surface with their conical ends removed, as reaction chambers, using ultraviolet curing glue (Norland optical adhesive 63) under UV light for 5 min. The coverslips were then treated in a Zepto B (Diener Electronic) plasma oven for 12 min at 30 W under 1 L/h airflow. Immediately after, vesicle mixtures were added to reaction chambers, and after letting the vesicles settle for 4 min 3 mM CaCl<sub>2</sub> was added to enhance vesicle fusion on the activated surface.

Chambers were incubated for 1 hour at 37°C, washed with PBS through serial washes by vigorous pipetting, incubated with 0.1% fatty acid-free BSA (Sigma-Aldrich) in protein

storage buffer for 30 min to which 2 ug/ml final concentration of zebrafish EcadECD or mouse E-cadherin/Fc/6xHis chimera (E2153, Sigma) was added. Protein was incubated on bilayers for 45 min at RT before changing to a prewarmed imaging medium with serial washes.

## 2. 3 Zebrafish lines and handling

Zebrafish (*Danio rerio*) handling was performed as described<sup>135</sup>. Embryos were raised at 28.5–31°C in E3 medium (5 mM NaCl, 0.17 mM KCl, 0.33 mM CaCl, 20.33 mM MgSO<sub>4</sub>) and staged as previously described<sup>91</sup>. The following lines were used: WT ABxTL, Tg(actb2:My12.1-eGFP)<sup>136</sup>, Tg(cdh1-tdTomato)xt18<sup>137</sup>, Tg(cdh1-mlanYFP)xt17<sup>137</sup> and Tg(ctnna-citrine)ct3a<sup>138</sup>, Tg(actb1:mCherry-utrCH)<sup>136</sup>, Tg(actb2:Tpm3.1-mNeongreen) and Tg(actb2:ArpC2-mNeongreen) (both created by Roland Kardos in the Heisenberg Lab). Fish were bred in the aquatics facility of IST Austria according to local regulations, and all procedures were approved by the Ethics Committee of IST Austria regulating animal care and usage.

## 2. 4 Cloning of expression constructs

PCR products from plasmids pEGFP-RhoA Biosensor (gift from Michael Glotzer, Addgene plasmid # 68026) and GFP-AHPH-DM (gift from Alpha Yap, Addgene plasmid # 71368) were subcloned with following primers to create Gateway attB PCR products: pEGFP-RhoA

5'-GCAGGATCCCATCGATTATGGTGAGCAAGGGCGAG-3', 5'-

CGTAATACGACTCACTATAGTTTCAAGGCTTTCCAATAGGTTTGTAGCAA-3',

GFP-AHPH-DM

5'-

AATACAAGCTACTTGTCTTTTTGCAGGATCCCATCGATTATGGTGAGCAAGGGCG  
AG-3'

5'-

TCTGGATCTACGTAATACGACTCACTATAGTTCTAGAGGCTCAAGGCTTTCCAATA  
GGTTTGTAGC-3'.

cDNA sequence coding for Ftractin (IP3KA\_RAT, 10M to 52G) was codon-optimized and ordered as a gBlocks Gene Fragment (IDT) with attB arms.

Zebrafish E-cadherin-GFP plasmid (a gift from Erez Raz<sup>139</sup>, and E-cadherin full-length PCR product was subcloned using the Gateway primers:

5'-GGGGACAAGTTTGTACAAAAAAGCAGGCTTAACCATGGCCTGCGTGAC-3'

5'-GGGGACCACTTTGTACAAGAAAGCTGGGTTGTCCTCTCCGCCACCGT-3'

All products were recombined with pDONR(P1-P2) (Lawson#208) to create entry clones, and further recombined with with p3E mNeonGreen (Allelebiotech), p3E mKO2, p3E-3xmCherry or p3E-polyA (Chien#302) and pCS2-Dest (Lawson #444) to create expression plasmids.

E-cadherin- $\Delta$ cyto-GFP fusion was created by removing the cytoplasmic domain by amplifying the full-length plasmid with the following primers:

5'-GATCTCGAGGTGTCCAAAGGCG-3'

5'-CAGCAGAGGCTCTTTCTTGCTG-3'

## 2. 5 Embryo microinjections

Zebrafish embryos were injected using glass capillary needles (30-0020, Harvard Apparatus), which were prepared by a needle puller (P-97, Sutter Instruments) and attached to a microinjector system (PV820, World Precision Instruments).

All embryos were microinjected with 100 pg lefty1 mRNA at the 1-cell stage to induce ectoderm fate. Additionally, to visualize F-actin 60pg of Ftractin-NG or 75 pg Lifeact-RFP mRNAs<sup>136</sup>; to visualize RhoA activity 80 pg of GFP-AHPH-WT<sup>140</sup> or GFP-AHPH-DM mRNAs<sup>141</sup>; to decrease endogenous Cdh1 amounts, 4 ng *cdh1* morpholino (5'-TAAATCGCAGCTCTTCCTTCCAACG-3', GeneTools)<sup>142</sup>; to decrease Myosin-2 activity 75 pg CA-Mypt mRNA<sup>84</sup>, to increase RhoA activity 3 pg caRhoA mRNA<sup>84</sup>, to decrease Rac1 activity 100 pg DN-Rac1 mRNA<sup>143</sup>, to overactivate Ezrin 150 pg CA-Ezrin mRNA<sup>144</sup> and for actin single molecule imaging 0.125 ng actin protein from rabbit skeletal muscle labeled with TRITC (Cytoskeletal, Inc.) were injected to 1-cell stage embryos.

To exchange endogenous Ecad with designed constructs, following morpholino injection, 200pg Ecad-mCherry (full-length) or 200 pg E-cadherin- $\Delta$ cyto-GFP were injected into the 1-cell-stage embryos.

Synthetic mRNAs were produced using the SP6 mMessage mMachine kit (Ambion), while actin protein was handled according to manufacturer protocols.

## 2. 6 Embryo cell cultures

Embryos were first transferred to prewarmed (28.5-31°C) DMEM/F12 medium (Sigma-Aldrich) (supplemented with GlutaMAX (Gibco), PenStrep and diluted to 90% with cell culture grade water to better match the osmolarity of the *in vivo* environment) at time of cell culture preparation for live imaging. The animal cap was cut from the yolk cell at sphere stage with forceps and these explants were transferred to eppendorf tubes using glass pipettes. For each condition, one embryo was used to minimize variability and for all conditions embryos from the same batch of embryos from a single couple were used. In case of inhibitor use, media in the eppendorfs were accordingly exchanged 10 min before cell seeding. All explants were dissociated by gentle tapping and seeded on bilayers covered with control or treatment media at 29°C.

## 2. 7 Inhibitor treatments

DMEM/F12 medium or DMSO (0.1%) were used as controls depending on the solvent of the pharmacological inhibitors. The final concentrations used were 0.1% for DMSO, 10  $\mu$ M for para-nitroblebbistatin (10 mM stock dissolved in DMSO) (Optopharma Ltd.), 20

nM for 1-Oleoyl lysophosphatidic acid sodium salt (LPA) (5 mM stock dissolved in water) (Tocris), 20 nM for Jasplakinolide (100  $\mu$ M stock dissolved in DMSO) (Sigma-Aldrich), 100  $\mu$ M CK666 (stock in DMSO), 25  $\mu$ M SMIFH2 (stock in DMSO), 1  $\mu$ M Damnacanthal (stock in DMSO), 50  $\mu$ M LimKi3 (stock in DMSO).

## 2.8 Phalloidin staining

Cell cultures were prepared on bilayers as described and kept at 28°C for 30 min. Cells were fixed by adding 4% PFA (diluted from methanol-free 16% solution (Agar Scientific)) into the media, to a final 2% concentration. After 5 min of fixation, cells were rinsed 5x with CSK buffer (10mM PIPES/KOH (1M, pH 6.8), 100 mM NaCl, 300 mM Sucrose, 1 mM EGTA, 1mM MgCl<sub>2</sub>, 1mM DTT, 1 tablet protease inhibitor per 50 ml), permeabilized for 10 min with 0.1% Triton in CSK buffer, blocked for 10 min with 2% BSA and stained with Atto 565 phalloidin (dissolved and aliquoted in DMSO) (Sigma Aldrich, 94072) in blocking solution. Cells were washed 3x with CSK buffer and an anti-fade mounting solution was added for samples that were not imaged on the day.

## 2. 9 Imaging tools

### 2.9.1 PDMS confinement

In the case of bilayers without the EcadECD (except for adherence assay, see below), cells were imaged under PDMS confinement to increase the contact area that is imaged. Bilayers were formed on coverslips glued to the bottom of plastic dishes containing a 17-mm round hole, on which a chamber was created by gluing a ring cut from a 15 ml falcon tube. Cells were seeded into these chambers.

1:10 PDMS mixtures (Sylgard 184, Ellsworth Adhesives) were prepared as previously described<sup>72</sup>, degassed for 2 min at 2,000 rpm (mix) and for 2 min at 2,200 rpm (defoam) in a mixer/defoamer (ARE-250, Thinky). PDMS was poured onto a wafer and 10-mm round coverslips that were activated by plasma cleaning were pressed onto this mix. The wafer was baked at 95 °C for 15 min and the 16- $\mu$ m-high micropillar-coated coverslips were gently removed from the wafer to be used as confiners. Before use, a confiner was incubated for 5 min with FBS, washed with PBS and kept in a culture medium. For imaging, the confiner was placed on a soft pillar attached to a magnetic glass lid, and closed on the cells. During imaging, it was kept in place using a magnetic ring underneath the dish.

### 2.9.2 Hydrogel microwells

My Polymer 132 (My Polymers) hydrogel microwells to trap cell doublets were prepared as previously described<sup>145</sup>. Briefly, microwells with a diameter of 30  $\mu$ m and depth of 50  $\mu$ m were prepared by pressing the pattern-containing PDMS stamps to droplets of polymer on Mattek glass-bottom dishes. These patterns were cured using a UV lamp (Thorlabs UV-light-emitting diode 365 nm) in nitrogen atmosphere for up to 1 hour, and the PDMS stamps were peeled off. Before usage, hydrogel patterns were passivated for 5 min with BSA and kept in PBS until use.

## 2. 10 Microscopy and Data Analysis

Imaging was performed using microscopes with heating chambers preheated to 29°C. For contact formation imaging, the acquisition was started as soon as cells were seeded. For steady contact imaging, cells were imaged 10-30 min post seeding. Cultures were imaged for around 1h maximum, dividing and apoptotic cells were excluded from analysis.

Contacts were imaged using an LSM800 equipped with an Airyscan detector using a Plan-APOCHROMAT 63x/1.4 oil objective (Zeiss). For time-lapse imaging of Ecad and AHPH signals that were weaker and subject to higher photobleaching, Andor Dragonfly 505 equipped with 1x Andor Zyla sCMOS detector using a CFI Apochromat TIRF 60x/NA 1.49/WD 0.13 mm oil objective (Nikon) was used. A TILL Photonics iMic TIRF System equipped with Andor TuCam detection was used with a 100x/1.49 (Olympus) oil objective for imaging bilayers, single molecules and FRAP experiments.

All micrographs were adjusted for contrast and saved as figures using Fiji. The rest of the data for analysis were processed raw.

### 2.10.1 FRAP

To measure the diffusion constant of the protein on different bilayer compositions, photobleaching experiments were performed using Cy5-labeled EcadECD. With a frame rate of 2 s per frame, 5 pre-bleach frames were acquired, followed by photobleaching of an area of about  $10 \mu\text{m} \times 10 \mu\text{m}$ . Recovery of the signal was analyzed using the `frap_analysis`<sup>146</sup> program implemented in MATLAB (The MathWorks, Natick, MA).

FRAP experiments for cellular Ecad were performed using the Ecad-mlanYFP expressing cells. With a frame rate of 0.5 s per frame, 5 pre-bleach frames were acquired, followed by photobleaching of an area of about  $5 \mu\text{m} \times 5 \mu\text{m}$  at the cell contact. A photobleach correction due to the imaging process was performed using an un-bleached area of the contact and the photobleach curve was normalized to the first pre-bleach data point. To obtain the recovery times and immobile fractions, monoexponential functions were fitted to the recovery curves.

### 2.10.2 Adherence assay

To check for the specificity of cell-bilayer adhesions, bilayers were kept EcadECD-free or Ecad was reduced in cells using the morpholino. Contact areas were quantified using the particle analysis function of ImageJ, under a certain value ( $150 \mu\text{m}^2$ ) cells were considered non-adherent, where smaller contact areas were attributed to non-specific interactions.

### 2.10.3 Average intensity and coverage at the contact

Contact intensity over time was measured using a custom Python script, by taking ratios of the total intensity after background subtraction to total area determined by local thresholding. For AHPH and F-tractin constructs, values were normalized to maximum to remove injection-based variations between samples. We found the AHPH construct to

localize diffusely, as well as in a few cortical foci. These foci were homogeneously spread at the contact-free interface and after the contact area stabilized, they localized to the contact rim, which seemed to correlate with contractile activity in the cells. Nevertheless, we excluded them from our average intensity analysis, given that not all RhoA biosensors show such structures<sup>147</sup>.

As Myosin-2 filaments could be detected, masks for these positive signals at the contact interface were created using ILASTIK<sup>148</sup>. Next, using a custom Python<sup>149</sup> script, percentages of total area positive for signal were determined in segmented images. To get enrichment of a signal at the rim, rim and center intensities at the contact were separately calculated and rim-to-center ratio was used as a measure of enrichment where the contact rim was the 1-1.5  $\mu\text{m}$ -thick ring at the contact edge and contact center was the remainder area.

Contact diameters were estimated from the measured contact areas as most contacts were symmetrical.

#### 2.10.4 Colocalization and line profiles

Dual color images acquired with the confocal mode of LSM800 from Ecad-tdTom expressing cells injected with AHPH-NG, and Ecad-mlanYFP expressing cells injected with Ftractin-mKO2 were used for colocalization analysis. Images were analyzed using Just Another Colocalization Plugin (JACoP)<sup>150</sup> ([https://github.com/fabricecordelieres/IJ-Plugin\\_JACoP](https://github.com/fabricecordelieres/IJ-Plugin_JACoP)) in ImageJ. After adjusting the thresholds manually to detect positive signals, Manders' coefficients M1 and M2 (0 to 1)<sup>151</sup>, which give a fraction of overlap between positive pixels, and Li's Intensity Correlation Quotient (Li's ICQ) (-0.5 to 0.5)<sup>152</sup>, which gives a value based on the correlation of intensity changes at two channels, were calculated.

In order to visualize the colocalization, intensity profiles over a 0.3  $\mu\text{m}$ -thick line for both channels were plotted together.

#### 2.10.5 Radial intensity profiles

Radial averages of intensity profiles in symmetrical contacts were generated using the transform function in ImageJ to rotate a single snapshot by 1-359°. The resulting rotations were averaged to get the mean radial intensity and plotted by a line profile along the contact diameter. Profiles were normalized to contact length first, and second, to mean intensity, before averaging radial profiles from multiple cells.

#### 2.10.6 F-actin and Ecad flows

Time-lapse images of Ftractin-NG or Ecad-mlanYFP expressing cells were used for flow analysis. The built-in Fiji<sup>153</sup> function Multi Kymograph was used to get single kymographs along each cell's diameter. For analysis, kymographs were split into two pieces from the position of center of mass to get radial kymographs. The motion of fluorescent particles within was detected using a deep learning automated kymograph analysis software, KymoButler<sup>154</sup> in Mathematica 12.1 (Wolfram Research, Inc.). BiKymoButler function was

used to detect bidirectional tracks with a particle size of 0.3  $\mu\text{m}$  and a minimum of 10 seconds. From these tracks, net velocity of particle movements with respect to the center of mass and track durations were calculated.

For experiments with Jasp, network movement was detected also using PIVlab<sup>155</sup> to get a spatial map, as filaments were stable enough for movements to be detected with particle image velocimetry. Extracted velocity vectors were averaged over time and using a custom Python script, radial velocities were plotted with respect to the center of mass.

### 2.10.7 Actin network density

Ftractin-NG labeled F-actin networks were extracted using a software for quantification of biopolymers networks, SOAX<sup>156</sup>. For time-lapse images, parameters were adjusted for each movie based on inspection of some frames and the corresponding extracted networks; the saved parameters were later used to batch process the movies. Extracted network coordinates were used to plot networks using a custom Python script, total network lengths were measured using Skan library<sup>157</sup> functions and divided by contact areas to get network density values.

### 2.10.8 Actin single particle tracking

TRITC-injected cells were imaged on the Imic TIRF microscope with  $\sim 100$  nm pixel size, using a 561-nm laser line with 100 ms exposure. Acquisition intervals of 1 s, 2 s and 3 s were used to capture at least 200-frame time lapses. Particle detection and tracking were performed using the TrackMate plugin<sup>158</sup> in ImageJ, based on a Gaussian fit with an estimated diameter of 0.3  $\mu\text{m}$ . 0.2  $\mu\text{m}$  maximum linking distance and gaps of maximum 2 frames were allowed to account for failures to detect particles. Thresholds were adjusted manually for each experiment and tracks were verified by overlaying with the raw data. Average lifetime of actin at contacts were calculated as previously described<sup>159</sup>. Briefly, effective lifetime was given by fitting a monoexponential decay function to the lifetime distribution of tracks obtained from each cell. This value was corrected for photobleaching using the varying acquisition intervals to obtain the photobleaching constant, giving a corrected dissociation rate. Photobleach corrected lifetimes obtained from each experiment (with at least 3 different movies) were plotted as single data points.

## 2. 11 Statistics and Reproducibility

Data were plotted and statistical tests were performed in Prism 6 (Graphpad). Details for each experiment are described in figure legends. In summary, first, a D'Agostino-Pearson normality test was performed and based on the results, a two-tailed Student's *t*-test for parametric distributions and a Mann–Whitney *U*-test for non-parametric distributions were used to compare two groups. To compare cumulative distributions of velocity histograms between two samples, Kolmogorov-Smirnov test was performed. To compare more than two groups, an analysis of variance (ANOVA) for parametric distributions and a Kruskal–Wallis test for non-parametric distributions were used. Independent experiments (N) denote a single embryo, where controls and experiments are taken from the egg lay of a single couple, and n denotes the number of imaged/analyzed cells from this embryo.

# 3. Results

## 3. 1 Reconstitution of adhesion on bilayers

In order to visualize contact formation dynamics with high spatiotemporal resolution, we aimed to establish a biomimetic system where zebrafish ectoderm progenitor cells adhere to supported lipid bilayers, which carry mobile and correctly-oriented E-cadherin (Ecad) ectodomains (EcadECDs) (Fig. 7). We chose ectoderm cells as they made strong contacts compared to other progenitor cells<sup>86</sup>, and formed a stereotypical contact architecture - showing a ring-like accumulation of Ecad and F-actin at the contact rim. Another advantage of ectoderm progenitors was that they only expressed Ecad, which helped us keep our system minimal.

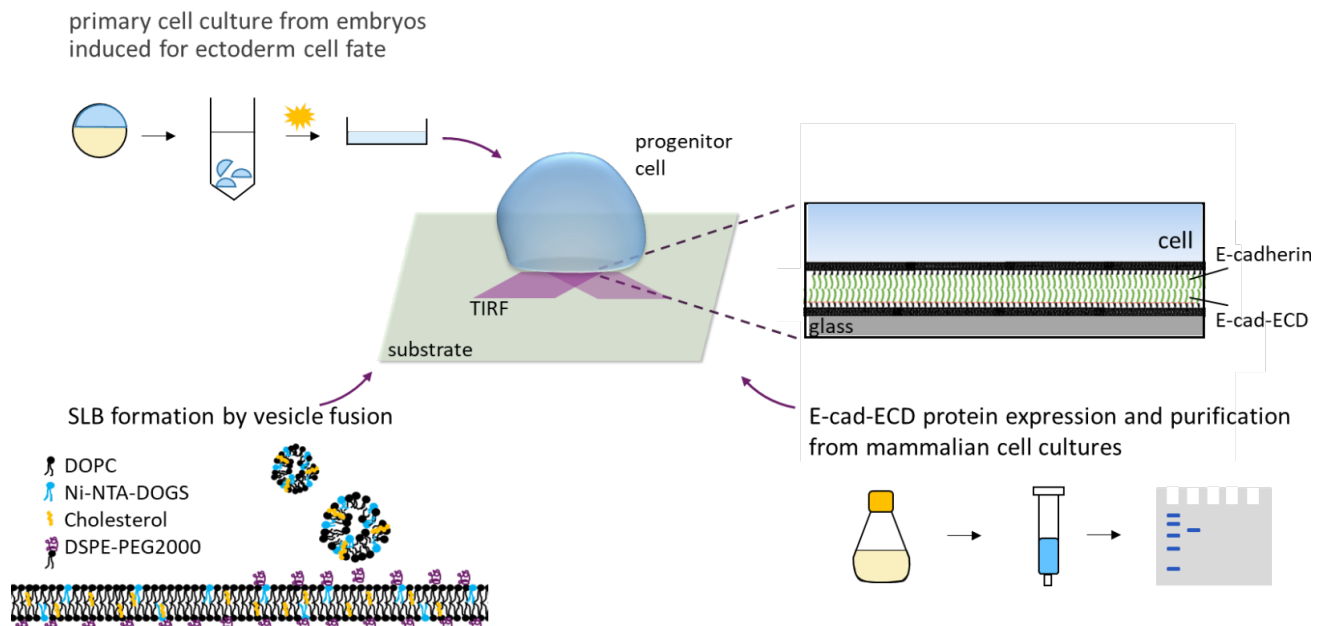


**Figure 7. Schematic of the biomimetic cell-cell adhesion assay.** Ectoderm progenitor cells seeded for the adhesion assay were obtained by dissociating fate-induced embryos at sphere stage. The supported lipid bilayer was formed by small unilamellar vesicles comprising fluid-phase phosphatidylcholines, Ni-chelated lipids, cholesterol to decrease fluidity and PEG-ylated lipids to mimic non-specific interactions with a glycocalyx-like layer. EcadECD protein was purified from HEK293 suspension and tagged to the bilayers with its 12xHis tag. This platform provided us with a contact at a single z-plane which could be observed using confocal microscopes or more techniques such as total internal reflection microscopy (TIRF), thanks to its closeness to the coverslip.

As a proof of concept, we wanted to know whether contacts would form when one of the cells missed a functional cellular link to its E-cadherin. To test this, we injected embryos at the one-cell stage with *cdh1* morpholino (MO) to knock-down E-cadherin in the cells. We either rescued the cadherin expression by injecting a full-length (FL) Ecad-encoding

mRNA in red or a cytoplasmic-deletion truncated version ( $\Delta$ cyto) of the same construct to mimic the situation of bilayers, lacking their link to the cytoskeleton. We measured contact lengths between doublets of these cells. While the homophilic Ecad $\Delta$ cyto contacts did not expand, we could rescue the contacts in EcadFL doublets. The hybrid Ecad $\Delta$ cyto-EcadFL contacts had contacts that expanded as much as the EcadFL-EcadFL contacts, showing that a single cell with a functional Ecad complex could be enough to drive adhesion (Fig. 8). Therefore, we assumed the bilayer assay we planned could mimic cell-cell adhesion with cell-bilayer contacts.

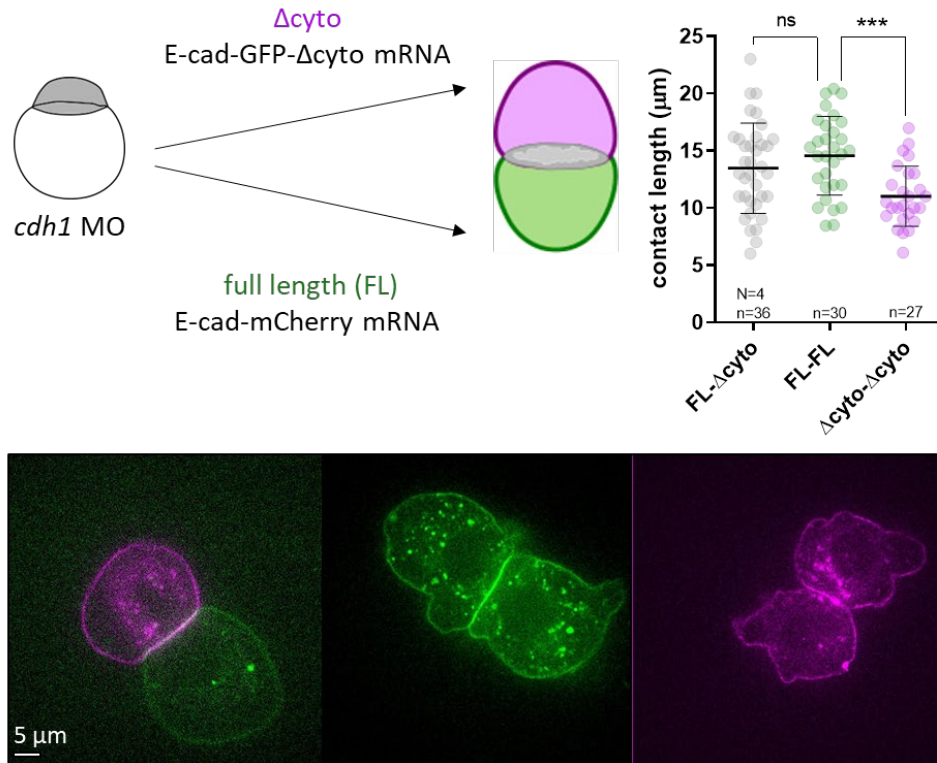


**Figure 8. Hybrid EcadFL-Ecad $\Delta$ cyto contacts compare to homotypic EcadFL-EcadFL contacts.** A schematic of the experiment is given on the top left. At the bottom, representative images of 3 different contact combinations are given. Contact length quantifications of homotypic and heterotypic contacts with EcadFL or Ecad $\Delta$ cyto are given on the top right. From  $N=4$  independent experiments,  $n$  denotes the number of doublets quantified for each condition in the plot, where error bars show mean  $\pm$  s.e.m. Student's  $t$ -test.

In order to purify zebrafish EcadECD with 12xHis, we opted to use a mammalian expression system to keep its glycosylation patterns (Fig. 9a). Previously, constructs expressed with insect or bacteria cultures were found to be inactive (a supplier providing insect-purified human E-cadherin (sinobiological.com) removed the protein from their selection later on). Our initial expression trials gave no yields, however adding  $\text{CaCl}_2$  to the cell cultures 2 days post transfection (as stated in a thesis from Harrison Lab) stabilized the EcadECD that was secreted into the culture medium even though it killed most of the cells in cultures (Fig.9b). We checked the activity of the protein via a  $\text{CaCl}_2$

aggregation assay as calcium is needed for Ecad activity. Beads coated with zebrafish EcadECD only aggregated in the presence of  $\text{CaCl}_2$  (Fig. 9c). This activity seemed to last around 10-12 months for the EcadECD kept at  $-80^\circ\text{C}$  or in liquid nitrogen, suggesting some improvement to the storage buffer might be necessary.

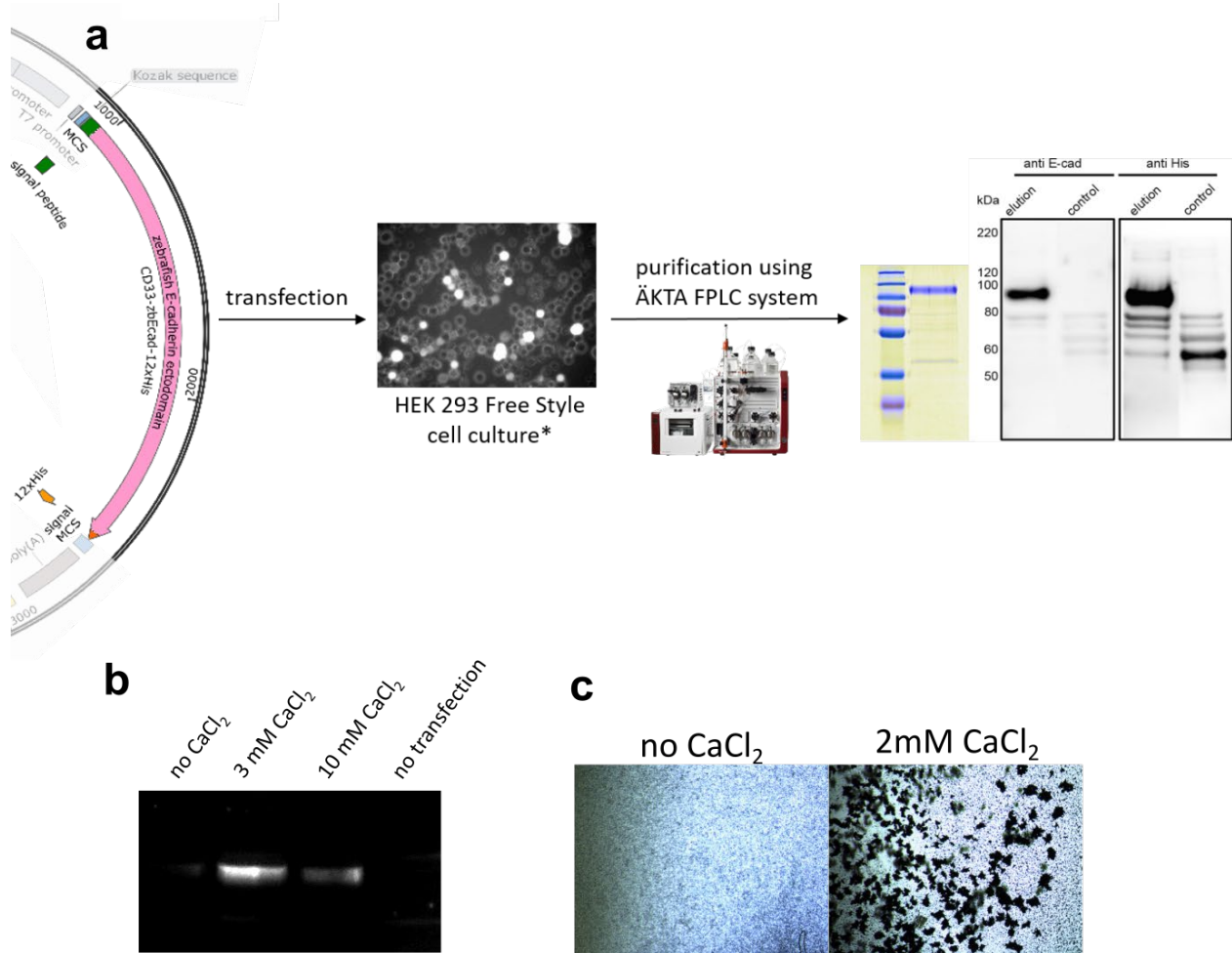


**Figure 9. Zebrafish EcadECD purification and activity.** Expression and purification strategy of EcadECD. A pcDNA(3.1-) plasmid that carries the codon-optimized zebrafish E-cadherin ectodomain sequence was placed downstream to CD33 signaling peptide and finished with a 12xHis tag. HEK 293 Freestyle cells in suspension were used for expression, a representative image transfected using polyethyleneimine with cytoplasmic GFP is shown. SDS-PAGE of purified protein is on the left side of gels, followed by western blots against zebrafish Ecad with an ectodomain recognizing antibody and against His tag. Controls are from culture media that have not been transfected with the EcadECD plasmid (a). Effects of extra calcium addition to expression media. Different amounts of calcium were added to expression media 2 days after transfection and a western blot against Ecad was carried out with samples from the culture media directly after 5 days with calcium (b). EcadECD activity assay. Cobalt-based magnetic beads incubated with zebrafish EcadECD in the presence or absence of calcium show different aggregation kinetics (c).

As it would ease the protocol, first, we tested a commercially available mouse EcadECD which carries His- and Fc-tags to induce cell-bilayer adhesion. This construct had been used in zebrafish studies from our lab before, in *in vivo* settings, to induce adhesion<sup>93,160</sup>. In order to simplify the adhesion assay, we started with gel-phase (DPPC) bilayers which would provide an immobile ligand as we measured by FRAP experiments (Fig. 10a), given that many labs successfully induced contacts with a functionalized glass of polymer surfaces with non-diffusive ligand arrays to study Ecad-mediated adhesion. However, we did not see contact formation between the mouse EcadECD functionalized bilayers and ectoderm progenitors, as the cells continued rolling on the bilayers as if on passivated surfaces (Fig. 10b). We assumed that our assay required a more specific interaction to be functional, as the mouse and zebrafish EcadECDs showed only 63% similarity in sequence (Fig. 10c).

Next, we tried our new zebrafish EcadECD construct with the same settings, with gel-phase bilayers to check the adhesive activity of the protein. The diffusion constant of the EcadECD, which was FRAPped after labeling it with Cy5, was slower than the lipid bilayer, which might be due to the protein being a bulkier structure than the lipids but also a result of cis interactions of cadherins on the bilayer surface (Fig. 9a). Many cells in cultures spread nicely on the functionalized bilayers, while *cdh1* MO cells did not spread on the bilayers and when bilayers were left undecorated cells also did not spread (Fig. 9d,e). This proved that our EcadECD construct was functional and cells spread on them due to specific adhesions. Still, it was interesting to see a spread phenotype from the cells as this is not the case when cell doublets are brought together. Therefore we looked into these contacts in more detail by imaging alpha-catenin with higher resolution. Interestingly, alpha-catenin seemed to localize to radial defined structures, reminding us of stress fibers. This observation, given that such observations were made when switching from mobile to immobile bilayers or other immobile stiff substrates before (see 1.3.2) suggests that immobile substrates might be mimicking structures formed in matrix-cell interactions rather than cell-cell interactions. This is plausible as some adhesion complex-actin linker proteins such as vinculin, also recently alpha-catenin have been found to participate in cell-cell and matrix-cell adhesions respectively, contrary to their traditional roles<sup>127,161</sup>.

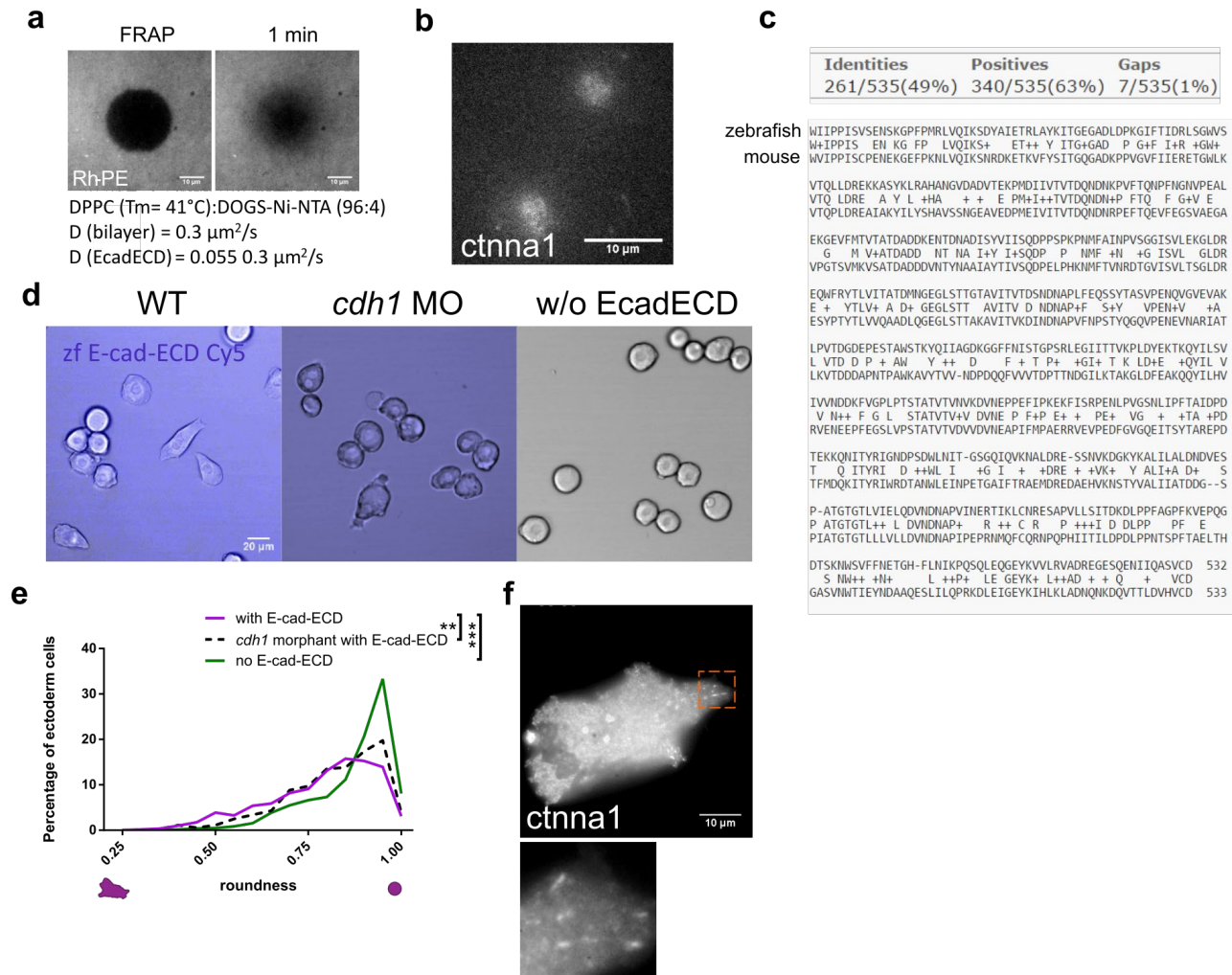


**Figure 10. Mouse and zebrafish EcadECD on gel-phase bilayers.** FRAP experiment of the gel-phase bilayer shows the slow recovery of the lipids labeled with 0.1 molar % rhodamine PE. Measured diffusion constants for rhodamine PE and EcadECD-Cy5 are given (a). Bilayer-ectoderm cell interface of cells expressing alpha-catenin-citrine seeded on mouse EcadECD functionalized gel bilayers (b). Amino acid sequence comparison between zebrafish and mouse E-cadherin ectodomains (c). Exemplary images of ectoderm progenitor cells in wild-type conditions seeded on zebrafish EcadECD functionalized gel bilayers (left), ectoderm progenitors injected with *cdh1* MO (middle), and wild-type ectoderm progenitors seeded on empty bilayers (right) (d). Quantification of contact roundness under different conditions (e). An exemplary image of alpha-catenin-citrine expressing ectoderm cell-gel-bilayer contact, below is the zoomed-in image denoted in the image above (f). Student's *t*-test (e).

Following these results, we wanted to recapitulate cell-cell adhesion on fluid bilayers to better mimic the natural architecture of nascent adhesions. We started optimizing the fluid bilayers for adhesion after seeing cells did not adhere to them right away (Fig. 11a), suggesting the viscosity of the bilayers and therefore the dragging force cellular Ecad can apply to the Ecad on the bilayer is an important factor in contact formation. We first tested various ligand densities by changing Ni-chelated lipid amounts, and on fluid bilayers, only

above 5% molar Ni-NTA lipids, we could induce adhesion. These values were already at the limit of cadherin width, showing we might have got a dense layer of EcadECD at those values, also evident by their decreased diffusion constant (Fig. 11a). Also at these values of Ni-NTA lipids we could not be sure that the bilayers would be homogenous. Therefore we went down to 4% which is commonly used in immune synapse studies. This first titration had already shown us the importance of cadherin diffusivity in inducing adhesions, so we tried decreasing the fluidity of the bilayers next to affect protein mobility. We opted for introducing cholesterol into the lipid mixture as this proved a cleaner and more homogenous method of decreasing fluid bilayer diffusion than other methods. At molar ratios of 4% Ni-NTA and 40% cholesterol, we obtained partially-fluid bilayers on which the tethered EcadECD diffused at  $0.34 \pm 0.04 \mu\text{m}^2/\text{s}$  (Fig. 11c). Cells seeded on these bilayers made large (more than  $15\mu\text{m}$  in diameter) contacts, while the contacts formed with bilayers which lacked EcadECD or used Cdh1-morphant cells remained small (Fig. 11d). Together, these observations supported that E-cadherin-functionalized partially-fluid bilayers could support E-cadherin-specific interactions with progenitor cells and form a 2D imaging platform to observe contacts.

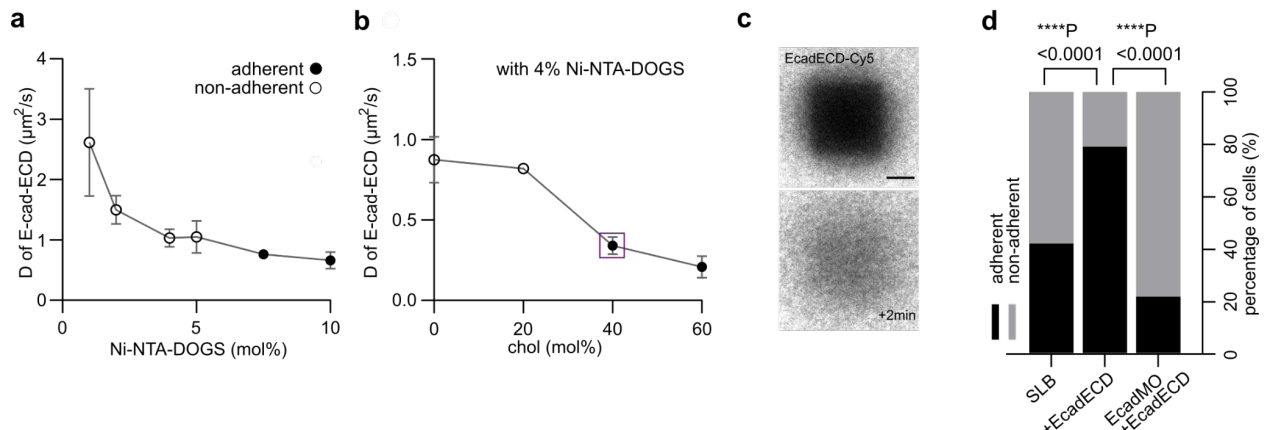


**Figure 11. Optimization of fluid bilayers.** The plot shows the diffusion constant of EcadECD-Cy5 on DOPC bilayers with Ni-NTA-DOGS titration. Empty circles denote conditions where no adhesion is seen (a). Plot shows the diffusion constant of EcadECD-Cy5 on DOPC with 4 molar % Ni-NTA-DOGS bilayers and cholesterol titration (b). An exemplary image of FRAP experiment from the working bilayer, purple rectangle in figure (b) (c). Percentage of cells adhering to empty bilayers ( $N=3$ ,  $n=48$ ), bilayers functionalized with EcadECD ( $N=3$ ,  $n=50$ ), and using *cdh1* MO injected cells on functionalized bilayers ( $N=3$ ,  $n=50$ ). Kruskal-Wallis test (d). Scale bar:  $5 \mu\text{m}$ .

## 3. 2 Contact formation dynamics

### 3.2.1 E-cadherin-mediated contact formation regulates cortical actomyosin

We first used our assay to investigate the initial steps of contact formation and recorded time-lapse movies of newly-forming contacts as they increased and stabilized in size. Cells made symmetrical contacts reminiscent of the *in vivo* situation on our working bilayer. We used the Tg(*cdh1*-mIanYFP)xt17 line to monitor the endogenous Ecad, and imaged contact formation with total internal reflection fluorescence (TIRF) microscopy,

which minimized photobleaching. The concentration of Ecad at the contact increased within 2-3 minutes of contact formation, concomitant with the contact area increase (Fig. 12a,b), in line with previous studies showing Ecad to concentrate at intercellular contacts by a diffusion-trap mechanism following trans binding (Yamada 2007, Wu 2010). On the contrary, cells seeded on bilayers without EcadECD, which we imaged under slight confinement to increase the imaging area without changing mechanical properties of the cells<sup>162</sup>, displayed characteristics of the contact-free interface and had lower Ecad intensity at their cell-bilayer interfaces (Fig.12e,f). This once again supported that the ectoderm progenitors bound specifically to the EcadECD on bilayers.

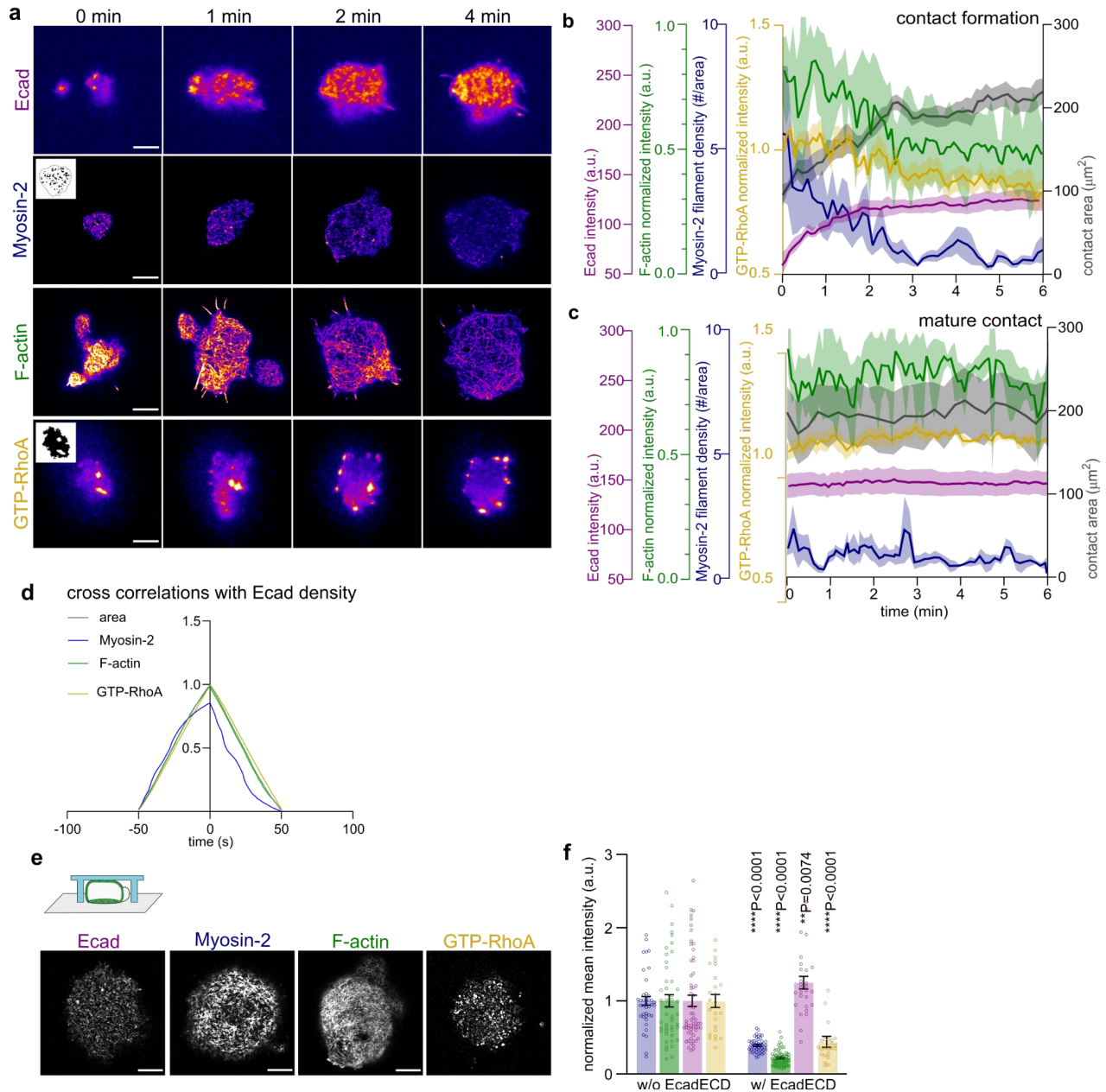


Figure 12. Dynamics of contact formation. Representative TIRF images of Ecad, Airyscan images of Myosin-2, Airyscan images of F-tractin/F-actin and TIRF images of

*AHPH/GTP-RhoA during contact formation (a). Inlets in Myosin-2 and GTP-RhoA show exemplary masks for positive signals used in intensity calculation. Plot of Ecad, Myosin-2, F-actin, GTP-RhoA fluorescent intensities and contact area over time during contact formation (on the left; Ecad N=4, n=10; Myosin-2 N=4, n=4; F-actin N=6, n=6; GTP-RhoA N=3, n=11) and at mature contacts (on the right; Ecad N=3, n=20; Myosin-2 N=3, n=4; F-actin N=5, n=7; GTP-RhoA N=4, n=7) (b,c). Cross correlations in time for the graph in (b) (d). Schematic of confined contacts on bilayers without EcadECD, and representative images of Ecad, Myosin-2, F-actin and GTP-RhoA (e). Comparison of mean intensities with and without EcadECD on bilayers for Ecad, Myosin-2, F-actin and GTP-RhoA (without EcadECD; Ecad N=3, n=33; Myosin-2 N=3, n=20; F-actin N=4, n=23; GTP-RhoA N=2, n=25; with EcadECD; Ecad N=6, n=26; Myosin-2 N=7, n=50; F-actin N=3, n=35; GTP-RhoA N=4, n=27). Mean  $\pm$  s.e.m. are shown. Mann-Whitney test (f). Scale bars are 5  $\mu$ m.*

Next, we checked whether our previous observation of actomyosin downregulation at progenitor cell-cell contacts<sup>86</sup> could be recapitulated with our reconstitution assay. We imaged Myosin-2 and F-actin separately to image them both at high resolution with Tg(actb2:Myl12.1-eGFP) transgenic line and F-actin-mNeonGreen using Airyscan imaging as these markers did not show strong photobleach. Myosin-2 appeared as filaments, initially richly decorating the cortex, as in the contact-free interface (Fig. 12a,e). As the appearance and disappearance of Myosin-2 filaments were highly dynamic throughout contact formation, we quantified the average density of filaments in the contact area. Myosin-2 was reduced at the contacts concurrently with the contact area expansion, ultimately becoming absent from the contacts and appearing only at the contact rim during retraction of protrusions such as blebs (Fig. 12a,b), that frequently travel on the contact-free surfaces of progenitor cells. These results supported that homotypic Ecad interactions led to the downregulation of Myosin-2, specifically at the contacts. Previously, studies in similar culture systems have shown F-actin to get depleted from intercellular contacts during contact expansion<sup>45,86</sup>. We noted that average F-actin intensity decreased as contacts expanded, similar to Myosin-2 however, it reached stable levels when the contact area stabilized as an F-actin network at the contact remained. Overall, the correlation between Ecad, Myosin-2 and F-actin amounts during contact expansion confirmed the increasing Ecad concentration and decreasing actomyosin levels to be coupled to promote contact expansion (Fig. 12d), and intercellular signaling activity of Ecad was active in our reconstitution assay. When looked at mature contacts (>10 min), these changes were not evident and all plotted quantifications seemed stable, confirming that the plots showing decreases in intensities did not show these trends due to photobleaching (Fig. 12c) and that the contacts had already reached maturity in terms of protein levels within the first 6 minutes they were observed.

### 3.2.2 Small GTPases for contact regulation

Small GTPases Rac and RhoA have been implicated to function at cell-cell contact sites before<sup>163</sup>, and they could modulate both Myosin-2 activity and F-actin levels. To see whether we could find a downstream link between Ecad homophilic binding and actomyosin reduction, we started screening the function of these GTPases. Rac1 was previously suggested to become active at nascent contacts and to downregulate RhoA

activity there. We tried to inhibit Rac1 function using an inhibitor, as well as a dominant negative version of the zebrafish Rac1 (DN-Rac1)<sup>143</sup>. With Rac inhibitor, we did not see a difference in the relative actin levels at the cell-cell contact vs contact-free interface (Fig. 13a). When we looked at DN-Rac1, which is functional in mesendoderm cell migration, we did not see differences in distributions of Myosin-2 or F-actin at contact interfaces (Fig. 13b,c). These observations led us to believe that Rac1 did not play an active role in the contact formation of zebrafish ectoderm progenitors.

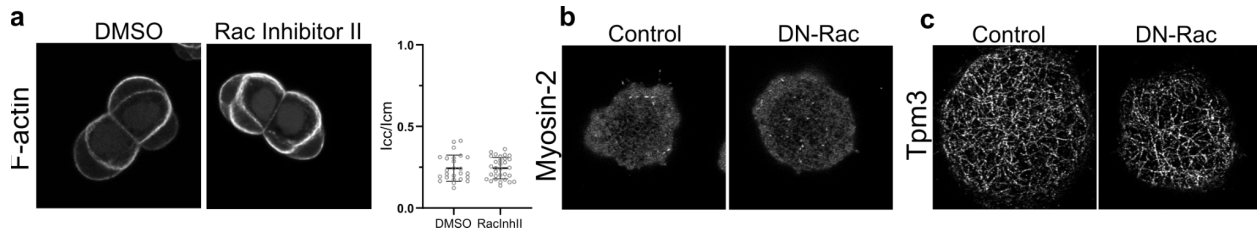


**Figure 13. Rac1 inhibition does not affect cell-cell contacts.** Single plane representative images of F-actin expressing cell doublets treated with DMSO as control or Rac Inhibitor II, with cell-cell to cell-matrix intensity ratios (DMSO N=2, n=25; RacInhII N=2, n=31). Mean  $\pm$  s.e.m. are shown. Student's t-test,  $p = 0.9969$  (a). Representative images of Myosin-2 and Tropomyosin3 (as an F-actin marker) at the cell-bilayer interfaces of control and DN-Rac1 expressing cells (b,c).

In a similar attempt to determine whether there might be decreased RhoA activity at the contacts, we tried increasing RhoA activity and seeing the changes it causes in cell doublet adhesion. When expressing a constitutively active form of RhoA (CA-RhoA), cell doublets showed smaller contact sizes as reported before<sup>145</sup>. To our surprise, this did not correlate with an enhanced decrease of actomyosin at the contact site as a result of increased global contractility. But the actomyosin amounts at the cell-cell contact seemed to increase more relative to contact-free surfaces (Fig. 14), suggesting CA-RhoA expression might have overwritten the actomyosin downregulation at the contacts of cell doublets.

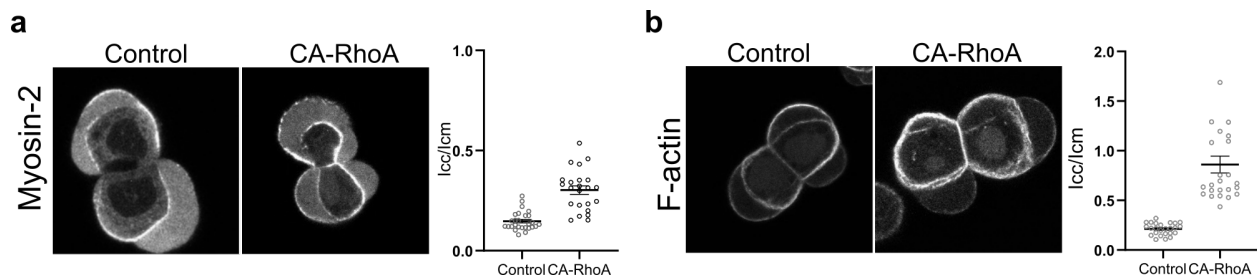


**Figure 14. RhoA overactivity affects cell-cell doublets.** Single plane representative images of Myosin-2 at the cell doublets of control and CA-RhoA expressing cells, with cell-cell to cell-matrix intensity ratios (Control N=3, n=27; CA-RhoA N=3, n=23). Mean  $\pm$  s.e.m. are shown. Mann-Whitney test, \*\*\*\* $P < 0.0001$  (a). Single plane representative images of F-actin/F-actin at the cell doublets of control and CA-RhoA expressing cells, with cell-cell to cell-matrix intensity ratios (Control N=2, n=25; CA-RhoA N=2, n=23). Mean  $\pm$  s.e.m. are shown. Mann-Whitney test, \*\*\*\* $P < 0.0001$  (b).

To investigate the WT situation further, we visualized active RhoA during contact formation using a biosensor. We tried mouse and enhanced (2xrGBD) Xenopus Rhotekin-based sensors with no success (only giving cytoplasmic signal even with CA-RhoA) and found that a human sequence construct based on Anillin Rho binding domain (GTP-RhoA) was previously used successfully in zebrafish<sup>164</sup>. Its correct localization was also evident during cytokinesis at the contractile ring, so we performed further analysis with this construct. Limited by the low signal intensity of the construct, we acquired time-lapse movies with TIRF microscopy to avoid photobleaching. We found the construct to localize diffusely at the contact site, as well as in a few cortical foci (Fig. 12a). These foci were homogeneously spread at the contact-free interface (Fig. 12e,f), and after the contact area stabilized, they localized only to the contact rim (Fig. 12a). Similar to decreases in Myosin-2 and F-actin, GTP-RhoA levels decreased at the contacts during the first 2-3 minutes of contact expansion (Fig. 12a-d).

As a control, we imaged a mutant version of the biosensor that does not bind to active RhoA (GTP-RhoA<sup>A740D E758K</sup>). In contrast to the GTP-RhoA, Levels of this construct slightly increased as contacts formed (Fig. 15a,b), validating the measured decrease in GTP-RhoA during contact expansion. Furthermore, dual-color images of Ecad and GTP-RhoA showed that Ecad clusters and GTP-RhoA lack overlap (Fig. 15c-f). This suggested that Ecad-mediated signaling at the contact locally repressed RhoA activity, which could downregulate Myosin-2 and F-actin levels. To test this hypothesis further, we imaged cells injected with CA-RhoA as they formed contacts. In CA-RhoA-injected cells, while Ecad levels increased similarly as the contact area increased, GTP-RhoA levels did not decrease (Fig. 15g,h), showing that the decrease of GTP-RhoA was overwritten at these contacts. Furthermore, neither F-actin nor Myosin-2 decreased at the contacts, and contacts maintained a dense cortex decorated with Myosin-2 filaments with a small contact area. Together, these findings led us to conclude that homotypic Ecad interactions promote contact expansion by downregulating RhoA activity at the contacts.

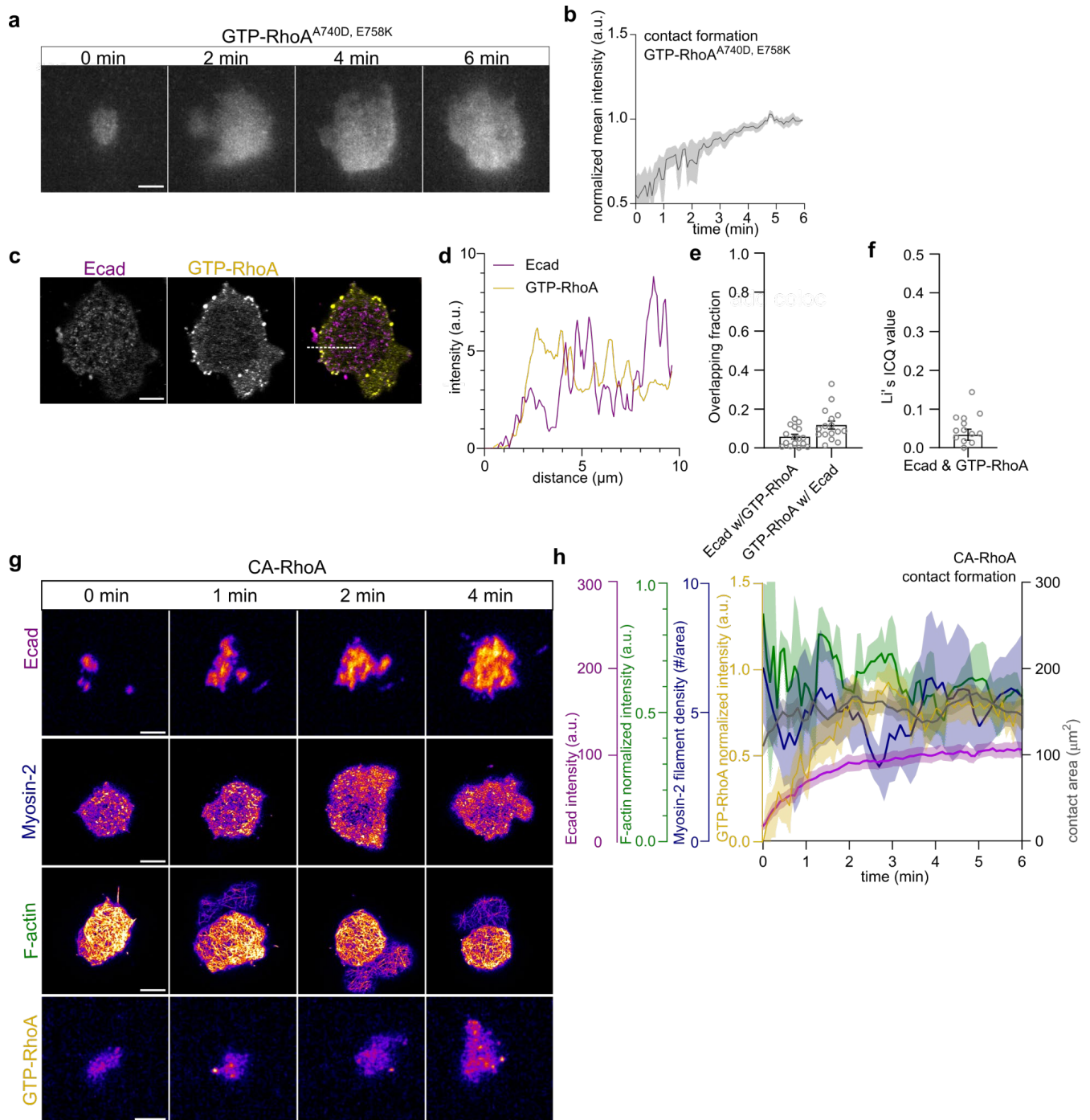


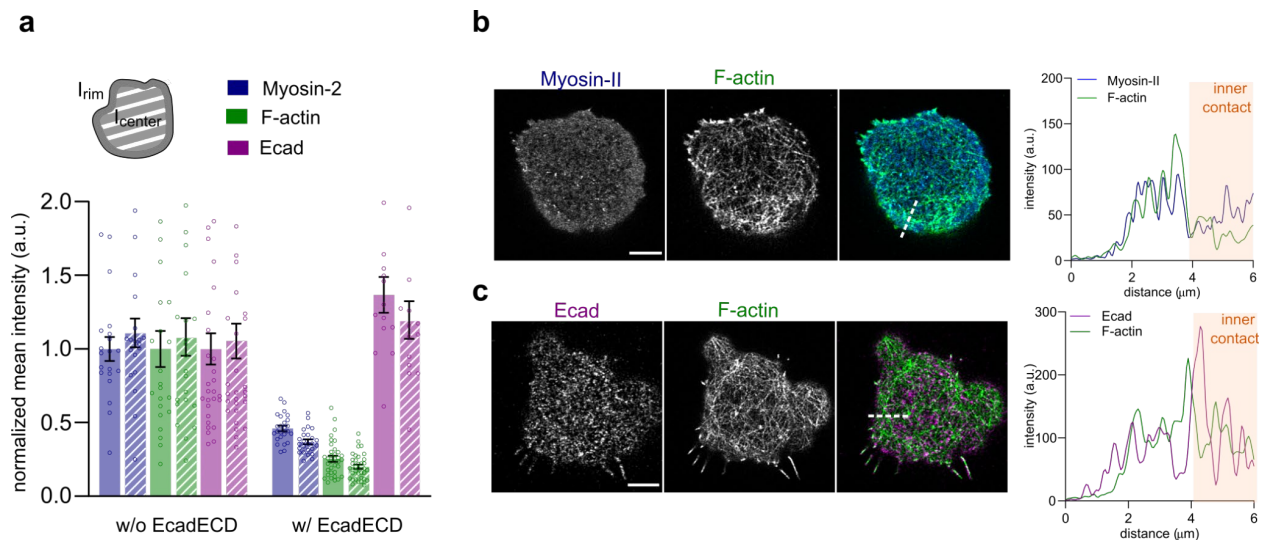
**Figure 15. RhoA-mediated changes at the contact.** Representative TIRF images of the mutant AHPHA740D E758K/GTP-RhoAA740D E758K during contact formation (a). The plot of mean intensity at the contact over time for GTP-RhoAA740D E758K ( $N=4$ ,  $n=7$ ) (b). Representative dual-color images of Ecad-Tom cells expressing GTP-RhoA-NG, in the merged tab Ecad is labeled purple and GTP-RhoA yellow (c). The plot of intensities for Ecad and GTP-RhoA signals over the dashed line in (c) (d). Bar plots of Manders' coefficients for colocalization quantification of Ecad with GTP-RhoA (left) and GTP-RhoA with Ecad (right). (e). Bar plot of Li's ICQ value for colocalization quantification of Ecad and GTP-RhoA (f). Mean  $\pm$  s.e.m. are shown. ( $N=1$ ,  $n=14$ ) (e,f). Representative

TIRF images of Ecad, Airyscan images of Myosin-2, Airyscan images of F-actin/F-actin and TIRF images of AHPH/GTP-RhoA during contact formation (g). Plot of Ecad, Myosin-2, F-actin, GTP-RhoA fluorescent intensities and contact area over time during contact formation (Ecad  $N=2$ ,  $n=13$ ; Myosin-2  $N=3$ ,  $n=5$ ; F-actin  $N=3$ ,  $n=3$ ; GTP-RhoA  $N=3$ ,  $n=9$ ) (h). Scale bars are 5  $\mu\text{m}$ .

### 3. 3 Centrifugal flows redistribute F-actin and E-cadherin

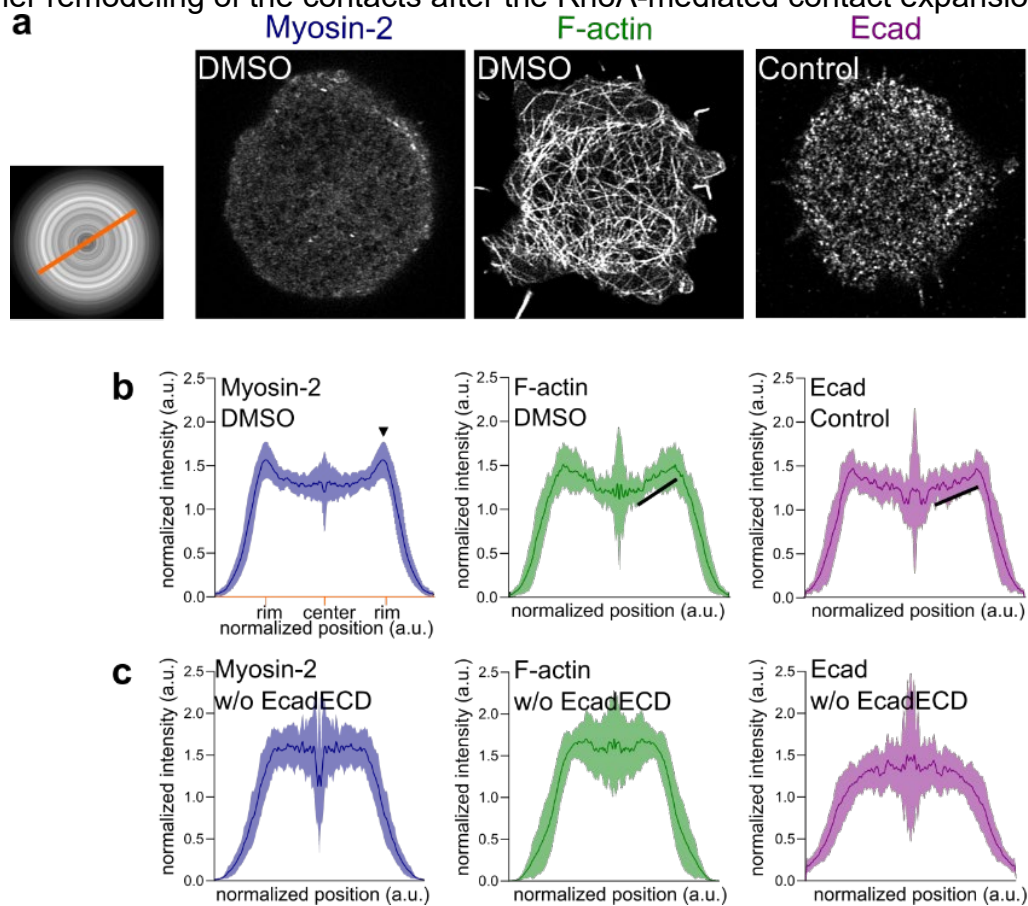
Next, we examined whether the Ecad and F-actin accumulated at the contact rim, as seen in the cell doublets of the ectoderm cells at the cell-bilayer contacts. We found that even though a general reduction in actomyosin was present as we measured (Fig. 12a,b), actomyosin reduction was less pronounced at the contact rim than the contact center; and while Ecad increased overall in the whole contact, it accumulated more at the contact rim (Fig. 16a).

The ring-like accumulation of F-actin separated distinct cortical organizations: we can think of this accumulation as an actin arc, seen in immune synapses, as it forms mostly circumferential arrays of actin sporadically decorated with Myosin-2 filaments, though weaker than the actin arc of the immune synapse as it gets disorganized easily with cell protrusions sometimes (Fig. 16b). The narrow zone between the F-actin arc and the contact edge exhibits a contractile cortex, reminiscent of the contact-free cortex above it. This cortex was not always visible (sometimes the edge was the actin arc itself), but mostly when blebs occurred and got retracted, a dense network of actin got built there in a fast fashion, and Myosin-2 minifilaments decorated it, possibly helping with the bleb retraction as described in literature before<sup>165</sup>. Due to these retractions, this zone showed occasional fast centripetal F-actin flows starting at the cell edge and ending at the arc, which marks the outer edge of the “real contact”, and the blebs cannot go further than it. Compared to the outer zone, the inner zone showed a less dense and more stable F-actin network. Notably, Ecad accumulation occurred at the edge of this inner zone, as it did not get into the actin arc (Fig. 16c).



**Figure 16.** Contact architecture at the contact rim vs. center. Plot of mean intensities for Myosin-2, F-actin and Ecad at the contact rim and contact center on bilayers with or without EcadECD. Mean  $\pm$  s.e.m. are shown (a). Representative dual-color images of Myosin-2-GFP; Utrophin-mCherry line cells, in the merged tab Myosin-2 is labeled blue and F-actin green, with plot of intensities for Myosin-2 and F-actin signals over the dashed line in (b). Representative dual-color images of Ecad-YFP line cells expressing Ftractin-KO, in the merged tab Ecad is labeled purple and F-actin green, with the plot of intensities for Ecad and F-actin signals over the dashed line in (c). Scale bars are 5  $\mu$ m.

To further investigate the architecture of Ecad-mediated contacts, we built radial intensity profiles of Myosin-2, F-actin and Ecad at mature contacts (Fig. 17a,b). This analysis showed Myosin-2 to peak specifically at the contact rim, showing a rather binary response to biochemical changes. Meanwhile, F-actin and Ecad formed a continuous gradient along the contact radius, increasing levels from the center towards the rim of the mature contacts. Such gradients were not seen in contacts without EcadECD, showing the specificity of these contacts to E-cad-mediated adhesion (Fig. 17c). The gradients appeared during the fast contact expansion phase and continued to get steeper for 2-3 min after the total amounts of F-actin and Ecad were stabilized (Fig. 17d,e), suggesting further remodeling of the contacts after the RhoA-mediated contact expansion.



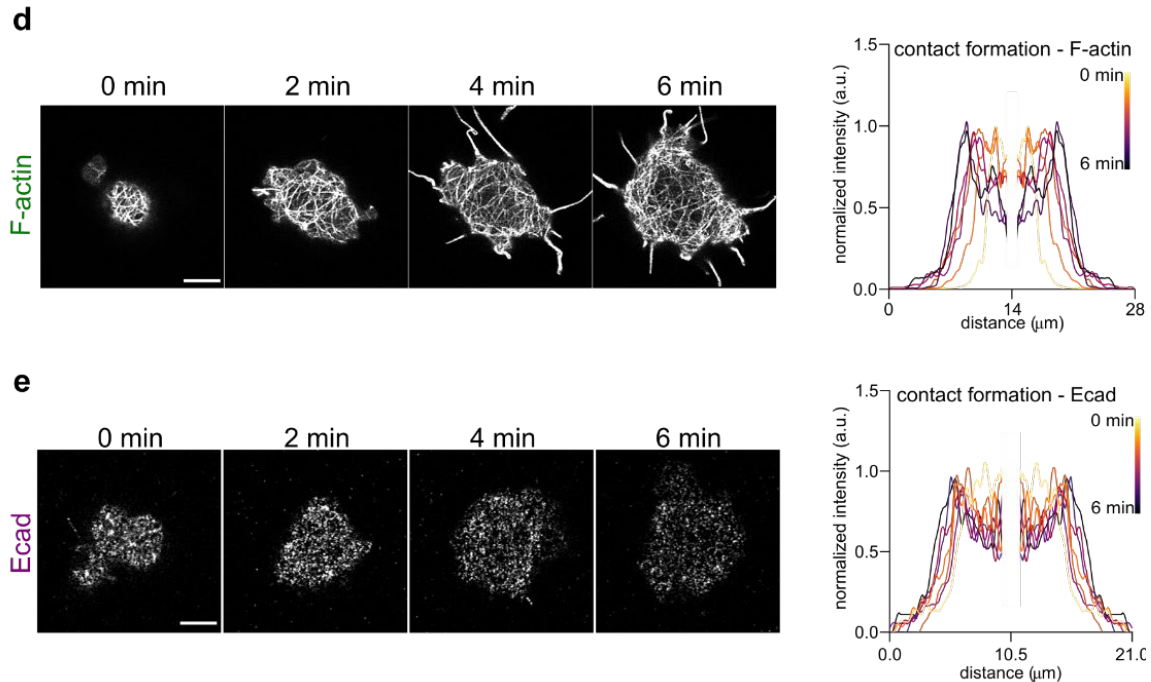


**Figure 17. Radial intensity profiles at the contact.** Airyscan snapshots of Myosin-2, F-actin/F-actin and Ecad at the contact, given with an exemplary radial intensity image where the profile is calculated along the orange line (a). Radial intensity plots, which are normalized by contact length and average intensity, for Myosin-2 treated with DMSO, F-actin treated with DMSO and Ecad (Myosin-2  $N=3$ ,  $n=22$ ; F-actin  $N=3$ ,  $n=20$ ; Ecad  $N=4$ ,  $n=20$ ). Arrowhead points to the Myosin-2 peak, and lines show the gradual increases in F-actin and Ecad profiles (b). Radial intensity plots for Myosin-2, F-actin and Ecad on bilayers without EcadECD (Myosin-2  $N=3$ ,  $n=18$ ; F-actin  $N=3$ ,  $n=19$ ; Ecad  $N=3$ ,  $n=29$ ) (c). Representative images of F-actin during contact formation and intensity profiles from indicated times, normalized to maximum intensity (d). Representative images of Ecad during contact formation, along with intensity profiles from indicated times, normalized to maximum intensity (d). Mean  $\pm$  s.e.m. are shown (b,c). Scale bars are 5  $\mu\text{m}$ .

To confirm these results with a second approach, we analyzed the F-actin network density at the maturing contacts (Fig. 18a). In a fashion temporarily similar to the F-actin gradient establishment, network density decreased for several more minutes after the fast contact expansion phase, diluting the actin network at the contact even further (Fig. 18b). Network density formed a gradient similar to F-actin intensity, suggesting that the radial intensity profile of F-actin is due to changes in network density (Fig. 18c). Overall, these results hinted at the possibility of a different mechanism, which spatially redistributed the maintained pools of F-actin and Ecad at the contact.

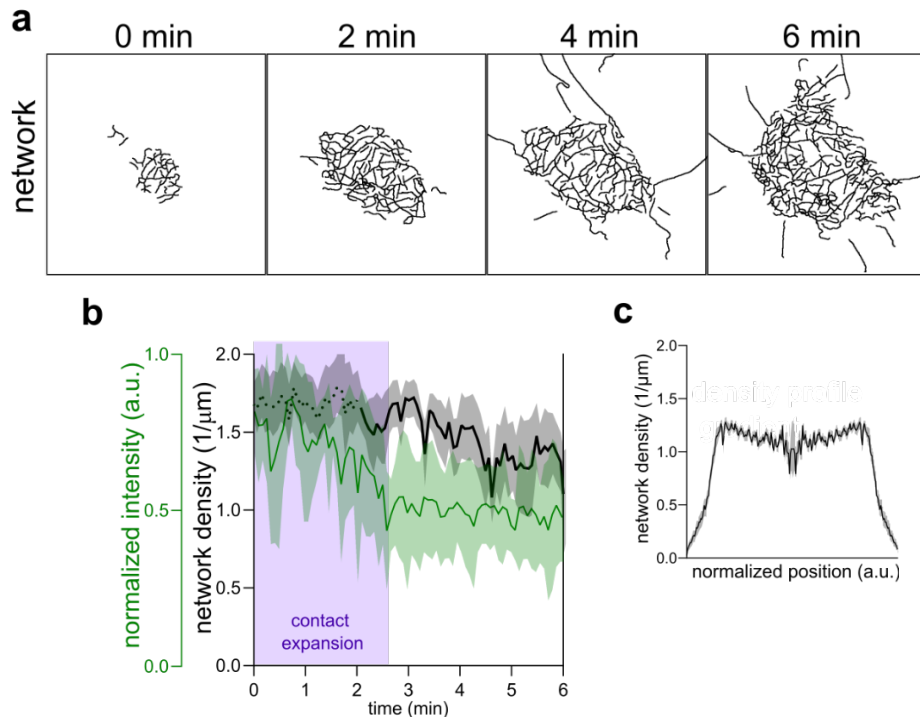


**Figure 18.** *F-actin network density at the contact. Representative images of the SOAX-skeletonized F-actin network during contact formation of Fig. 17d (a). The plot of F-actin fluorescent intensity (repeated from (Fig. 12b) and F-actin network density over time during contact formation (F-actin network density  $N=6$ ,  $n=6$ ). The contact expansion phase of initial minutes is indicated in purple (b). Radial network density profile of F-actin ( $N=5$ ,  $n=23$ ). Mean  $\pm$  s.e.m. are shown (b,c).*

As contact formation disrupts the uniform distribution of the contractility indicator Myosin-2 at the cortex, we asked whether this anisotropy would induce cytoskeletal flows directed toward the contact rim with peak Myosin-2 levels. We hypothesized that such centrifugal flows could mechanically mediate the translocation of proteins outwards. We sought to demonstrate the presence of centrifugal flows via kymographs along the inner contact diameter where Ecad accumulates. This analysis showed that F-actin filaments move predominantly from the contact center towards the rim ( $0.22 \pm 0.09 \mu\text{m}/\text{min}$ ) in mature contacts, consistent with our hypothesis (Fig. 19a-c). The flows appear during contact formation and continue in mature contacts, supporting the idea that a protected Myosin peak activity could cause them (Fig. 19d). To understand how these flows are established and related to the concomitant accumulation of Ecad at the contact edge, we turned to Myosin-2, previously shown to represent the main determinant of cortical actin contractility and flow. To address the possibility that flows might be Myosin-2 mediated, we blocked Myosin-2 activity in the contacting cell by exposing it to the Myosin-2 inhibitor para-nitroblebbistatin (pnBb) and analyzed resultant changes in F-actin flows at the contact<sup>166</sup>. Centrifugal F-actin flows at the contact were not detectable anymore upon pnBb treatment (Fig. 19c,i), and pnBb-treated contacts displayed higher F-actin network density (Fig. 19k), alongside radial profiles showing no enrichment towards the contact rim for F-actin (Fig. 19h) supporting the notion that such flows are generated by the

asymmetric distribution of Myosin-2 at the contact edge and contribute to further dilution of the F-actin network at the contacts.

We analyzed changes in Ecad distribution at the contact disc to explore further whether and how the centrifugal flows of F-actin at the contact disc are related to the graded distribution and accumulation of E-cadherin at the contact edge. Since Ecad clusters have previously been shown to be taken along by F-actin flows (see 1.2.2), we hypothesized that the observed centrifugal F-actin flows at the contact disc might trigger similar flows of Ecad, leading to Ecad gradient formation and contact edge accumulation. Kymograph analysis revealed single Ecad clusters flowing centrifugally (Fig. 19a-c) with an average net velocity ( $0.28 \pm 0.64 \mu\text{m}/\text{min}$ ) similar to F-actin filaments (Fig. 19b,c), supporting the notion of Ecad flowing towards the contact edge by advection with the centrifugal F-actin flow. In order to check whether low contractility halts Ecad flows as well, we used CA-Mypt-expressing Ecad-YFP cells as pnBb treatment caused Ecad-mlanYFP signal-to-noise ratio to weaken. CA-Mypt-expressing contacts were similar to pnBb-treated contacts in which they demolished the rim enrichment of F-actin and resulted in higher network densities at the contact (Fig. 19j,k). CA-Mypt-expressing contacts did not show any enrichment for Ecad (Fig. 19h) and halted centrifugal Ecad cluster flows (Fig. 19c,i). A control experiment we did with pnBb using Ecad-Tom-expressing cells that could be imaged without bleaching for a short while gave a distribution of Ecad similar to CA-Mypt-expressing contacts (Fig. 19l), validating our observations of pnBb and CA-Mypt can be used interchangeably within our context.

Further analysis of colocalization of distinct Ecad clusters showed a partial colocalization of Ecad clusters with the F-actin filaments (Fig. 19f,g), suggesting that not all Ecad clusters were directly linked to F-actin, consistent with Ecad flowing by advection rather than direct transport by the F-actin network.

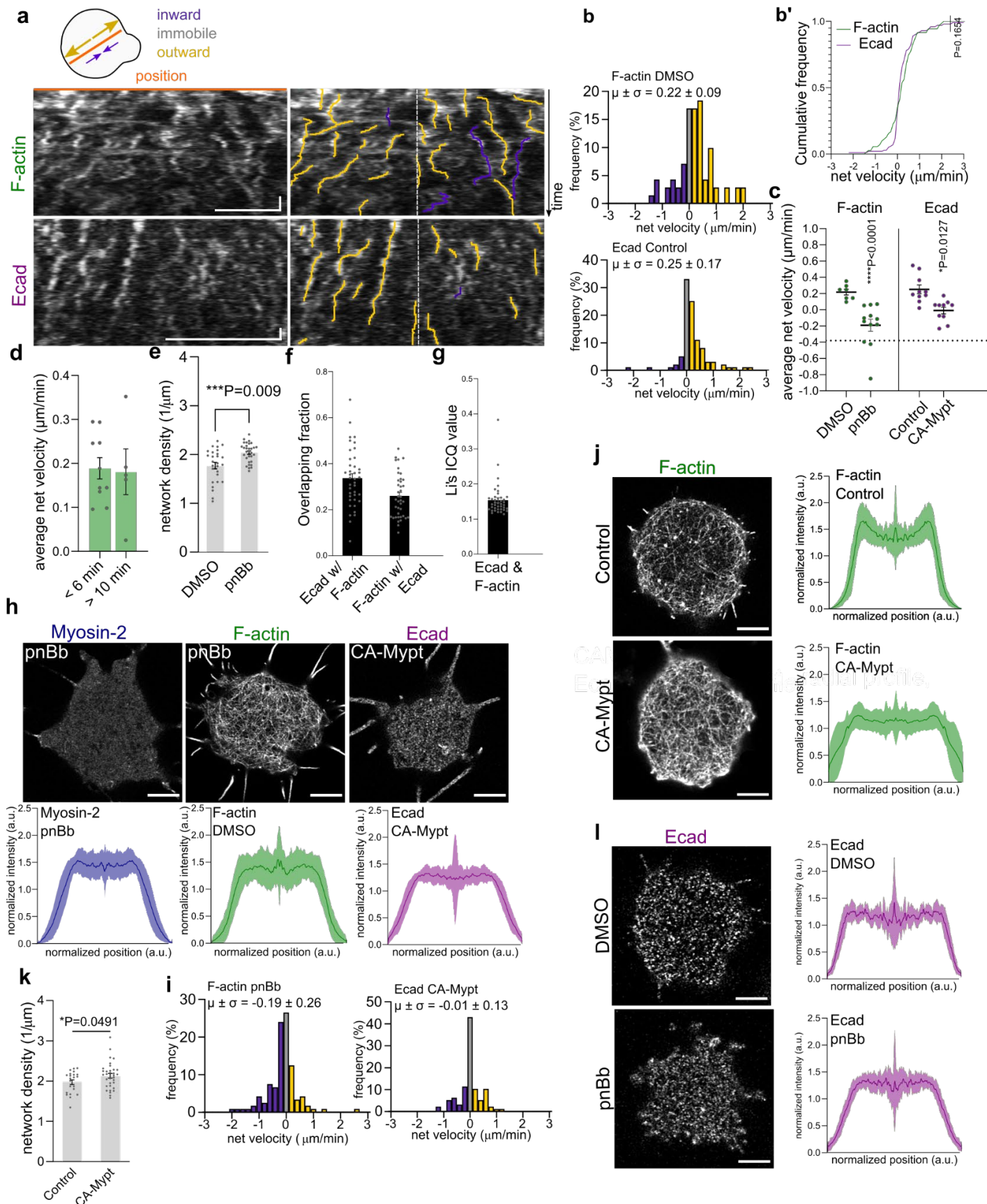


*Figure 19. Myosin-2-activity-dependent flows of F-actin and Ecad. Schematic of the contact showing contact diameter excluding protrusions as the kymograph position and giving allocation of flow direction. Kymographs of the contacts expressing F-actin (above) and Ecad (below), along with tracks superimposed on the raw data (right). Outward-directed tracks are labeled in yellow, and inward-directed tracks are labeled in purple (a). Histograms of net track velocities for F-actin treated with DMSO and Ecad (F-actin N=5, n=7; Ecad N=4, n=10; 10 tracks from each cell)(b). The plot of cumulative net velocities of data shown in (b), Kolmogorov-Smirnov test (b'). The plot of average net track velocity per cell. DMSO or pnBb-treated F-actin-labeled cells and control or CA-Mypt-injected Ecad-expressing cells are quantified (F-actin DMSO N=5, n=7; F-actin pnBb N=8, n=12; Ecad control N=4, n=10; Ecad CA-Mypt N=3, n=10). Mann-Whitney test (c). Average net velocities of F-actin tracks for newly-forming contacts (N=4, n=10) and mature contacts (N=5, n=5). Mann-Whitney test. P=ns. (d). Comparison of F-actin network density for DMSO-treated and pnBb-treated contacts (DMSO N=3, n=27; pnBb N=3, n=25). Student's t-test. (e). Bar plots of Manders' coefficients for colocalization quantification of Ecad-Tom-expressing cells injected with F-actin-KO as F-actin marker (N=2, n=40)(f). Bar plot of Li's ICQ value for colocalization quantification of the same cells as in (f)(g). Airyscan snapshots of Myosin-2 treated with pnBb, F-actin treated with pnBb and Ecad injected with CA-Mypt at the contact, with radial intensity plots, which are normalized by contact length and average intensity, for each marker below (Myosin-2 pnBb N=3, n=20; F-actin pnBb N=3, n=24; Ecad CA-Mypt N=3, n=25) (h). Histograms of net track velocities for F-actin treated with pnBb and Ecad injected with CA-Mypt (F-actin pnBb N=8, n=12; Ecad CA-Mypt N=3, n=10; 10 tracks from each cell)(i). Representative Airyscan images of F-actin for control and CA-Mypt-expressing cells, along with radial intensity plots (F-actin control N=3, n=31; F-actin CA-Mypt N=3, n=25) (j). Comparison of F-actin network density for control and CA-Mypt-expressing contacts (Control N=4, n=22; CA-Mypt N=4, n=34). Student's t-test (k). Representative Airyscan images of Ecad-Tom for DMSO-treated and pnBb-treated cells, along with radial intensity plots (Ecad DMSO N=2, n=15; Ecad pnBb N=2, n=24) (l). Scale bars are 5  $\mu$ m on the x-axis and 1 min on the y-axis.*

As the flows are contractility-dependent, we wondered how increased contractility would impact the contact dynamics. We treated cells with lysophosphatidic acid (LPA), a contractility amplifier, and analyzed the radial distribution of proteins at the contact. F-actin showed a very strong peak at the contact rim (Fig. 20a,c), in line with our previous study where LPA increased rim accumulation of F-actin<sup>145</sup>. While Ecad did not show a strong peak like F-actin, it formed a steeper gradient than the control (Fig. 20a,c). The differences in distribution profiles of F-actin and Ecad support that the profiles may not be maintained via direct coupling. The network density of F-actin had dropped in comparison to the control, as expected by more F-actin being carried to the rim, leading to higher rim accumulation (Fig. 20cb). Next, we measured flow velocities at LPA-treated contacts, and to our surprise, flow velocities did not show an increase (Fig. 20d,e). When carefully inspecting the contacts, we realized that most LPA-treated contacts had some ectopic F-actin foci, which could explain why the flows would not get faster, as these foci would create instabilities in the contractility gradient. Indeed, the foci were also positive for Myosin-2 (Fig. 20f), forming local peaks of contractility in the normally Myosin-free contact zone. Interestingly, local recruitment of Ecad was present around the ectopic actomyosin

foci (Fig. 20g), and we observed centripetal F-actin and Ecad flows towards them (Fig. 20e), opposite in direction to what we had so far observed at the contacts. This observation strengthens our hypothesis that cortical flows of F-actin and Ecad, arising due to Myosin-2 anisotropy, result in Ecad enrichment around higher-contractility sites.

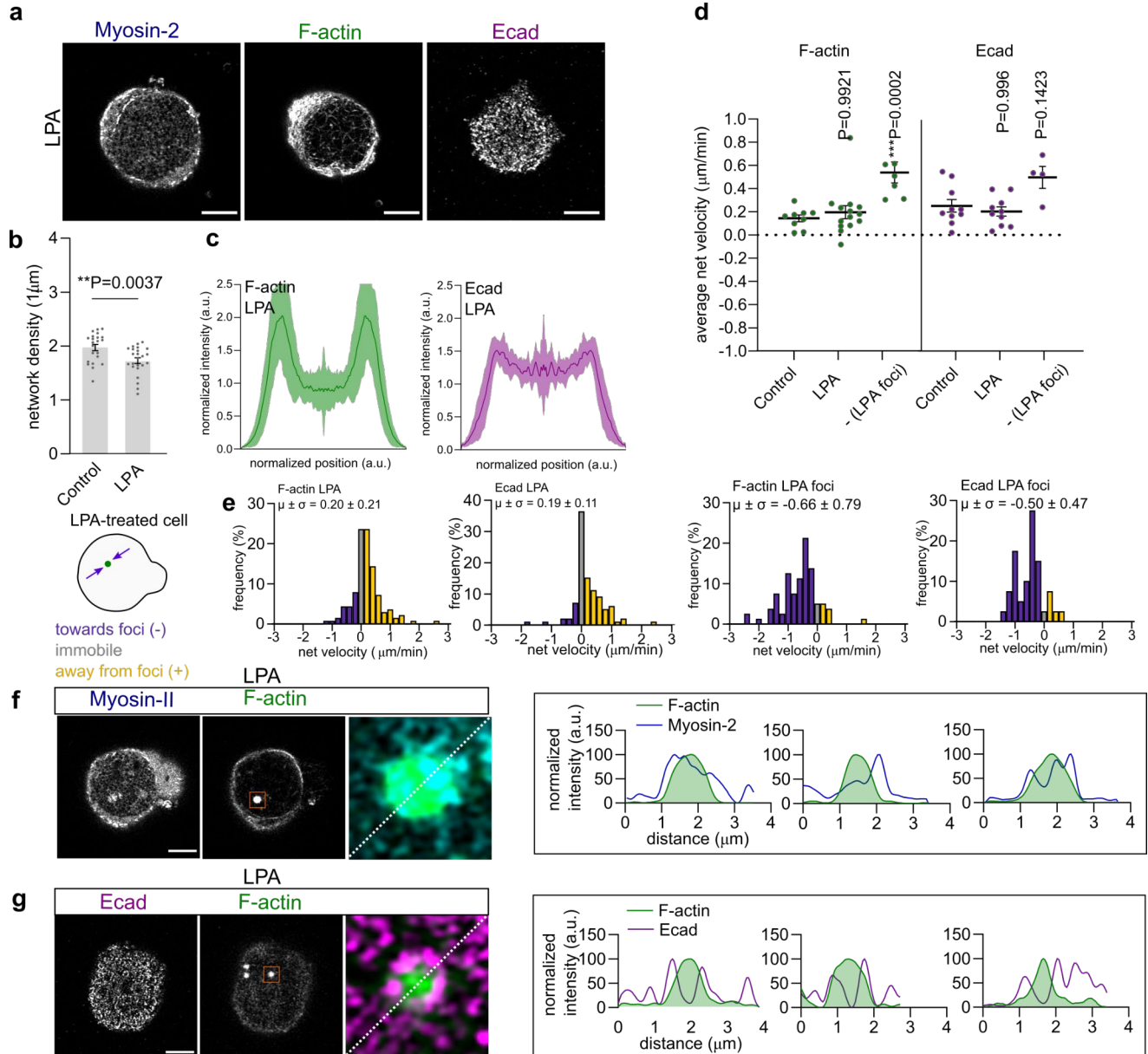


**Figure 20. Contractility-enhanced contact dynamics.** Airyscan snapshots of Myosin-2, F-actin and Ecad treated with LPA (a). Comparison of F-actin network density for control and LPA-treated contacts (control  $N=3$ ,  $n=22$ ; LPA  $N=2$ ,  $n=24$ ). Student's  $t$ -test (b). Radial intensity plots of LPA-treated contacts for F-actin and Ecad (F-actin Control  $N=8$ ,  $n=11$ ; F-actin LPA  $N=3$ ,  $n=34$ ; Ecad LPA  $N=3$ ,  $n=16$ ) (c). The plot of average net track velocity per cell. LPA-treated contacts and local flows around LPA-induced foci are quantified (F-actin Control  $N=6$ ,  $n=9$ ; F-actin LPA  $N=7$ ,  $n=14$ ; F-actin LPA foci  $N=3$ ,  $n=5$ , 7 foci; Ecad LPA  $N=6$ ,  $n=10$ ; Ecad LPA-foci  $N=3$ ,  $n=4$ , 4 foci). Mann-Whitney test. Ecad

*control is repeated from Fig. 19c (d). Histograms of net track velocities for F-actin and Ecad treated with LPA (F-actin LPA N=7, n=14; F-actin LPA foci N=3, n=5, 7 foci; Ecad LPA N=6, n=10; Ecad LPA-foci N=3, n=4, 4 foci; 10 tracks from each cell)(e). Representative dual-color images of Myosin-2-GFP; Utrophin-mCherry line cells. In the merged tab, zoom-in of the rectangle in the middle picture is shown; Myosin-2 is labeled blue and F-actin green, with the plot of intensities for Myosin-2 and F-actin signals over the dashed line (leftmost) and two more examples of line intensities taken over foci from different contacts (f). Representative dual-color images of Ecad-YFP line cells injected with Ftractin-KO as F-actin marker. In the merged tab, zoom-in of the rectangle in the middle picture is shown; Ecad is labeled purple and F-actin green, with the plot of intensities for Ecad and F-actin signals over the dashed line (leftmost) and two more examples of line intensities taken over foci from different contacts (g). Error bars show mean  $\pm$  s.e.m. (c,d).*

With these observations, we identified two critical mechanisms underlying cortical actomyosin depletion at the contact disc and Cadherin accumulation at the contact edge: downregulation of RhoA signaling downstream to trans-bound E-cadherin depletes Myosin-2 and decreases F-actin levels at the forming contact. This localized downregulation of cortical actomyosin contractility at the contact versus the remainder of the cell cortex leads to centrifugal flows of F-actin and E-cadherin towards the contact edge, causing their accumulation there. As we had manipulations of cortical tension to support this hypothesis, we checked the amounts of F-actin and Ecad under these conditions (Fig. 21a). Following our conclusions, when treating cells with LPA or pnBb, there were no significant changes in the Ecad amounts, suggesting the initial homophilic binding stage is relatively passive. F-actin amounts also did not differ between conditions showing that the Ecad-mediated downregulation occurs rather homogeneously between different conditions. The second phase, which is based on the contractility differences between the contact and the contact-free surface, redistributes the available pool of Ecad and F-actin within the contact. As for F-actin quantification, we used Ftractin, a marker we injected into the embryos. Therefore we wanted to double-check this observation using phalloidin staining, an unquestionable marker of F-actin (Fig. 21b). We quantified within single cells, the intensity differences at the contact in comparison to the contact-free interface. LPA-treatment enhanced the differences, but the low contractility conditions did not differ significantly from their respective controls. This observation is different from the cell doublet situation; when two cells are brought together under Blebbistatin treatment, we would not expect them to make large contacts, and their F-actin levels would not be significantly reduced in the barely formed contacts, as in this case, contact expansion through contact-free cortex tension would not take place. However, on bilayers, the geometry is different, probably since an infinite pool of adhesion molecules exists providing a high adhesion tension, the low surface tension of the pnBb or CA-Mypt cells can be broken and cells can easily spread on the surface (Fig. 21c) possibly through a wetting mechanism, different from cell doublets. This discrepancy helps us see that as soon as cadherin adhesion exists, actomyosin reduction can occur through signaling.

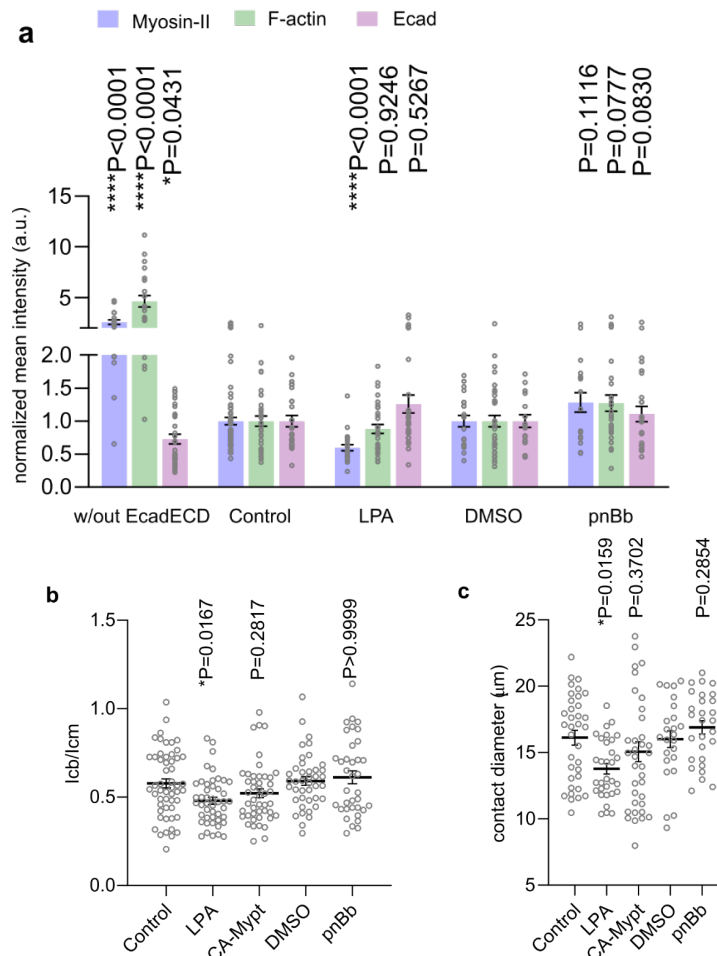


**Figure 21. Contact manipulations.** Plot of mean intensities for Myosin-2, F-actin and Ecad at the contact for contacts without EcadECD, control, LPA treatment, DMSO treatment and pnBb treatment. (w/out EcadECD Myosin N=3, n=20; F-actin N=4, n=23; EcadYFP N=3, n=33; Control Myosin-2 N=7, n=50; F-actin N=3, n=35; EcadYFP N=6, n=26; LPA Myosin-2 N=3, n=25; F-actin N=3, n=30; EcadYFP N=4, n=29; DMSO Myosin-2 N=3, n=21; F-actin N=3, n=39; EcadTom N=2, n=16; pnBb Myosin-2 N=3, n=16; F-actin N=3, n=28; EcadTom N=2, n=25) Kruskal-Wallis test for w/outECD, Control and LPA. Student's t test for Myosin-2 DMSO and pnBb. Mann-Whitney test for F-actin and Ecad DMSO and pnBb. w/out EcadECD and Control are repeated from Fig12f (a). Quantification of cell-bilayer/contact-free interfaces intensity ratios for phalloidin staining of DMSO-treated, pnBb-treated, control, LPA-treated and CA-Mypt-expressing cells (DMSO N=2, n=41; pnBb N=2, n=36; control N=2, n=53; LPA N=2, n=; CA-Mypt N=2, n=48) (b). Plot of contact diameters for control, LPA-treated, CA-Mypt-expressing, DMSO-treated and pnBb-treated cells (Control N=3, n=35; LPA N=3, n=31; CA-Mypt N=3, n=36; DMSO N=3, n=24; pnBb N=2, n=28). Kruskal-Wallis test for Control, LPA and CA-Mypt. Student's t test for DMSO and pnBb (c). Mean  $\pm$  s.e.m. are shown.

## 3. 4 Effects of turnover on contact dynamics

### 3.4.1 Reduced actin turnover increases rim accumulation

Increased turnover, also via LPA, was previously shown to reduce actin and Ecad turnovers<sup>45,145</sup>. As these contacts had more rim accumulation even though their flow velocity did not differ from contacts and decreased network density, we sought whether the results we saw could be due to reduced actin turnover, allowing more time for the network to be carried centrifugally. We treated cells with low amounts of Jasp, in order not to stabilize contacts completely, and ran radial profile, network density and flow analysis. As shown before, Jasp-treated contacts had high rim accumulation of F-actin and Ecad (Fig. 22a,b). F-actin seemed more bundled, and these structures accumulated circumferentially. These bundles made tracing quite easy, and we observed flows faster than the control for F-actin and Ecad, showing the flows are coupled (Fig. 22c,d). Faster flows could be due to a more connected network, experiencing the forces from rim more efficiently. These faster flows and increased network stability led to a more diluted actin network, as expected (Fig. 22e).

Clear dynamics of the Jasp-treated contacts allowed us to analyze F-actin flow profiles with particle image velocimetry (PIV) at these contacts in a more spatially-resolved way. Recapitulating our observations, LPA addition did not change Jasp-treated flow velocities, yet pnBb abolished them (Fig. 22f,g). The average flow velocities, averaged over circumferential rings starting from the center of mass, increased from the center towards the contact rim and stopped at the rim, resulting in compression accumulating F-actin and Ecad at the rim.

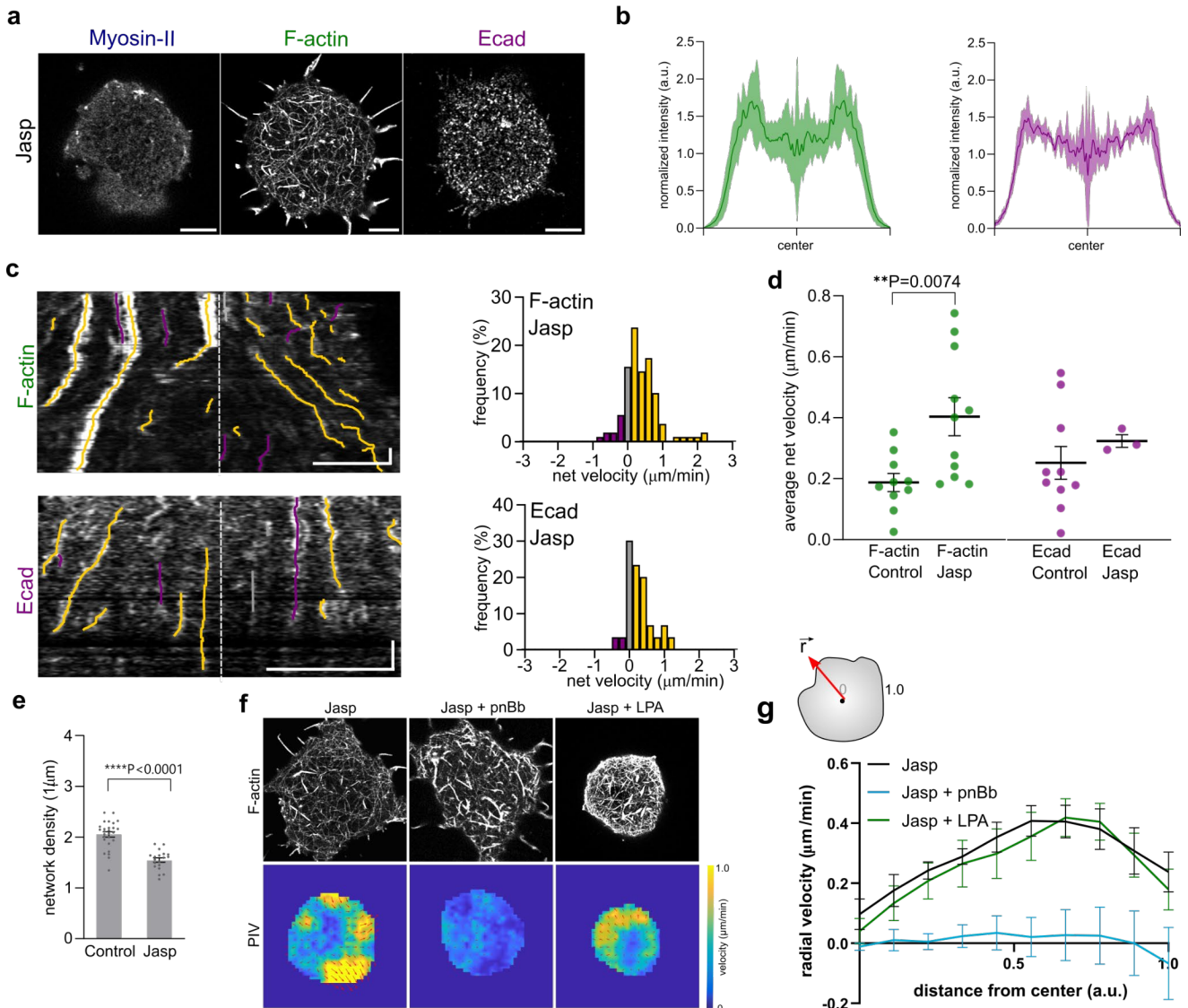


**Figure 22. Jasp-treated contacts.** Airyscan snapshots of Myosin-2, F-actin and Ecad treated with Jasp (a). Radial intensity plots of Jasp-treated contacts for F-actin and Ecad (F-actin Jasp  $N=4$ ,  $n=23$ ; Ecad Jasp  $N=2$ ,  $n=6$ ) (b). Kymographs of Jasp-treated contacts expressing F-actin (above) and Ecad (below), tracks superimposed on the raw data. Outward-directed tracks are labeled in yellow, and inward-directed tracks are labeled in purple. Histograms of net track velocities for F-actin and Ecad treated with Jasp (F-actin  $N=8$ ,  $n=11$ ; Ecad  $N=2$ ,  $n=3$ ; 10 tracks from each cell) (c). Plot of average net track velocity per cell for Jasp-treated contacts (F-actin  $N=8$ ,  $n=11$ ; Ecad  $N=2$ ,  $n=3$ ) Control is repeated from Fig. 20c. Mann-Whitney test. Control is repeated from Fig. 19c (d). Comparison of F-actin network density for Control (repeated from Fig. 20b) and Jasp-treated contacts (Jasp  $N=4$ ,  $n=19$ ) Student's  $t$ -test. (e). Airyscan snapshots of F-actin for Jasp-treated, Jasp plus pnBb-treated and Jasp plus LPA-treated cells (above), with PIV maps averaged over time lapses (below) (f). Plot of radial net velocities of Jasp-, Jasp plus pnBb- and Jasp plus LPA-treated cells along the contact radius (Jasp  $N=2$ ,  $n=3$ ; Jasp+pnBb  $N=3$ ,  $n=6$ ; Jasp+LPA  $N=3$ ,  $n=5$ ). Mean  $\pm$  s.e.m. are shown. Scale bars are  $5 \mu\text{m}$  on the  $x$ -axis and  $1 \text{min}$  on the  $y$ -axis.

### 3.4.2 Molecular turnover measurements

As Myosin-2 driven accumulation of F-actin and Ecad at the contact edge not only depends on their centrifugal flow velocities but also on their turnover, we measured actin lifetime by single-molecule imaging of injected TRITC-Actin protein and Ecad lifetime using FRAP.

As actin-GFP mRNA injection gave a homogenous cytoplasmic signal, TRITC-Actin protein injection proved the best option to measure actin lifetime. Injection of this protein in small quantities at the one-cell stage resulted in single molecules roughly  $0.5\ \mu\text{m}$  apart from each other (Fig. 23a). Even when we tried higher concentrations, we could never label filaments thoroughly, and very high concentrations were also lethal for the embryos. For spot detection, we used the TrackMate algorithm of ImageJ and measured track lengths at contacts. Most longer tracks seemed randomly distributed, with many in the center. From the obtained tracks, we constructed decay curves with track counts for differing lifetimes that fit mono exponentials, optimizing the quality thresholds we used in TrackMate for each experimental day (Fig. 23b-d). The decay constants that were extracted from these curves give a sum of the F-actin dissociation rate and a photobleaching rate. By varying the acquisition intervals (see Methods), we got separate estimates of photobleaching and a corrected dissociation rate for F-actin (Fig. 23e-f).

In line with previous reports, we found a lifetime of  $26.3 \pm 2.8\ \text{s}$  for actin in controls (Fig. 23g). LPA treatment increased actin lifetime as expected, which would result in more accumulation at the rim of the contact. Also, pnBb treatment increased the actin lifetime at the contact significantly, in accordance with reports of suppressed Myosin-2 activity reducing actin turnover (Sonal 2018) however, this increased lifetime would not predict more rim accumulation as the outward flows were suppressed with pnBb treatment.

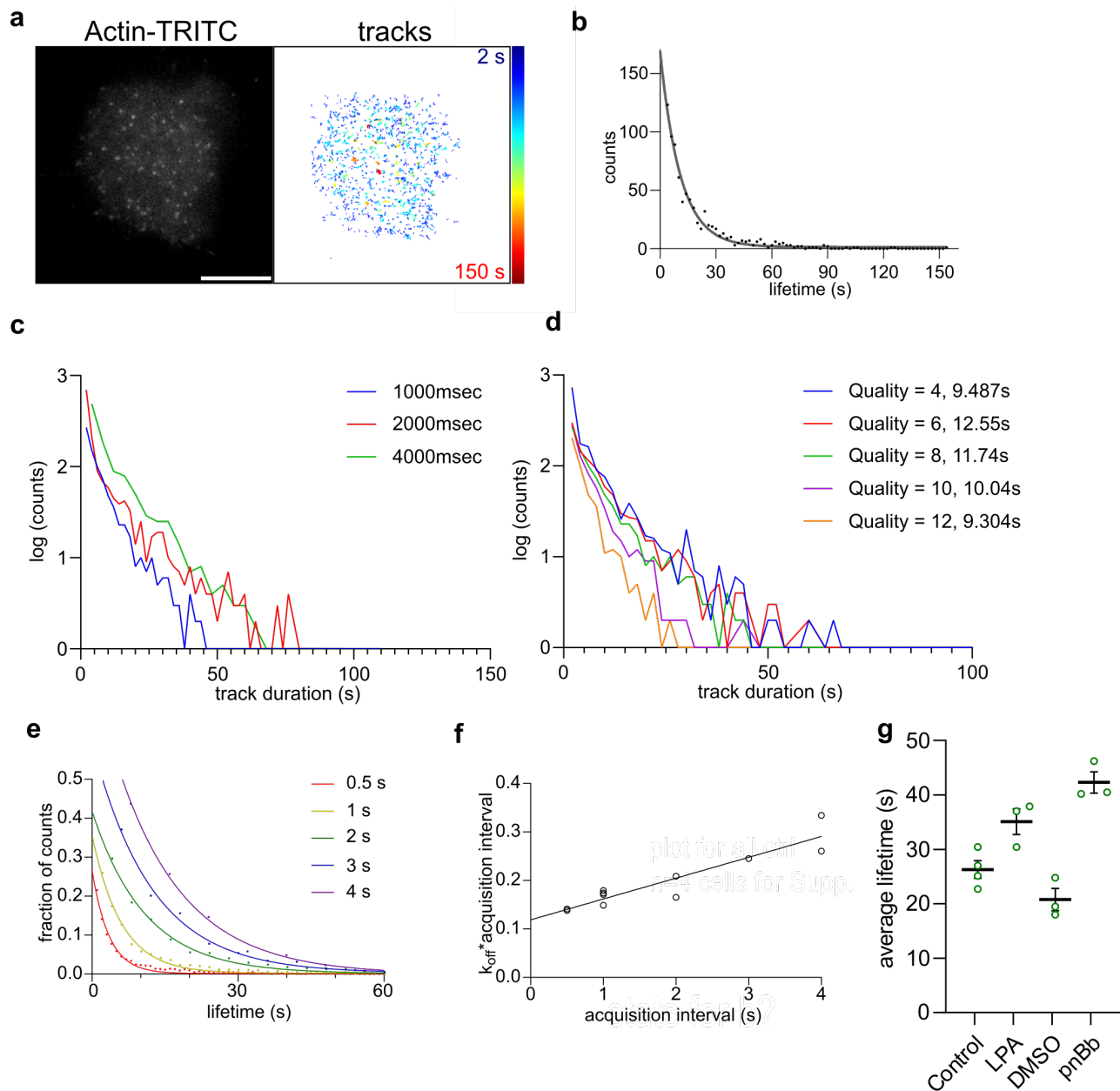


**Figure 23. Actin single molecule imaging.** TIRF image of a TRITC-Actin-labeled contact, along with tracks detected using TrackMate (a). An exemplary plot of track duration distribution from a single movie, showing exponential decay (b). Decay curves for different acquisition intervals were plotted using the log scale to check for linearity (c). Decay curves for the same data with different quality thresholds picked in TrackMate,  $k_{\text{eff}}$  values are given (d). Fraction of counts given for differing lifetimes for 3 cells acquired with differing time intervals (0.5, 1, 2, 3, 4s), raw decay data is given by dots, and best monoexponential fits are given by lines (e). Plot of acquisition interval vs acquisition interval \* effective dissociation constant for data shown on the left. The line indicates fit to  $k_{\text{eff}} t_{\text{ti}} = k_{\text{off}} t_{\text{ti}} + k_{\text{pb}} t_{\text{ex}}$ , where  $k_{\text{eff}}$  is the effective dissociation constant,  $k_{\text{off}}$  is the real dissociation constant,  $k_{\text{pb}}$  is the photobleaching rate,  $t_{\text{ex}}$  is the exposure time and  $t_{\text{ti}}$  is the acquisition interval (f). The plot of actin average lifetimes for control, LPA-

treated, DMSO-treated and *pnBb*-treated contacts (Control  $N=4$ ; LPA  $N=3$ ; DMSO  $N=3$ ; *pnBb*  $N=3$ ;  $n$  is at least 3 (differing acquisition intervals and cells) for each  $N$ ). Mean  $\pm$  s.e.m. are shown (e). Scale bar: 5  $\mu$ m.

Following actin measurements, we continued with measuring Ecad lifetime to see whether we would lower values for it as Ecad formed a less steep gradient than F-actin. We opted to use FRAP to measure Ecad recovery times as we had a knock-in line, and any single molecule technique would require overexpression of Ecad in the cells. As we checked the recovery curves, they fit well to a one-phase association curve, suggesting the imaged Ecad pool does not show significantly different dynamics based on their clustering or F-actin association (Fig. 24a,b). This is probably because of the high Ecad turnover, 11.69  $\pm$  4.71 s of recovery time for control, which limits detection of different pools even if they exist. When two-phase associations were tried; the taus for two phases were not differing an order of magnitude; therefore we could not use this method reliably. In line with this, the clusters also seemed to have similar recoveries as with more diffusive monomers (Fig. 24a). Still, we also detected a low fraction of immobile pool (Fig. 24c), which increased in percentage with LPA-treatment. Moreover, Ecad turnover seemed to correlate with tension in the cell, as LPA-treated contacts showed slower turnover. The CA-Mypt-expressing contacts on the contrary showed faster turnover compared to control but the difference was not significant suggesting control conditions may not have high contractility to start with. We also did not see a correlation between Ecad and F-actin turnovers, especially under low contractility, showing Ecad and actin turnovers may not always be linked (Fig. 24a,b). The details of the recovery process are not very clear through this analysis, as we could not detect clear differences at the edge vs center of the FRAPped regions suggesting an apparent diffusion-based recovery, but also FRAP areas of different sizes seemed to have slightly different recovery profiles. In preliminary experiments where we FRAPped the whole contacts, we got values around 15 s for recovery; more experiments are needed to figure contributions of lateral diffusion vs cytoplasmic turnover, yet both might be contributing to it based on the current preliminary observations.

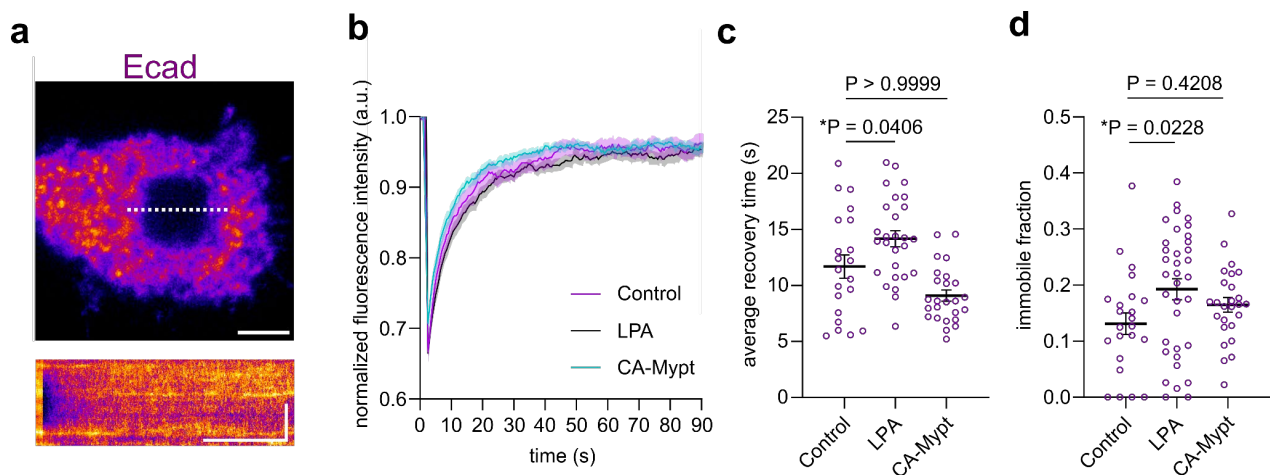


**Figure 24. Ecad recovery after bleaching.** TIRF image of FRAPped contact labeled for Ecad (above), along with a kymograph of the acquired timelapse along the dashed line (below) (a). Exemplary recovery curves after bleaching for Control, LPA-treated and

CA-Mypt-expressing contacts (Control n=11; LPA n=9; CA-Mypt n=9) (b). Plot of average recovery times at Control, LPA-treated and CA-Mypt-expressing contacts (Control N=3, n=35; LPA N=4, n=28; CA-Mypt N=3, n=24) (b). The plot of immobile fractions for the data shown in (c)(d). Mean  $\pm$  s.e.m. are shown (e). Kruskal-Wallis test. The scale bar is 5  $\mu$ m on the x-axis for the image above and y-axis for the image below, 1 min for the x-axis for the image below.

It is expected that the already observed Myosin-2 localization differences in cell doublets would give rise to flows. Previously the actin network at the contacts was not clearly visualized, and the Myosin-2 was completely absent, so only with our study it became possible to assume flows and observe them. As we managed to get measurements for flows and turnovers thanks to the resolution we have with lipid bilayers, it should be possible to feed these parameters to a mathematical model and see how much accumulation at the rim would be possible. Our collaborators are working on this with the extracted parameters (Table 1).

	Contact diameter (um)	Actin average flow velocity (um/min)	Actin average lifetime (s)	Ecad average flow velocity (um/min)	Ecad average recovery time (s)	Ecad immobile fraction
control	16.12 $\pm$ 3.28	0.18 $\pm$ 0.06	24.9 $\pm$ 1.8	0.25 $\pm$ 0.17	11.69 $\pm$ 4.71	0.13 $\pm$ 0.09
LPA	13.77 $\pm$ 2.24	0.20 $\pm$ 0.21	35.1 $\pm$ 3.3	0.20 $\pm$ 0.13	14.17 $\pm$ 3.73	0.19 $\pm$ 0.11
DMSO	16.01 $\pm$ 3.11	0.22 $\pm$ 0.09	20.77 $\pm$ 2.92			
pnBb	16.89 $\pm$ 2.64	-0.19 $\pm$ 0.26	42.3 $\pm$ 2.76			
CA-Mypt1	15.06 $\pm$ 4.49			-0.01 $\pm$ 0.13	9.10 $\pm$ 2.51	0.16 $\pm$ 0.07

Table 1. A summary of the flow and turnover parameters at the contact.

### 3. 5 Actin architecture at the contact

As mentioned above, the diffuse network of actin we observed at the contact was rather unexpected. Therefore when we first visualized it, we wanted to confirm those findings with cell doublets. Previously, our lab had published a study where doublets were stacked into microwells so that the contacts could be visualized *en face*<sup>145</sup>. We used a bright actin labeling line, overexpressing Tropomyosin3(Tpm3)-NeonGreen, to look at doublets with the microwell method. Even though this marker is not a ubiquitous F-actin maker, and Tropomyosins have been shown to bind specific pools of actin, we could observe a diffuse actin network at the contact in live cells (Fig. 25a), confirming our bilayer results. Similarly, phalloidin-stained cell-doublets also showed diffuse actin structures at the contacts rather than only at the rim (Fig. 25b).

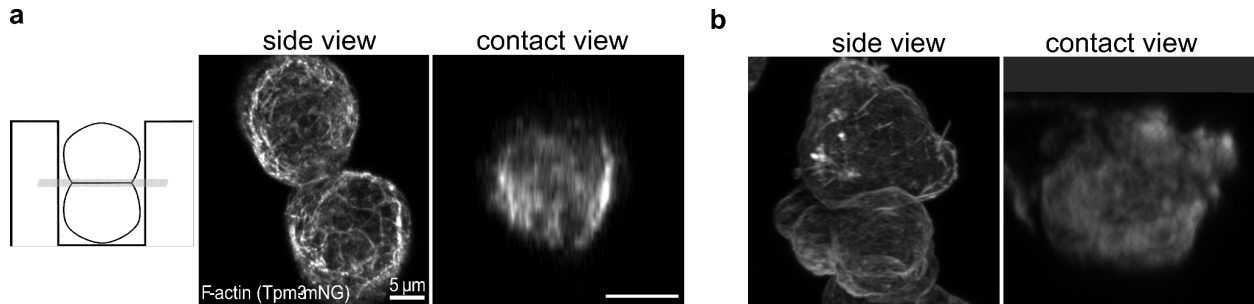


**Figure 25.** *Actin at the contacts of cell doublets. Schematic of the experimental design (left), side view and contact view for exemplary Tpm3-expressing contacts are shown (a). Side view and contact views of exemplary phalloidin-stained contacts are shown (b).*

As the nature of this actin network needed to be clarified, we did treatments with a general formin inhibitor (SMIFH2) and Arp2/3 inhibitor to see whether we could deduce the contributions of these networks to the local actin structure at the contacts. Formin inhibition increased Myosin-2 localization to the actin network and the actin network increased its network density upon treatment (Fig. 26a,b). Previously similar observations were made in stem cells, and Myosin-2 was suggested to be recruited thanks to the change in actin network density, implying that in control conditions Myosin-2 gets excluded spatially as the actin density decreases<sup>167</sup>. However, this needs to be investigated in more detail. Another explanation of actin density changes could be SMIFH2 treatment's decrease of contractility, resulting in a phenotype similar to pnBb<sup>168</sup>. As for Arp2/3 inhibition, we did not observe a difference in actin network density (Fig. 26b). Unfortunately, the fluorescent formin lines that were created in the lab or immunostainings against Arp2/3 complex components did not work. Therefore we could not get more details on the question of actin's nature at the contact. The only fluorescent line that worked was ArpC2, which labeled structures that colocalized with transient actin foci, that might be polymerization hotspots, and the edge of protrusions (Fig. 26c).

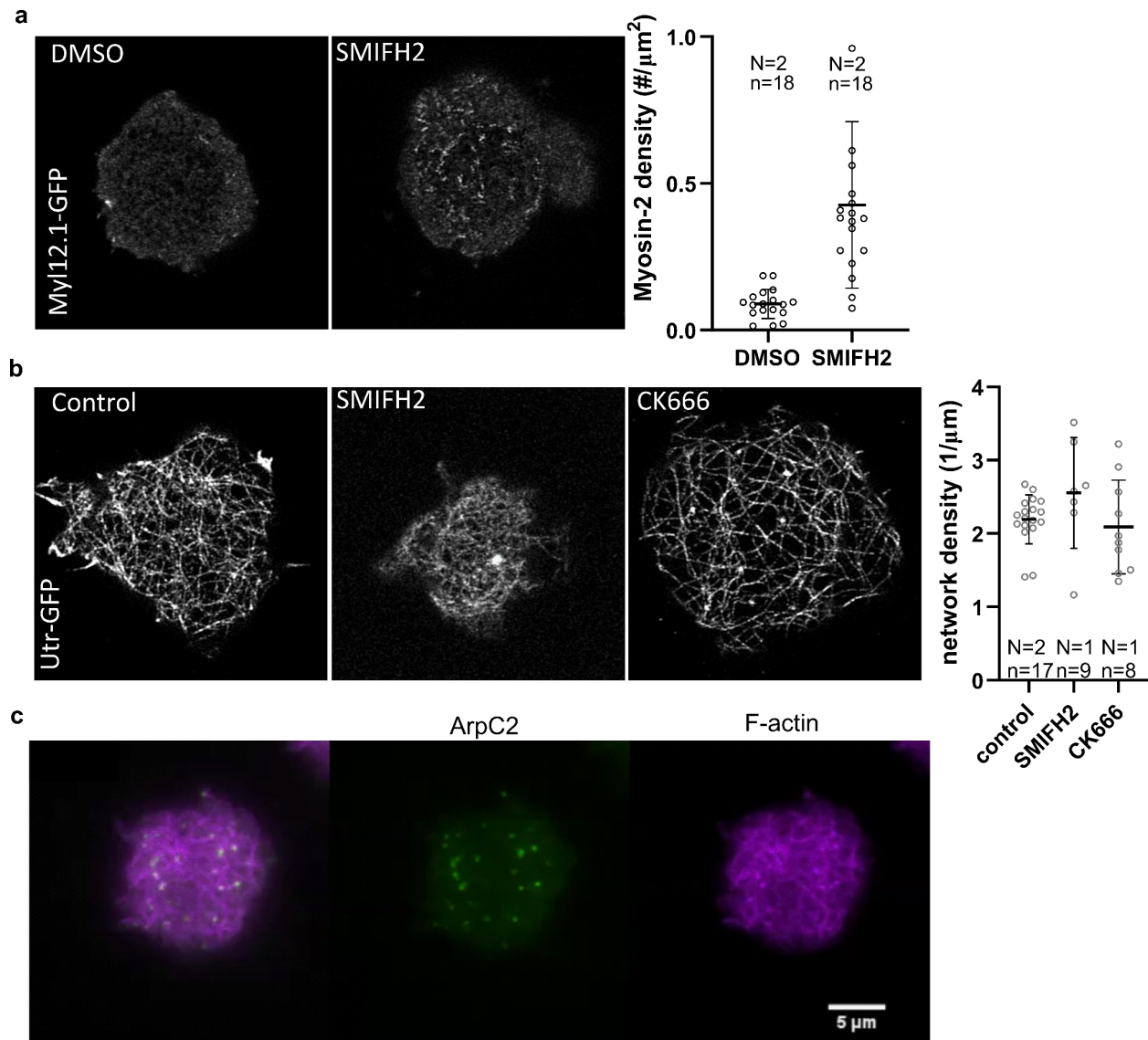


**Figure 26. Formin and Arp2/3 inhibitor treatments.** Representative images of Myosin-2 for DMSO- and SMIFH2-treated cells, along with the comparison of Myosin-2 density for these conditions, sample numbers are given in figure (a). Representative F-actin images for Control, SMIFH2- and CK666-treated cells, along with the comparison of F-actin network density for these conditions, sample numbers are given in figure (b). Representative dual-color images of ArpC2-mNeongreen cells, injected with Lifeact-RFP, in the merged tab Lifeact/F-actin is labeled purple and ArpC2 green (c).

We also checked whether cofilin might be active in decreasing network density at the cell contacts. Unfortunately, the antibodies we tried did not work in our hands, and the inhibitors of the LIM kinase (Damnacanthal and LimKi3), which phosphorylates cofilin and decreases its activity, did not give any differences in the network (Fig. 27).

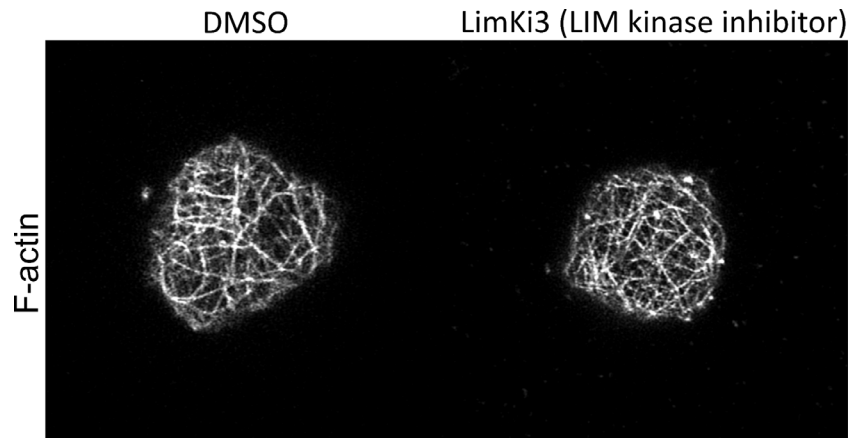


Figure 27. Inhibitors of actin depolymerization. Representative snapshots of F-actin/Fractin for DMSO- and LimKi3-treated contacts.

Another important note is on the selection of F-actin markers used. We realized during this project, thanks to the high resolution we obtained, that there is a preference for actin markers on specific pools of actin (Fig. 28). Utrophin was labeling the newly polymerizing actin network faster. It localized mainly to the protrusions and the ring-like accumulation at the edge, suggesting these networks might be more Arp2/3 mediated. On the contrary, Tpm3 labeled actin more slowly, and it seemed to bind more stable filaments in the contact center. Tpm3 was previously shown to label formin-mediated networks specifically, raising the question of whether it might be binding a formin-mediated network more readily in our contacts. Since we saw that F-actin labeled the actin structures more homogeneously than these two markers, we opted to use F-actin for most of our study.

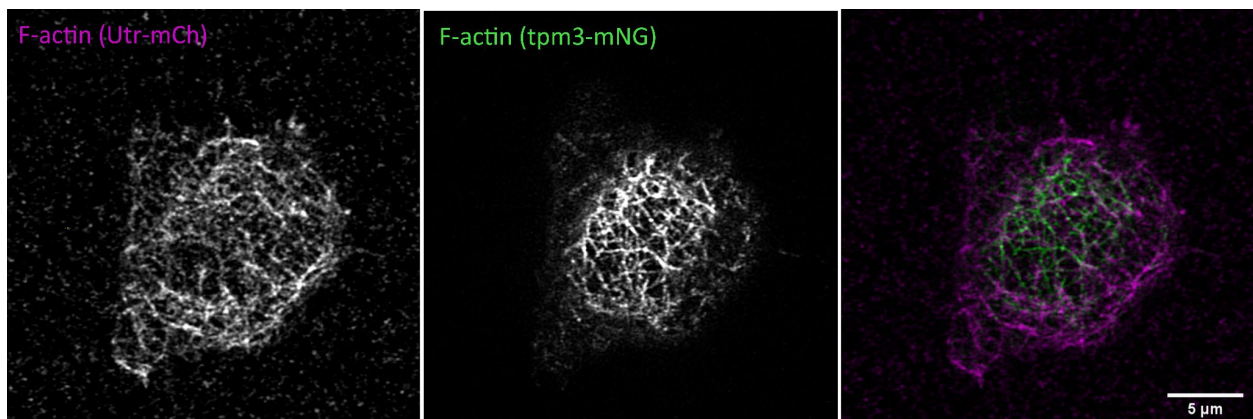


Figure 28. F-actin markers. Representative dual-color images of Utr-mCherry and Tpm3-mNeongreen cells, in the merged tab Utrophin is labeled purple and Tpm3 green.

### 3. 6 Contribution of blebs to F-actin and Ecad rim accumulation

Even though for most of this thesis we focused on accumulation that is mediated from center towards the actin ring, as mentioned before, the cells are decorated with blebs that get retracted at the contact site. We wondered whether these persistent blebs might also mediate remodeling at the contacts, for instance in the case of LPA, when blebs are

increased, similar to the idea that filopodia at the contacts might mediate Ecad clustering<sup>129</sup>.

We started by looking at the correlation of blebs with rim enrichment. At contacts of F-actin, as blebs got retracted, we observed an enrichment in the signal at the rim. It seemed like with blebs, the signal at the contact's edge, both for F-actin and Ecad, looked more diffuse, and with retraction, it came back to an enriched form (Fig. 29a,b). When we looked with kymographs at bleb retractions, we observed accumulations of F-actin and the formation of Ecad clusters at the stem of blebs in most cases (Fig. 29c). These observations were suggestive of blebs contributing to the remodeling of F-actin and Ecad at the contacts, yet it is unclear whether this is a meaningful contribution or cause transitional responses.

In order to investigate this phenomenon further, we tried to find a way to decouple bleb numbers and contractility. As it was used before for zebrafish progenitors<sup>144</sup>, we injected cells with a constitutively active form of Ezrin (CA-Ezrin2) to decrease bleb numbers by increasing membrane-cortex interactions. Unfortunately, in my hands, this method that I tried early on in my thesis (therefore, handling of cells may also not be excellent) could have given more consistent results. Only in some cases, CA-Ezrin2 decreased bleb numbers effectively, and the contacts in CA-Ezrin2-expressing cells were smaller and seemed to have less of a rim accumulation for alpha-catenin (Fig. 29d-g). Unfortunately, as reproducibility was a problem, I did not continue on this project further. As an alternative agent to reduce blebs, I also tried wheat germ agglutinin (WGA), as it binds glycoproteins of the cell membrane, yet after realizing it also affected Ecad clustering, I also did not continue further with that method. Other methods, such as osmolarity modulation, also did not have enough literature to guess the effects of such treatments very clearly. Therefore the question still stands whether retrograde retractions occurring through blebs outside of the contacts also matter for rim accumulation or not. Inducing blebs might also be an interesting take on this. For instance, laser cuts to the cortex of progenitor cells result in bleb formation, yet we did not have a good enough cutter system to investigate the results of a cut at the full cell contact at the time.

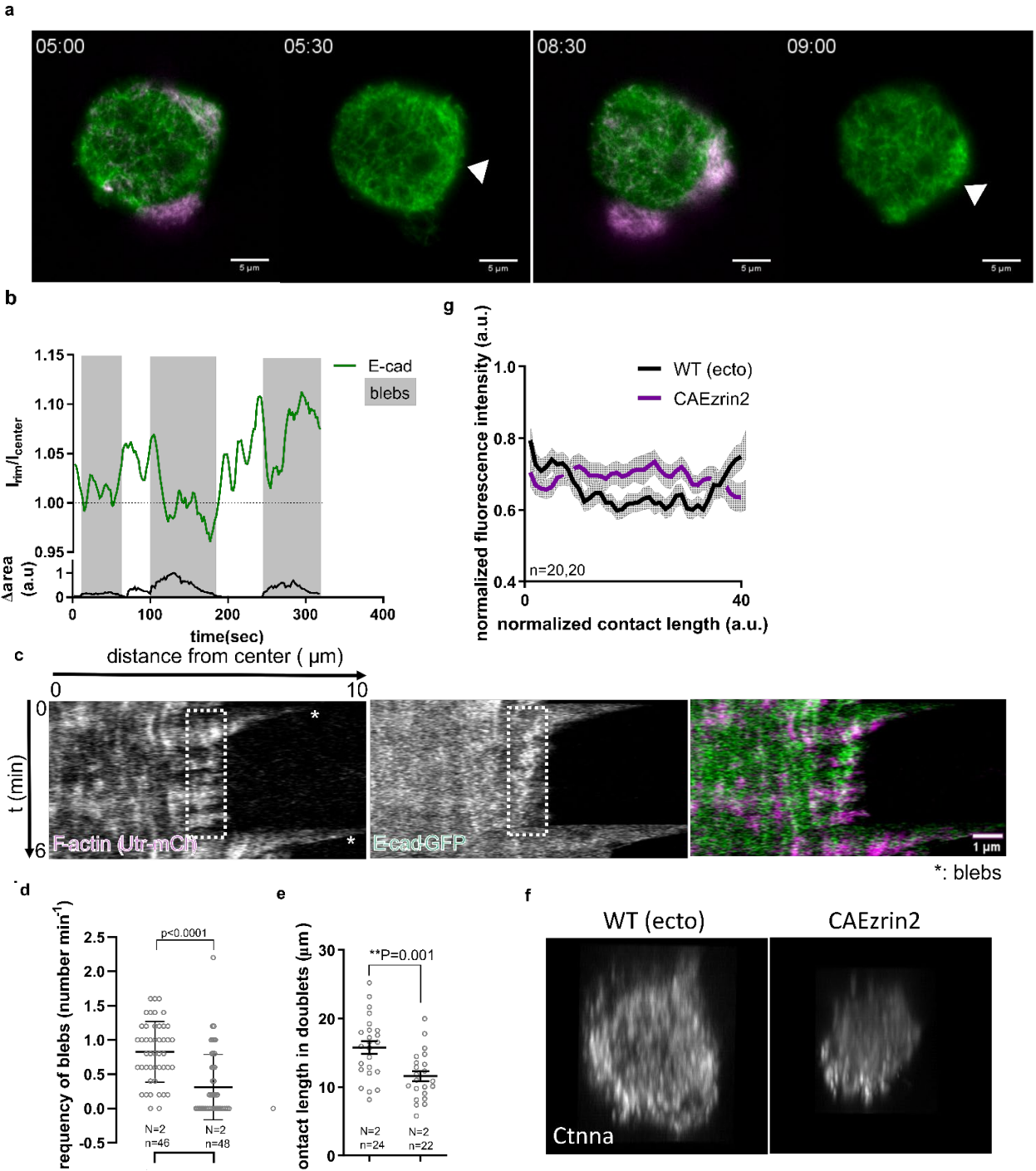


**Figure 29. Enrichment of proteins with bleb retractions.** Images from a time-lapse of F-actin/Utrophin, where area changes (blebs) are labeled in purple (a). Rim-to-center intensity ratios of an Ecad-labeled contact over time, with area changes indicating when blebs occur (b). Kymographs of a dual-colored contact radius injected F-actin/Utrophin is labeled in purple and injected Ecad-GFP is labeled in green. The rectangle shows the stem of bleb retractions (blebs are labeled with \*), where accumulations occur (c). Comparison of bleb frequencies in control and CA-Ezrin2-expressing cells. Student's t-

test. Sample numbers are given (d). Comparison of contact lengths between the cell doublets of control and CA-Ezrin2-expressing cells. Student's t-test. Sample numbers are given (e). Representative images of alpha-catenin contacts of control and CA-Ezrin2-expressing cells reconstructed from z-stacks (f). Quantification of radial intensity for control and CA-Ezrin2-expressing contacts (reconstructed as in f). Sample numbers are given (g).

## 4. Discussion and Conclusions

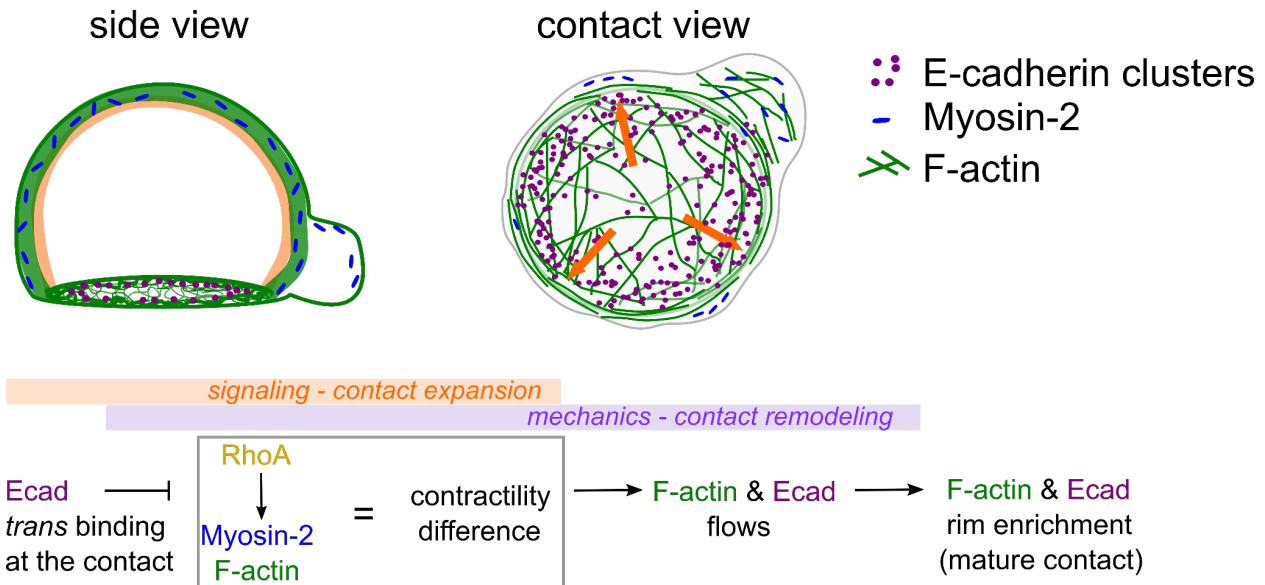


Figure 30. Ecad homophilic binding induced cortical acto-cadherin flows lead to rim accumulation.

Our main finding in this thesis explains how Ecad mediates its own rim accumulation in nascent contacts (Fig. 30). We show that in the initial minutes of contact formation, Ecad density at the contact increases, and this leads to a decrease in RhoA GTPase activity, which mediates downregulation of F-actin and Myosin-2 levels. After this initial phase, the protein amounts at the contact zone stabilize. Moreover, physical remodeling takes place. Possibly as soon as the Myosin-2 distribution becomes asymmetric due to the total exclusion of Myosin-2 at the contact, F-actin starts flowing from the low-contraction contact center towards the high-contraction contact rim. Ecad follows similarly. With the same velocities seen for F-actin flows it goes centrifugally towards the rim. We show that the average actin lifetime is around 30 seconds and Ecad recovers much faster, in around 10 seconds; this correlates with how steep the gradients of these proteins are along the cell radius. Therefore, the cortical flows of F-actin and Ecad, created through biochemical means by Ecad itself, remodel the Ecad-mediated cell-cell contacts.

We observed the changes at the contacts with high spatiotemporal resolution thanks to the SLB systems we employed in this thesis work to reconstitute cell-cell adhesion. We induced adhesion between cells and the bilayers using partially-fluid bilayers via

cholesterol addition to fluid PC components. Significantly, cells could remodel on these bilayers as seen by the spatial distribution of proteins similar to cell-cell doublets and increased Ecad levels at their contacts. We have not investigated the importance of Ecad density increase at the contact site in this study; however, it is a well-established phenomenon in cell cultures<sup>163</sup>. It might be interesting to characterize the RhoA-mediated and cytoskeletal responses with a titration of bilayer fluidities, therefore with various diffusion constants for available E-cadherin on the bilayer. For instance, Rac1 response<sup>124</sup> and actin bundling<sup>118</sup> were shown to differ on mobile and immobile substrates. Both force responses due to changes in bilayer viscosity and density-dependent clustering of cadherins<sup>122</sup> might differ as the substrate mobility changes. Previously on fluid bilayers, cadherin density increase was observed without mature contact formation<sup>126</sup>. Whether this density response was needed or necessary levels were reached to induce adhesion formation is not clear. In order to decouple the importance of cadherin enrichment vs the drag force cells required to apply to it, it would also be possible to titrate only the ligand density on partially-fluid bilayers. Unfortunately, we could not carry out such studies due to limitations in cell cultures, as there was much variability in the quality of the cells and contacts they made day by day and embryo batch by embryo batch. It would be exciting to carry out such experiments using a more robust culture system such as established cell lines.

We could also see how the maturation processes would differ from our nascent embryonic contacts using epithelial lines. In our contacts, we observed a complete downregulation of Myosin-2, and a diffuse network of F-actin does not seem to be oriented. It would be interesting to look at the contacts of enveloping cell layer (EVL) from the embryo, which carried Myosin-2 and actin foci at their contacts with bilayers as, from time to time, we ran into these cells. Similarly, in mature epithelial contacts, one would expect Myosin-2 at the contact, and it would be interesting to see whether they would have similar initial steps and how actin organization, presumably running as parallel bundles in those cells, would emerge. Radial or parallel bundles of actin were seen on immobile substrates of E-cadherin before (see 1.3.2.1), it would be interesting to investigate whether this response was a side effect of the ligand immobility or whether mature contacts also reach such conformations at our system.

Regarding cell-to-cell differences in contacts, an open question remains within the embryonic stage we study. During gastrulation, initially, ectoderm and mesendoderm cells differentiate from each other. It would be interesting to try out mesendoderm cells systematically using our system. One could see whether cells would break symmetry and start migrating in such a system and what variables could mediate such a response. It would be possible to change stiffness using PDMS support<sup>118</sup> or polymer-stacked bilayers<sup>133</sup> to investigate such properties and image contacts with high resolution at the same time. In cell clusters it would be interesting to see how cell-cell contacts would affect cell-bilayer contacts as well, by systematically changing contacting cell numbers and visualizing the contacts. Moreover, adding Ncad to the synthetic system would be valuable in studying mesendoderm contacts as they also start expressing this protein. Ecad and Ncad both make homophilic interactions, yet they were shown to make heterotypic interactions as well. There is still no clear understanding on how heterotypic

vs homotypic interactions affect the contact architecture, even though it is known that differential expression of cadherins mediates robust patterning in space<sup>169</sup>.

Previously, Rho and Rac signalings have been implicated in junction formation<sup>163</sup>. We did not observe any change in our contacts with the elimination of Rac signaling, while Ecad and active RhoA signals were found not to overlap, suggesting Ecad clusters to downregulate the RhoA signaling at the contact. However, we still need to figure out the cascade of events leading to RhoA downregulation. The link between Rho GTPases and Ecad signaling needs to be well-established as there seem to be differences from junction to junction. Rac activity might be required for filopodia or lamellipodia formation, which were shown to initiate *de novo* contacts before<sup>129,163</sup>. However, in zebrafish ectoderm progenitors, we do not observe these protrusions in culture but rather blebs as the dominant protrusions, which may be why Rac activity does not have a major role in these cells. Rac activity, which peaked at contact initiation, was suggested to downregulate RhoA activity by recruiting a RhoGAP to p120-catenin<sup>170,171</sup>. Whether such an interaction could occur independent of Rac activity, and the role of p120-catenin in the downregulation of actomyosin via RhoA could be investigated further.

Following RhoA downregulation, F-actin levels decrease (we also observed significant downregulation of F-actin amounts when using a dominant negative form of ROCK, this similarity suggests F-actin levels could also be regulated via Rho/ROCK pathway in ectoderm progenitors). Nevertheless, there is Myosin-2 activity at the contact rim where there is protrusive activity, as well as a richer circumferential actin network reminiscent of immune synapse actin arcs. Ecad accumulation at the rim seems to be a consequence of the high actomyosin contractility at the rim. It may not be surprising that the accumulation of such proteins, also probably RhoA activity, occurs at the contact rim, where the component of contact-free cortical tension that is normal to the contact interface is the highest. Of course, this is a prediction<sup>172</sup>, and it would be interesting to measure the values and how force correlates with actin and Ecad gradual profiles. FRET sensors that were developed for E-cadherin could be used to investigate this<sup>44</sup>. The contact edge seems a critical place to hold the two mechanically-interacting matrices together against this normal force. One question in this context is whether the tension difference is mediated only via Myosin-2 activity differences or whether the density of actin might be important as well<sup>173</sup>.

Reports show Ecad clustering, F-actin stabilization, Myosin-2 and Vinculin localizations to the cell contact edge<sup>45,86,145,174</sup>. The next question is how the rim-like accumulation is mediated. If there were a simple mechanism as we suggest, where Ecad homophilic interactions downregulate actomyosin, the whole contact would have the same actomyosin downregulation. On top, as only normal force and diffusion trap could cause a passive coffee ring effect for Ecad distribution, a decrease in actomyosin, maybe even more so than at the contact with less Ecad, would be expected at the contact rim. However, what we see is an actomyosin ring at the rim and Ecad being accumulated not at this ring but inside it, suggesting another factor to cause the actomyosin accumulation, which contradicts ideas such as a bigger Ecad cluster zone at the rim to activate RhoA opposite to the contact center, to form a circumferential actomyosin network typical of

zonula adherens<sup>141</sup>. Still, one could check the localization of mediators of this process, such as the RhoGEF Ect2, an upstream activator of the RhoA pathway<sup>175</sup>, in progenitor cells, to completely eliminate this hypothesis.

The actin architecture at the contact still needs to be better understood after this study, as it is resolved to this extent for the first time. It looks more complex than previously thought and has distinct regions with different structures. It will be exciting, as this architecture, to some extent, resembles immune synapses and stem cell contacts, to better understand the contact architecture of actin. As seen by Ecad accumulation within the inner side of the actin accumulation, this actin arc structure either spatially excludes Ecad or may not be a part of the real contact. It would be very interesting to check the distance of cells from the bilayers using RICM with some spatial resolution to understand the distance different actin architectures stand at from the cell-bilayer contacts and to see whether Ecad receptors might be excluded from this zone due to their size<sup>176</sup>. Another hypothesis could be that the actin ring is an extension of the upper cortex, and the high actomyosin levels of the cortex override the Ecad-dependent effects there. As any microscope we use would image around a 200-nm z section, it would be hard to image such an effect without superresolution. It is also possible that this actomyosin richer zone is just the expanding contact edge, labeled “contact edge”, and is free of Ecad in papers from the Nelson Lab<sup>163</sup>. It is possible that this edge with a more expansive property could act in preventing the collapse of contacts. There might also be an effect of geometry, due to the right angle of the cortex at the contact edge or protrusions, or the actin polymerization might be polarized in the cell. It might be interesting to follow up on our observations, especially with formin inhibitors, which were essential to understanding how Myosin-2 is recruited to the actin network at the contacts and what nucleators are active. It might be possible that the rim and center actin networks are nucleated via different proteins as in the immune synapse and have different stabilities and interacting proteins, resulting in the differential architecture of actin as well as Ecad exclusion from one of these zones. Another explanation could be blebs; as they bring Myosin-2, they also bring in actin towards the rim during retractions. Such transient accumulations could as well break the symmetry of the contacts.

The Myosin-2 signal at the contact has a cytoplasmic component, which might be non-specific as we see mini-filaments. Interestingly, with this signal, in addition to mini-filaments, the cytoplasmic background also gets weaker at the center of the contact. The center within the overlying cell cortex is dense and has vesicles, which appear as dark spots against the cytoplasmic signal, and the blebs are empty inside in comparison. This contact structure would be interesting to study further and realize the roles of many vesicles at the contact zone, some of which might be carrying ecad, and see their release mechanisms; for instance, whether this might also be a cause for the differential amounts of Ecad at the contact center vs underneath the actomyosin rich edge. Regarding Myosins, we looked at only Myosin-2 activity and localization and could explain most of our observations via that as Myosin-2 activity blockers could stop flows and affect the dilution of the F-actin network at the contact. Nevertheless, other Myosins are also implicated in cell-cell adhesions, such as Myosin-6, which was found to regulate vinculin recruitment to mature contacts<sup>177,178</sup>. Understanding the molecular architecture better will

be crucial and will also lead to better theoretical models to describe the contacts. This characterization of the contacts will be possible in the future with more optimized antibody staining protocols and new fluorescent zebrafish lines. In addition to the actomyosin-related proteins, there might be other receptors mediating the contacts in addition to Ecad as well. For instance, epidermal growth factor receptor (EGFR) was previously shown to form complexes with Ecad, which was disrupted under force<sup>179</sup>, and IgSF member Nectins were shown to associate with Ecad in the formation of adherens junctions<sup>180</sup>.

With fluorescence microscopy, we are shining light literally on a single protein in the darkness of the whole cell, and it is intriguing to think what other molecules might be carried with the F-actin flows and get enriched at the rim. Candidates that would be interesting to look at are ezrin-radixin-moesin (ERM) proteins that link cell membranes to the cytoskeleton. As they also appear in retracting blebs, they could be expected to be locally recruited close to the contact edge from both sides if they were to be carried with centrifugal flows. ERM proteins are known to mediate actin architecture<sup>51</sup>. Thus it could be interesting to image them to search for correlations between their localization and the different actin layers we defined in the contact (see 1.2.1). Previous work also suggests cell membrane itself flows, and it is highly possible that F-actin flows would carry many proteins and the cell membrane towards the rim. It would be interesting to image membrane or membrane tension via recently developed sensors such as Flipper<sup>181</sup>, as flows could affect the lipid order, and membrane tension was shown to promote Ecad clustering before by imposing membrane flattening and facilitating aggregation of proteins<sup>182</sup>.

The Cadherin adhesion complex is mechanosensitive. Enrichment of Ecad could be due to higher contact-free cortical tension acting locally at the rim, stabilizing the mechanosensitive cadherin complex, specifically strengthening the cadherin-actin bonds under force through catch bond behaviors of  $\alpha$ -catenin and Vinculin, which is recruited to cryptic binding sites of  $\alpha$ -catenin. The mechanosensitivity of cadherin-actin complex might also modulate contacts by modulating actin turnover under force, decreasing E-cadherin/ $\alpha$ -catenin complex mobility<sup>102</sup>. Here we describe an additional level of mechanosensation of contacts that keeps the contact remodeling dynamic; a constant flow of Ecad from center to the rim makes sense in this context to keep it accumulated as turnover is around 10 seconds and probably required to keep the RhoA levels down everywhere. The mechanism we propose for progenitor cells here does not exclude these well-established mechanisms; however, we would like to suggest that it is important to discuss the context of these mechanisms, as, at different stages of adhesion and different cell types, various mechanisms of Ecad enrichment might be at play. We suggest that our proposed mechanism might dominate at weak, short-living contacts as in the early stages of a developing embryo. It would still be important to investigate the other mechanisms of Ecad enrichment further in our contacts. For instance, replacing E-cadherin with forms that cannot respond to force to see whether a rather passive accumulation of Ecad if Myosin-2 difference persisted would be very interesting. This would require very carefully-devised experimental approaches, as a complete replacement might interfere with contact formation on the bilayers completely as in the case of Ecad knock-down, and overexpression of mutant cadherins may not give very indicative results if the mutant can

still cis cluster and follow wildtype Ecad dynamics thanks to that. However, it is worth noting that so far, we observed a very fast turnover of Ecad at the contacts, that did not seem to give differences at the rim vs center, agreeing with our idea that the mechanosensitivity of cadherins may not be much in play at our contacts (please see 1.2.3 for a more detailed introduction to zebrafish progenitor contacts).

Jasp-treated contacts exhibited thick bundles of actin. Mainly the flows of these thick structures were detected, which turned out to be faster than the controls. In line with these results, Ecad flows also increased velocity, proving the two are linked. Jasp-treated contacts, in conclusion, led to more accumulation of actin and Ecad, while the actin bundles were the main accumulated structures, there was no such pattern to Ecad, showing that even though the flows are linked, it may not be a direct link. Ecad pattern still seemed homogenous. The fast flows of Jasp-treated contacts might be because of a better connected actin network due to its increased stability. This proves that actin flows with a force that is sensed at the rim.

An observation we could not completely explain was the similar flow velocities LPA-treated cells showed, both for F-actin and Ecad. We had assumed that LPA treatment would increase the differences in contractility of contact-free surfaces and the contact, and the F-actin indeed showed an expected profile: a strong actomyosin ring surrounded the diffuse actin network of smaller contacts. Ecad profile also had a steeper gradient but was not changed as strongly. LPA contacts were not easy to analyze as the F-actin intensities differed too much within the contact; just by looking at them, some variability was present as some contacts had dense F-actin networks, some sparse, and some had several foci of actomyosin. We attributed the dense networks to too high contractility, which blocked proper contact formation. Most contacts did not look very silenced and even without stable big foci, had some excited profile as they formed and dispersed small actin foci. We assumed such activity at the normally more stable contacts could be the cause slowing the flows. Yet, it is also possible that the reason is geometry, as smaller contacts of LPA-treated cells might be more viscous and therefore slow the flow down. Another possibility is that within these contacts, Ecad limits the flow velocity (if there is some intrinsic limit to it that is reached at these contacts) if the link between actin and Ecad is stronger due to higher tension and the friction between them is increased. Of course, this still may not be explaining the high actomyosin signal at the rim. It may be because the contact-free cortex is much more contractile and higher in signal, which also translates to the contact plane. At the same time, also blebs are increased, and they seem to show more clustering of Ecad on them, and therefore it is possible they carry more meaningful-than-control amounts of material during their retraction towards the rim, increasing accumulation therein. To understand the LPA-treated contacts, it will be necessary to look into these hypotheses further. It also does not help that its exact mechanism of action is not very straightforward. Therefore we tried other contractility-increasing techniques, such as CA-RhoA injection, which gave a different phenotype at the contact and alternative drugs to increase contractility, such as Calyculin A were too toxic for the cultures. Other alternatives should be tried and compared to better dissect the effect of LPA treatment.

Our study exemplifies how a biochemical process can give rise to a mechanical process and how a mechanochemical process can drive the spatiotemporal regulation of contacts. When the cells are dividing, contractility in progenitor cells seems to increase; they round up as they homogenize their cortices and increase actomyosin activity at the contact. This reverses the contact formation process we observed and detaches cells from each other. Such dynamic contacts form and disappear throughout development, especially fast in the early stages in many vertebrate embryos. Visualizing this phenomenon or its effects *in vivo* would be extremely important. Such visualization depends on developments in imaging, yet one can already perform experiments to see whether it is possible to engage the cortices of neighboring cells via flows; for instance, by changing actin properties such as stability and contractility, which we defined as important parameters in determining flows in one cell, and investigating if these effects determine the distributions of proteins in the other contacting cell. One could assume such flows that are synchronized on both sides of the contacts via Ecad binding could provide positive feedback on each other, therefore, be faster and mature contacts faster. Through modeling, and by carefully analyzing the distribution of contact proteins over time, it might be possible to infer flow velocities *in vivo* and to see whether, with contractility changes whether cells change the mechanism they use for contact remodeling, for instance, by invoking a switch from flows to conformational mechanosensitive changes in the cadherin complex to mature long-lasting contacts. Flows can also be indirectly detected using beads that can be injected or placed with an optical tweezer to cell contacts; cytoplasmic beads that are close enough to the membrane so they can be carried with the cortical flows could prove their existence *in vivo*, although some trials of bead injections I had did not give any positive results even on bilayers. The bead could also be membrane-bound, which could also check whether other receptors on membrane flow.

We propose flow-mediated contact remodeling as a new contact regulation mechanism, using synthetic substrates' resolution and controllability. Synthetic systems can also be used within the context of the embryo in the future. For instance, as functionalized vesicles mimicking cells, which carry surface receptors and ligands, or as mechanistically defined malleable substrates, that could be instrumental both in the characterization of the embryos and in developing new therapies. In my experience, reconstitution starts with an initial understanding and putting minimal components together; it can frustrate you as it teaches you how complex a biological system is and surprise you as you increase your understanding to more than your starting point. Step by step, synthetic and developmental biology interactions will create wonders.

## References

1. Brunet, T. & King, N. The origin of animal multicellularity and cell differentiation. *Dev. Cell* **43**, 124–140 (2017).
2. Buss, L. W. Evolution, development, and the units of selection. *Proc. Natl. Acad. Sci.* **80**, 1387–1391 (1983).
3. Cavalier-Smith, T. Origin of animal multicellularity: precursors, causes, consequences—the choanoflagellate/sponge transition, neurogenesis and the Cambrian explosion. *Philos. Trans. R. Soc. B Biol. Sci.* **372**, 20150476 (2017).
4. Brunet, T. *et al.* Light-regulated collective contractility in a multicellular choanoflagellate. *Science* **366**, 326–334 (2019).
5. Fujimori, T., Nakajima, A., Shimada, N. & Sawai, S. Tissue self-organization based on collective cell migration by contact activation of locomotion and chemotaxis. *Proc. Natl. Acad. Sci.* **116**, 4291–4296 (2019).
6. Krieg, M. *et al.* Tensile forces govern germ-layer organization in zebrafish. *Nat. Cell Biol.* **10**, 429–436 (2008).
7. Bakhti, M. *et al.* Loss of electrostatic cell-surface repulsion mediates myelin membrane adhesion and compaction in the central nervous system. *Proc. Natl. Acad. Sci. U. S. A.* **110**, 3143–3148 (2013).
8. Regina Todeschini, A. & Hakomori, S. Functional role of glycosphingolipids and gangliosides in control of cell adhesion, motility, and growth, through glycosynaptic microdomains. *Biochim. Biophys. Acta BBA - Gen. Subj.* **1780**, 421–433 (2008).
9. Fenderson, B. A., Zehavi, U. & Hakomori, S. A multivalent lacto-N-fucopentaose III-lyssyllysine conjugate decompacts preimplantation mouse embryos, while the free

- oligosaccharide is ineffective. *J. Exp. Med.* **160**, 1591–1596 (1984).
10. Thiery, J. P. Cell adhesion in development: a complex signaling network. *Curr. Opin. Genet. Dev.* **13**, 365–371 (2003).
  11. Takeichi, M. Cadherin Cell Adhesion Receptors as a Morphogenetic Regulator. *Science* **251**, 1451–1455 (1991).
  12. Nichols, S. A., Roberts, B. W., Richter, D. J., Fairclough, S. R. & King, N. Origin of metazoan cadherin diversity and the antiquity of the classical cadherin/ $\beta$ -catenin complex. *Proc. Natl. Acad. Sci.* **109**, 13046–13051 (2012).
  13. Murray, P. S. & Zaidel-Bar, R. Pre-metazoan origins and evolution of the cadherin adhesome. *Biol. Open* **3**, 1183–1195 (2014).
  14. Brümmerdorf, T. & Lemmon, V. Immunoglobulin superfamily receptors: cis-interactions, intracellular adapters and alternative splicing regulate adhesion. *Curr. Opin. Cell Biol.* **13**, 611–618 (2001).
  15. Ozaki-Kuroda, K. *et al.* Nectin Couples Cell-Cell Adhesion and the Actin Scaffold at Heterotypic Testicular Junctions. *Curr. Biol.* **12**, 1145–1150 (2002).
  16. Tachibana, K. *et al.* Two Cell Adhesion Molecules, Nectin and Cadherin, Interact through Their Cytoplasmic Domain-Associated Proteins. *J. Cell Biol.* **150**, 1161–1176 (2000).
  17. Finegan, T. M. & Bergstralh, D. T. Neuronal immunoglobulin superfamily cell adhesion molecules in epithelial morphogenesis: insights from *Drosophila*. *Philos. Trans. R. Soc. B Biol. Sci.* **375**, 20190553 (2020).
  18. Janiszewska, M., Primi, M. C. & Izard, T. Cell adhesion in cancer: Beyond the migration of single cells. *J. Biol. Chem.* **295**, 2495–2505 (2020).

19. Springer, T. A. Adhesion receptors of the immune system. *Nature* **346**, 425–434 (1990).
20. Dustin, M. L. Cell adhesion molecules and actin cytoskeleton at immune synapses and kinapses. *Curr. Opin. Cell Biol.* **19**, 529–533 (2007).
21. McEver, R. P. Selectins: initiators of leucocyte adhesion and signalling at the vascular wall. *Cardiovasc. Res.* **107**, 331–339 (2015).
22. Genbacev, O. D. *et al.* Trophoblast L-Selectin-Mediated Adhesion at the Maternal-Fetal Interface. *Science* **299**, 405–408 (2003).
23. den Elzen, N., Buttery, C. V., Maddugoda, M. P., Ren, G. & Yap, A. S. Cadherin adhesion receptors orient the mitotic spindle during symmetric cell division in mammalian epithelia. *Mol. Biol. Cell* **20**, 3740–3750 (2009).
24. Wang, X. *et al.* E-cadherin bridges cell polarity and spindle orientation to ensure prostate epithelial integrity and prevent carcinogenesis in vivo. *PLoS Genet.* **14**, e1007609 (2018).
25. Green, K. J. & Gaudry, C. A. Are desmosomes more than tethers for intermediate filaments? *Nat. Rev. Mol. Cell Biol.* **1**, 208–216 (2000).
26. Choi, C. K. *et al.* Actin and  $\alpha$ -actinin orchestrate the assembly and maturation of nascent adhesions in a myosin II motor-independent manner. *Nat. Cell Biol.* **10**, 1039–1050 (2008).
27. Changede, R. & Sheetz, M. Integrin and cadherin clusters: A robust way to organize adhesions for cell mechanics. *BioEssays* **39**, 1–12 (2017).
28. Kučera, O. *et al.* Anillin propels myosin-independent constriction of actin rings. *Nat. Commun.* **12**, 4595 (2021).

29. Humphries, J. D. *et al.* Vinculin controls focal adhesion formation by direct interactions with talin and actin. *J. Cell Biol.* **179**, 1043–1057 (2007).
30. Shibata, A. C. E. *et al.* Archipelago architecture of the focal adhesion: Membrane molecules freely enter and exit from the focal adhesion zone. *Cytoskeleton* **69**, 380–392 (2012).
31. Fritzsche, M., Erenkämper, C., Moeendarbary, E., Charras, G. & Kruse, K. Actin kinetics shapes cortical network structure and mechanics. *Sci. Adv.* **2**, e1501337 (2016).
32. Rak, G. D., Mace, E. M., Banerjee, P. P., Svitkina, T. & Orange, J. S. Natural Killer Cell Lytic Granule Secretion Occurs through a Pervasive Actin Network at the Immune Synapse. *PLOS Biol.* **9**, e1001151 (2011).
33. Brown, A. C. N. *et al.* Remodelling of Cortical Actin Where Lytic Granules Dock at Natural Killer Cell Immune Synapses Revealed by Super-Resolution Microscopy. *PLOS Biol.* **9**, e1001152 (2011).
34. Fritzsche, M. *et al.* Cytoskeletal actin dynamics shape a ramifying actin network underpinning immunological synapse formation. *Sci. Adv.* **3**, e1603032 (2017).
35. Hammer, J. A., Wang, J. C., Saeed, M. & Pedrosa, A. T. Origin, Organization, Dynamics, and Function of Actin and Actomyosin Networks at the T Cell Immunological Synapse. *Annu. Rev. Immunol.* **37**, 201–224 (2019).
36. Truong Quang, B.-A., Mani, M., Markova, O., Lecuit, T. & Lenne, P.-F. Principles of E-Cadherin Supramolecular Organization In Vivo. *Curr. Biol.* **23**, 2197–2207 (2013).
37. Erami, Z., Timpson, P., Yao, W., Zaidel-Bar, R. & Anderson, K. I. There are four

- dynamically and functionally distinct populations of E-cadherin in cell junctions. *Biol. Open* **4**, 1481–1489 (2015).
38. Chandran, R., Kale, G., Philippe, J.-M., Lecuit, T. & Mayor, S. Distinct actin-dependent nanoscale assemblies underlie the dynamic and hierarchical organization of E-cadherin. *Curr. Biol. CB* **31**, 1726-1736.e4 (2021).
  39. Hong, S., Troyanovsky, R. B. & Troyanovsky, S. M. Binding to F-actin guides cadherin cluster assembly, stability, and movement. *J. Cell Biol.* **201**, 131–143 (2013).
  40. Cavey, M., Rauzi, M., Lenne, P.-F. & Lecuit, T. A two-tiered mechanism for stabilization and immobilization of E-cadherin. *Nature* **453**, 751–756 (2008).
  41. Takeichi, M. Dynamic contacts: rearranging adherens junctions to drive epithelial remodelling. *Nat. Rev. Mol. Cell Biol.* **15**, 397–410 (2014).
  42. Vicente-Manzanares, M., Ma, X., Adelstein, R. S. & Horwitz, A. R. Non-muscle myosin II takes centre stage in cell adhesion and migration. *Nat. Rev. Mol. Cell Biol.* **10**, 778–790 (2009).
  43. Zhang, Y., Sivasankar, S., Nelson, W. J. & Chu, S. Resolving cadherin interactions and binding cooperativity at the single-molecule level. *Proc. Natl. Acad. Sci. U. S. A.* **106**, 109–114 (2009).
  44. Borghi, N. *et al.* E-cadherin is under constitutive actomyosin-generated tension that is increased at cell–cell contacts upon externally applied stretch. *Proc. Natl. Acad. Sci. U. S. A.* **109**, 12568–12573 (2012).
  45. Engl, W., Arasi, B., Yap, L. L., Thiery, J. P. & Viasnoff, V. Actin dynamics modulate mechanosensitive immobilization of E-cadherin at adherens junctions. *Nat.*

- Cell Biol.* **16**, 587–94 (2014).
46. Indra, I. *et al.* Spatial and temporal organization of cadherin in punctate adherens junctions. *Proc. Natl. Acad. Sci.* **115**, E4406–E4415 (2018).
  47. Slováková, J. *et al.* Tension-dependent stabilization of E-cadherin limits cell-cell contact expansion in zebrafish germ-layer progenitor cells. *Proc. Natl. Acad. Sci. U. S. A.* **119**, e2122030119 (2022).
  48. Hong, S., Troyanovsky, R. B. & Troyanovsky, S. M. Spontaneous assembly and active disassembly balance adherens junction homeostasis. *Proc. Natl. Acad. Sci. U. S. A.* **107**, 3528–3533 (2010).
  49. Fritzsche, M., Lewalle, A., Duke, T., Kruse, K. & Charras, G. Analysis of turnover dynamics of the submembranous actin cortex. *Mol. Biol. Cell* **24**, 757–767 (2013).
  50. Jodoin, J. N. *et al.* Stable Force Balance between Epithelial Cells Arises from F-Actin Turnover. *Dev. Cell* **35**, 685–697 (2015).
  51. Svitkina, T. The Actin Cytoskeleton and Actin-Based Motility. *Cold Spring Harb. Perspect. Biol.* **10**, a018267 (2018).
  52. Indra, I., Troyanovsky, R. B., Shapiro, L., Honig, B. & Troyanovsky, S. M. Sensing Actin Dynamics through Adherens Junctions. *Cell Rep.* **30**, 2820-2833.e3 (2020).
  53. Kovacs, E. M., Goodwin, M., Ali, R. G., Paterson, A. D. & Yap, A. S. Cadherin-Directed Actin Assembly: E-Cadherin Physically Associates with the Arp2/3 Complex to Direct Actin Assembly in Nascent Adhesive Contacts. *Curr. Biol.* **12**, 379–382 (2002).
  54. Verma, S. *et al.* Arp2/3 Activity Is Necessary for Efficient Formation of E-cadherin

- Adhesive Contacts\*. *J. Biol. Chem.* **279**, 34062–34070 (2004).
55. Hansen, S. D. *et al.*  $\alpha$ E-catenin actin-binding domain alters actin filament conformation and regulates binding of nucleation and disassembly factors. *Mol. Biol. Cell* **24**, 3710–3720 (2013).
56. Yamada, S., Pokutta, S., Drees, F., Weis, W. I. & Nelson, W. J. Deconstructing the Cadherin-Catenin-Actin Complex. *Cell* **123**, 889–901 (2005).
57. Wu, S. K. *et al.* Cortical F-actin stabilization generates apical–lateral patterns of junctional contractility that integrate cells into epithelia. *Nat. Cell Biol.* **16**, 167–178 (2014).
58. Kobiela, A., Pasolli, H. A. & Fuchs, E. Mammalian formin-1 participates in adherens junctions and polymerization of linear actin cables. *Nat. Cell Biol.* **6**, 21–30 (2004).
59. Vasioukhin, V., Bauer, C., Yin, M. & Fuchs, E. Directed actin polymerization is the driving force for epithelial cell-cell adhesion. *Cell* **100**, 209–219 (2000).
60. Bray, D. & White, J. G. Cortical Flow in Animal Cells. *Science* **239**, 883–888 (1988).
61. Kruse, K., Joanny, J. F., Jülicher, F., Prost, J. & Sekimoto, K. Generic theory of active polar gels: a paradigm for cytoskeletal dynamics. *Eur. Phys. J. E* **16**, 5–16 (2005).
62. Miller, A. L. The contractile ring. *Curr. Biol.* **21**, R976–R978 (2011).
63. Mayer, M., Depken, M., Bois, J. S., Jülicher, F. & Grill, S. W. Anisotropies in cortical tension reveal the physical basis of polarizing cortical flows. *Nature* **467**, 617–621 (2010).

64. Cytokinesis mediated through the recruitment of cortexillins into the cleavage furrow. *EMBO J.* **18**, 586–594 (1999).
65. Munro, E., Nance, J. & Priess, J. R. Cortical Flows Powered by Asymmetrical Contraction Transport PAR Proteins to Establish and Maintain Anterior-Posterior Polarity in the Early *C. elegans* Embryo. *Dev. Cell* **7**, 413–424 (2004).
66. Goehring, N. W. *et al.* Polarization of PAR Proteins by Advective Triggering of a Pattern-Forming System. *Science* **334**, 1137–1141 (2011).
67. Goswami, D. *et al.* Nanoclusters of GPI-Anchored Proteins Are Formed by Cortical Actin-Driven Activity. *Cell* **135**, 1085–1097 (2008).
68. Ashdown, G. W. *et al.* Live-Cell Super-resolution Reveals F-Actin and Plasma Membrane Dynamics at the T Cell Synapse. *Biophys. J.* **112**, 1703–1713 (2017).
69. Shi, Z., Graber, Z. T., Baumgart, T., Stone, H. A. & Cohen, A. E. Cell Membranes Resist Flow. *Cell* **175**, 1769-1779.e13 (2018).
70. Köster, D. V. & Mayor, S. Cortical actin and the plasma membrane: inextricably intertwined. *Curr. Opin. Cell Biol.* **38**, 81–89 (2016).
71. Illukkumbura, R., Bland, T. & Goehring, N. W. Patterning and polarization of cells by intracellular flows. *Curr. Opin. Cell Biol.* **62**, 123–134 (2020).
72. Reversat, A. *et al.* Cellular locomotion using environmental topography. *Nature* **582**, 582–585 (2020).
73. Molecular stretching modulates mechanosensing pathways - PubMed.  
<https://pubmed.ncbi.nlm.nih.gov/libraryproxy.ist.ac.at/28474792/>.
74. Alexandrova, A. Y. *et al.* Comparative dynamics of retrograde actin flow and focal adhesions: formation of nascent adhesions triggers transition from fast to slow flow.

*PloS One* **3**, e3234 (2008).

75. Altered Actin Centripetal Retrograde Flow in Physically Restricted Immunological Synapses | PLOS ONE.  
<https://journals.plos.org/plosone/article?id=10.1371/journal.pone.0011878>.
76. Ditlev, J. A. *et al.* A composition-dependent molecular clutch between T cell signaling condensates and actin. *eLife* **8**, e42695 (2019).
77. Murugesan, S. *et al.* Formin-generated actomyosin arcs propel T cell receptor microcluster movement at the immune synapse. *J. Cell Biol.* **215**, 383–399 (2016).
78. Pinheiro, D. *et al.* Transmission of cytokinesis forces via E-cadherin dilution and actomyosin flows. *Nature* **545**, 103–107 (2017).
79. Levayer, R. & Lecuit, T. Oscillation and polarity of E-cadherin asymmetries control actomyosin flow patterns during morphogenesis. *Dev. Cell* **26**, 162–175 (2013).
80. Rauzi, M. Cell intercalation in a simple epithelium. *Philos. Trans. R. Soc. B Biol. Sci.* **375**, 20190552 (2020).
81. Kametani, Y. & Takeichi, M. Basal-to-apical cadherin flow at cell junctions. *Nat. Cell Biol.* **9**, 92–98 (2007).
82. Noordstra, I. *et al.* Cortical actin flow activates an  $\alpha$ -catenin clutch to assemble adherens junctions. 2021.07.28.454239 Preprint at <https://doi.org/10.1101/2021.07.28.454239> (2021).
83. Peglion, F., Llense, F. & Etienne-Manneville, S. Adherens junction treadmill during collective migration. *Nat. Cell Biol.* **16**, 639–651 (2014).
84. Schwayer, C. *et al.* Mechanosensation of Tight Junctions Depends on ZO-1

- Phase Separation and Flow. *Cell* **179**, 937-952.e18 (2019).
85. Shimizu, T. *et al.* E-cadherin is required for gastrulation cell movements in zebrafish. *Mech. Dev.* **122**, 747–763 (2005).
  86. Maitre, J.-L. *et al.* Adhesion Functions in Cell Sorting by Mechanically Coupling the Cortices of Adhering Cells. *Science* **338**, 253–256 (2012).
  87. Chan, E. H., Chavadimane Shivakumar, P., Clément, R., LAUGIER, E. & Lenne, P.-F. Patterned cortical tension mediated by N-cadherin controls cell geometric order in the Drosophila eye. *eLife* **6**, (2017).
  88. Maître, J.-L., Niwayama, R., Turlier, H., Nédélec, F. & Hiiragi, T. Pulsatile cell-autonomous contractility drives compaction in the mouse embryo. *Nat. Cell Biol.* **17**, 849–855 (2015).
  89. Budnar, S. & Yap, A. S. A mechanobiological perspective on cadherins and the actin-myosin cytoskeleton. *F1000Prime Rep.* **5**, 35 (2013).
  90. Winklbauer, R. Dynamic cell–cell adhesion mediated by pericellular matrix interaction – a hypothesis. *J. Cell Sci.* **132**, jcs231597 (2019).
  91. Kimmel, C. B., Ballard, W. W., Kimmel, S. R., Ullmann, B. & Schilling, T. F. Stages of embryonic development of the zebrafish. *Dev. Dyn.* **203**, 253–310 (1995).
  92. A Hydraulic Feedback Loop Between Mesendoderm Cell Migration and Interstitial Fluid Relocalization Promotes Embryonic Axis Formation in Zebrafish by Karla Huljev, Shayan Shamipour, Diana Pinheiro, Friedrich Preußner, Irene Steccari, Christoph Markus Sommer, Carl-Philipp Heisenberg :: SSRN. [https://papers.ssrn.com/sol3/papers.cfm?abstract\\_id=4008562](https://papers.ssrn.com/sol3/papers.cfm?abstract_id=4008562).
  93. Petridou, N. I., Grigolon, S., Salbreux, G., Hannezo, E. & Heisenberg, C.-P.

- Fluidization-mediated tissue spreading by mitotic cell rounding and non-canonical Wnt signalling. *Nat. Cell Biol.* **21**, 169–178 (2019).
94. Solnica-Krezel, L. Conserved patterns of cell movements during vertebrate gastrulation. *Curr. Biol. CB* **15**, R213-228 (2005).
95. Kornberg, A. Biologic Synthesis of Deoxyribonucleic Acid. *Science* **131**, 1503–1508 (1960).
96. Annaluru, N. *et al.* Total Synthesis of a Functional Designer Eukaryotic Chromosome. *Science* **344**, 55–58 (2014).
97. Szent-Györgyi, A. G. The Early History of the Biochemistry of Muscle Contraction. *J. Gen. Physiol.* **123**, 631–641 (2004).
98. Litschel, T. *et al.* Reconstitution of contractile actomyosin rings in vesicles. *Nat. Commun.* **12**, 2254 (2021).
99. Liu, A. P. & Fletcher, D. A. Biology under construction: in vitro reconstitution of cellular function. *Nat. Rev. Mol. Cell Biol.* **10**, 644–650 (2009).
100. Glazier, R. & Salaita, K. Biochimica et Biophysica Acta Supported lipid bilayer platforms to probe cell mechanobiology ☆. *BBA - Biomembr.* **1859**, 1465–1482 (2017).
101. The Immune Synapse | SpringerLink. <https://link.springer.com/book/10.1007/978-1-4939-6881-7>.
102. Arslan, F. N., Eckert, J., Schmidt, T. & Heisenberg, C.-P. Holding it together: when cadherin meets cadherin. *Biophys. J.* (2021) doi:10.1016/j.bpj.2021.03.025.
103. Kong, X., Kapustka, A., Sullivan, B., Schwarz, G. J. & Leckband, D. E. Extracellular matrix regulates force transduction at VE-cadherin junctions. *Mol. Biol.*

Cell mbc.E22-03-0075 (2022) doi:10.1091/mbc.E22-03-0075.

104. Tabdili, H. *et al.* Cadherin-dependent mechanotransduction depends on ligand identity but not affinity. *J. Cell Sci.* **125**, 4362–4371 (2012).
105. Brown, A. C., Dysart, M. M., Clarke, K. C., Stabenfeldt, S. E. & Barker, T. H. Integrin  $\alpha 3\beta 1$  Binding to Fibronectin Is Dependent on the Ninth Type III Repeat. *J. Biol. Chem.* **290**, 25534–25547 (2015).
106. Tominaga, Y. *et al.* Affinity and kinetic analysis of the molecular interaction of ICAM-1 and leukocyte function-associated antigen-1. *J. Immunol. Baltim. Md 1950* **161**, 4016–4022 (1998).
107. Vendome, J. *et al.* Structural and energetic determinants of adhesive binding specificity in type I cadherins. *Proc. Natl. Acad. Sci.* **111**, (2014).
108. Cavalcanti-Adam, E. A. *et al.* Cell Spreading and Focal Adhesion Dynamics Are Regulated by Spacing of Integrin Ligands. *Biophys. J.* **92**, 2964–2974 (2007).
109. Doh, J. & Irvine, D. J. Immunological synapse arrays: patterned protein surfaces that modulate immunological synapse structure formation in T cells. *Proc. Natl. Acad. Sci. U. S. A.* **103**, 5700–5705 (2006).
110. Altered TCR Signaling from Geometrically Repatterned Immunological Synapses. [https://www-science-org.libraryproxy.ist.ac.at/doi/10.1126/science.1119238?url\\_ver=Z39.88-2003&rfr\\_id=ori:rid:crossref.org&rfr\\_dat=cr\\_pub%20%20pubmed](https://www-science-org.libraryproxy.ist.ac.at/doi/10.1126/science.1119238?url_ver=Z39.88-2003&rfr_id=ori:rid:crossref.org&rfr_dat=cr_pub%20%20pubmed).
111. Bachir, A. I., Horwitz, A. R., Nelson, W. J. & Bianchini, J. M. Actin-Based Adhesion Modules Mediate Cell Interactions with the Extracellular Matrix and Neighboring Cells. *Cold Spring Harb. Perspect. Biol.* **9**, a023234 (2017).

112. Ganz, A. *et al.* Traction forces exerted through N-cadherin contacts. *Biol. Cell* **98**, 721–730 (2006).
113. Kolahi, K. S. *et al.* Effect of Substrate Stiffness on Early Mouse Embryo Development. *PLOS ONE* **7**, e41717 (2012).
114. Yang, Y., Wang, K., Gu, X. & Leong, K. W. Biophysical Regulation of Cell Behavior—Cross Talk between Substrate Stiffness and Nanotopography. *Engineering* **3**, 36–54 (2017).
115. Collins, C., Denisin, A. K., Pruitt, B. L. & Nelson, W. J. Changes in E-cadherin rigidity sensing regulate cell adhesion. *Proc. Natl. Acad. Sci.* **114**, E5835–E5844 (2017).
116. Gavard, J. *et al.* Lamellipodium extension and cadherin adhesion: two cell responses to cadherin activation relying on distinct signalling pathways. *J. Cell Sci.* **117**, 257–270 (2004).
117. Ladoux, B. *et al.* Strength dependence of cadherin-mediated adhesions. *Biophys. J.* **98**, 534–542 (2010).
118. Andreasson-Ochsner, M. *et al.* Single cell 3-D platform to study ligand mobility in cell–cell contact. *Lab. Chip* **11**, 2876–2883 (2011).
119. Grakoui, A. *et al.* The immunological synapse: a molecular machine controlling T cell activation. *Science* **285**, 221–227 (1999).
120. Pautot, S., Lee, H., Isacoff, E. Y. & Groves, J. T. Neuronal synapse interaction reconstituted between live cells and supported lipid bilayers. *Nat. Chem. Biol.* **1**, 283–289 (2005).
121. Chen, Z. *et al.* Spatially modulated ephrinA1:EphA2 signaling increases local

- contractility and global focal adhesion dynamics to promote cell motility. *Proc. Natl. Acad. Sci.* **115**, E5696–E5705 (2018).
122. Thompson, C. J., Vu, V. H., Leckband, D. E. & Schwartz, D. K. Cadherin Extracellular Domain Clustering in the Absence of *Trans* -Interactions. *J. Phys. Chem. Lett.* **10**, 4528–4534 (2019).
123. Strale, P.-O. *et al.* The formation of ordered nanoclusters controls cadherin anchoring to actin and cell–cell contact fluidity. *J. Cell Biol.* **210**, 333–346 (2015).
124. Tsai, J. & Kam, L. C. Lateral Mobility of E-Cadherin Enhances Rac1 Response in Epithelial Cells. *Cell. Mol. Bioeng.* **3**, 84–90 (2010).
125. Nelson, W. J. Regulation of cell–cell adhesion by the cadherin–catenin complex. *Biochem. Soc. Trans.* **36**, 149–155 (2008).
126. Perez, T. D., Nelson, W. J., Boxer, S. G. & Kam, L. E-Cadherin Tethered to Micropatterned Supported Lipid Bilayers as a Model for Cell Adhesion. *Langmuir* **21**, 11963–11968 (2005).
127. Mukherjee, A. *et al.*  $\alpha$ -Catenin links integrin adhesions to F-actin to regulate ECM mechanosensing and rigidity dependence. *J. Cell Biol.* **221**, e202102121 (2022).
128. Charnley, M., Kroschewski, R. & Textor, M. The study of polarisation in single cells using model cell membranes. *Integr. Biol.* **4**, 1059–1071 (2012).
129. Biswas, K. H. *et al.* E-cadherin junction formation involves an active kinetic nucleation process. *Proc. Natl. Acad. Sci. USA.* **112**, 10932–10937 (2015).
130. Regulation of N-cadherin dynamics at neuronal contacts by ligand binding and cytoskeletal coupling - PubMed. <https://pubmed.ncbi.nlm.nih.gov/16319177/>.
131. Kusumi, A., Sako, Y. & Yamamoto, M. Confined lateral diffusion of membrane

- receptors as studied by single particle tracking (nanovid microscopy). Effects of calcium-induced differentiation in cultured epithelial cells. *Biophys. J.* **65**, 2021–2040 (1993).
132. Shilts, K. & Naumann, C. A. Tunable cell-surface mimetics as engineered cell substrates. *Biochim. Biophys. Acta BBA - Biomembr.* **1860**, 2076–2093 (2018).
133. Ge, Y. *et al.* N-cadherin-functionalized polymer-tethered multi-bilayer: a cell surface-mimicking substrate to probe cellular mechanosensitivity. *Soft Matter* **12**, 8274–8284 (2016).
134. Harrison, O. J. *et al.* Family-wide Structural and Biophysical Analysis of Binding Interactions among Non-clustered  $\delta$ -Protocadherins. *Cell Rep.* **30**, 2655-2671.e7 (2020).
135. WESTERFIELD, M. The Zebrafish Book : A Guide for the Laboratory Use of Zebrafish. [http://zfin.org/zf\\_info/zfbook/zfbk.html](http://zfin.org/zf_info/zfbook/zfbk.html) (2000).
136. Behrndt, M. *et al.* Forces Driving Epithelial Spreading in Zebrafish Gastrulation. *Science* **338**, 257–260 (2012).
137. Cronan, M. R. & Tobin, D. M. Endogenous Tagging at the *cdh1* Locus for Live Visualization of E-Cadherin Dynamics. *Zebrafish* **16**, 324–325 (2019).
138. Choe, C. P. *et al.* Wnt-Dependent Epithelial Transitions Drive Pharyngeal Pouch Formation. *Dev. Cell* **24**, 296–309 (2013).
139. Kardash, E. *et al.* A role for Rho GTPases and cell-cell adhesion in single-cell motility in vivo. *Nat. Cell Biol.* **12**, 47–53; sup pp 1-11 (2010).
140. Piekny, A. J. & Glotzer, M. Anillin is a scaffold protein that links RhoA, actin, and myosin during cytokinesis. *Curr. Biol. CB* **18**, 30–36 (2008).

141. Priya, R. *et al.* Feedback regulation through myosin II confers robustness on RhoA signalling at E-cadherin junctions. *Nat. Cell Biol.* **17**, 1282–1293 (2015).
142. Babb, S. G. & Marrs, J. A. E-cadherin regulates cell movements and tissue formation in early zebrafish embryos. *Dev. Dyn.* **230**, 263–277 (2004).
143. Pinheiro, D., Kardos, R., Hannezo, É. & Heisenberg, C.-P. Morphogen gradient orchestrates pattern-preserving tissue morphogenesis via motility-driven (un)jamming. 2022.05.16.492018 Preprint at <https://doi.org/10.1101/2022.05.16.492018> (2022).
144. Diz-Muñoz, A. *et al.* Steering cell migration by alternating blebs and actin-rich protrusions. *BMC Biol.* **14**, 74 (2016).
145. Slováková, J. *et al.* Tension-dependent stabilization of E-cadherin limits cell-cell contact expansion. <http://biorxiv.org/lookup/doi/10.1101/2020.11.20.391284> (2020) doi:10.1101/2020.11.20.391284.
146. Jönsson, P. frap\_analysis. *frap\_analysis* ([https://www.mathworks.com/matlabcentral/fileexchange/29388-frap\\_analysis](https://www.mathworks.com/matlabcentral/fileexchange/29388-frap_analysis)), MATLAB Central File Exchange. [https://ch.mathworks.com/matlabcentral/fileexchange/29388-frap\\_analysis](https://ch.mathworks.com/matlabcentral/fileexchange/29388-frap_analysis).
147. Mahlandt, E. K. *et al.* Visualizing endogenous RhoA activity with an improved localization-based, genetically encoded biosensor. <http://biorxiv.org/lookup/doi/10.1101/2021.02.08.430250> (2021) doi:10.1101/2021.02.08.430250.
148. Sommer, C., Straehle, C., Köthe, U. & Hamprecht, F. A. Ilastik: Interactive learning and segmentation toolkit. in *2011 IEEE International Symposium on*

*Biomedical Imaging: From Nano to Macro* 230–233 (2011).

doi:10.1109/ISBI.2011.5872394.

149. Van Rossum, G. & Drake, F. L. *Python 3 Reference Manual*. (CreateSpace, 2009).
150. Bolte, S. & Cordelières, F. P. A guided tour into subcellular colocalization analysis in light microscopy. *J. Microsc.* **224**, 213–232 (2006).
151. Measurement of co-localization of objects in dual- colour confocal images - MANDERS - 1993 - Journal of Microscopy - Wiley Online Library. <https://onlinelibrary-wiley-com.libraryproxy.ist.ac.at/doi/abs/10.1111/j.1365-2818.1993.tb03313.x>.
152. Li, Q. *et al.* A syntaxin 1, Galpha(o), and N-type calcium channel complex at a presynaptic nerve terminal: analysis by quantitative immunocolocalization. *J. Neurosci. Off. J. Soc. Neurosci.* **24**, 4070–4081 (2004).
153. Schindelin, J. *et al.* Fiji: an open-source platform for biological-image analysis. *Nat. Methods* **9**, 676–682 (2012).
154. Jakobs, M. A., Dimitracopoulos, A. & Franze, K. KymoButler, a deep learning software for automated kymograph analysis. *eLife* **8**, e42288 (2019).
155. Thielicke, W. & Stamhuis, E. PIVlab – Towards User-friendly, Affordable and Accurate Digital Particle Image Velocimetry in MATLAB. *J. Open Res. Softw.* **2**, e30 (2014).
156. Xu, T. *et al.* SOAX: A software for quantification of 3D biopolymer networks. *Sci. Rep.* **5**, 9081 (2015).
157. Nunez-Iglesias, J., Blanch, A. J., Looker, O., Dixon, M. W. & Tilley, L. A new Python library to analyse skeleton images confirms malaria parasite remodelling of

- the red blood cell membrane skeleton. *PeerJ* **6**, e4312 (2018).
158. TrackMate: An open and extensible platform for single-particle tracking - PubMed. <https://pubmed.ncbi.nlm.nih.gov/27713081/>.
159. Baranova, N. & Loose, M. Chapter 21 - Single-molecule measurements to study polymerization dynamics of FtsZ-FtsA copolymers. in *Methods in Cell Biology* (ed. Echard, A.) vol. 137 355–370 (Academic Press, 2017).
160. Friction forces position the neural anlage - PubMed. <https://pubmed.ncbi.nlm.nih.gov/28346437/>.
161. Huveneers, S. & de Rooij, J. Mechanosensitive systems at the cadherin-F-actin interface. *J. Cell Sci.* **126**, 403–13 (2013).
162. Venturini, V. *et al.* The nucleus measures shape changes for cellular proprioception to control dynamic cell behavior. *Science* **370**, eaba2644 (2020).
163. Yamada, S. & Nelson, W. J. Localized Zones of Rho and Rac Activities Drive Initiation and Expansion of Epithelial Cell-Cell Adhesion. *J. Cell Biol.* **178**, 517–527 (2007).
164. Gupta, S. *et al.* Enhanced RhoA signalling stabilizes E-cadherin in migrating epithelial monolayers. *J. Cell Sci.* **134**, jcs258767 (2021).
165. Life and Times of a Cellular Bleb - ScienceDirect. <https://www.sciencedirect.com.libraryproxy.ist.ac.at/science/article/pii/S0006349508706222>.
166. Képiró, M. *et al.* para-Nitroblebbistatin, the non-cytotoxic and photostable myosin II inhibitor. *Angew. Chem. Int. Ed Engl.* **53**, 8211–8215 (2014).
167. Xia, S. *et al.* Nanoscale Architecture of the Cortical Actin Cytoskeleton in Embryonic Stem Cells. *Cell Rep.* **28**, 1251-1267.e7 (2019).

168. Nishimura, Y. *et al.* The formin inhibitor SMIFH2 inhibits members of the myosin superfamily. *J. Cell Sci.* **134**, jcs253708 (2021).
169. Tsai, T. Y.-C. *et al.* An adhesion code ensures robust pattern formation during tissue morphogenesis. *Science* **370**, 113–116 (2020).
170. Wildenberg, G. A. *et al.* p120-Catenin and p190RhoGAP Regulate Cell-Cell Adhesion by Coordinating Antagonism between Rac and Rho. *Cell* **127**, 1027–1039 (2006).
171. Anastasiadis, P. Z. *et al.* Inhibition of RhoA by p120 catenin. *Nat. Cell Biol.* **2**, 637–644 (2000).
172. Winklbauer, R. Cell adhesion strength from cortical tension - an integration of concepts. *J. Cell Sci.* **128**, 3687–3693 (2015).
173. Chugh, P. *et al.* Actin cortex architecture regulates cell surface tension. *Nat. Cell Biol.* **19**, 689–697 (2017).
174. Regulation of  $\alpha$ -catenin conformation at cadherin adhesions | Semantic Scholar. <https://www.semanticscholar.org/paper/Regulation-of-%CE%B1-catenin-conformation-at-cadherin-Biswas/91522f9ed38d0fe05f55e0b6757733c75038a425>.
175. Ratheesh, A. *et al.* Centralspindlin and  $\alpha$ -catenin regulate Rho signalling at the epithelial zonula adherens. *Nat. Cell Biol.* **14**, 818–828 (2012).
176. Schmid, E. M. *et al.* Size-dependent protein segregation at membrane interfaces. *Nat. Phys.* **12**, 704–711 (2016).
177. Tamada, M., Perez, T. D., Nelson, W. J. & Sheetz, M. P. Two distinct modes of myosin assembly and dynamics during epithelial wound closure. *J. Cell Biol.* **176**, 27–33 (2007).

178. Maddugoda, M. P., Crampton, M. S., Shewan, A. M. & Yap, A. S. Myosin VI and vinculin cooperate during the morphogenesis of cadherin cell–cell contacts in mammalian epithelial cells. *J. Cell Biol.* **178**, 529–540 (2007).
179. Sullivan, B. *et al.* Mechanical disruption of E-cadherin complexes with epidermal growth factor receptor actuates growth factor-dependent signaling. *Proc. Natl. Acad. Sci. U. S. A.* **119**, e2100679119 (2022).
180. Tanaka, Y. *et al.* Role of Nectin in Formation of E-Cadherin–based Adherens Junctions in Keratinocytes: Analysis with the N-Cadherin Dominant Negative Mutant. *Mol. Biol. Cell* **14**, 1597–1609 (2003).
181. Colom, A. *et al.* A Fluorescent Membrane Tension Probe. *Nat. Chem.* **10**, 1118–1125 (2018).
182. Delanoë-Ayari, H., Al Kurdi, R., Vallade, M., Gulino-Debrac, D. & Riveline, D. Membrane and acto-myosin tension promote clustering of adhesion proteins. *Proc. Natl. Acad. Sci.* **101**, 2229–2234 (2004).